Adenosine Regulation of Adipose Tissue Lipid Metabolism

Mitchell Ethan Granade
Atlanta, GA

B.S. Biology, University of South Carolina, 2012

A Dissertation Presented to the Graduate Faculty of the
University of Virginia in Candidacy for the
Degree of Doctor of Philosophy

Department of Pharmacology

University of Virginia
May 2022

Thurl E. Harris, Ph.D.
Joel Linden, Ph.D.
Kevin R. Lynch, Ph.D.
Norbert Leitinger, Ph.D.
Matthew J. Wolf, M.D., Ph.D.

ABSTRACT

Adipose tissue is a critical regulator of energy balance that must rapidly shift its metabolism between fasting and feeding to maintain homeostasis. During feeding, adipose tissue acts as a physiological buffer for excess energy through lipid storage, while adipocyte lipolysis provides the body with a necessary source of energy through fatty acids during fasting. The dysregulation of these processes contributes to the development of metabolic syndrome and type 2 diabetes, so it is essential that we understand the pathways which regulate adipose tissue metabolism. Adenosine has been well characterized as an important regulator of adipocyte metabolism, and alterations in adenosine signaling are associated with obesity and metabolic syndrome. In this dissertation, we explore the regulation of adipose tissue metabolism by adenosine and its impacts on whole-body metabolic homeostasis. Adipose tissue is believed to be regulated by adenosine primarily through its actions on A_1 adenosine receptors (A1R), and we find that A1R augments insulin action in adipocytes and opposes catecholaminergic stimulation of adipocyte lipolysis *in vivo*. We also found that adenosine signaling in adipose tissue is not static but is dynamically shifted between fasting and feeding through transcriptional control of A1R and A_{2B} adenosine receptors. This shift in adenosine signaling may enable adipocytes to be more responsive to changing nutrient conditions.

ACKNOWLEDGMENTS

The path to my doctoral thesis has been far from a straightforward one. There have been stumbles, failures, sharp turns, and less severe course corrections. Alone, the end would have been impossible to reach, but I have been fortunate to have the help and support of countless people, both within the University of Virginia and without, who have enabled me to accomplish this goal. It would be impossible to adequately thank everyone here, but I sincerely appreciate everyone I have encountered along this journey.

First, I would like to thank my PI, Thurl Harris. I truly feel that you put the training of your students above all other considerations. It is due to your unwavering support in my goals that I have had so many opportunities for growth, from my training in the biotechnology training program and externship, to the numerous productive collaborations I have been able to take part in. You constantly encouraged me not only to persevere, but also to pursue my own hypotheses independently and challenge myself with new techniques and approaches. Your training has been paramount to my development as a scientist, and I am incredibly grateful for your mentorship.

After spending nearly six years in the Harris lab there are so many people to thank. I would first like to thank Katharina who initially trained me in the beginning of this project, taught me so much about mice and cardiovascular disease, and has always been so supportive. I would also like to thank Stefan for always being in the trenches of mouse work with me. I have learned so much from you, and without you I never could have completed the sheer volume of mouse experiments for my project. Vidisha and Katelyn, you were both there from the beginning and were truly wonderful friends and lab mates.

Salome, your training on the lipin and dgk assays was an invaluable foundation for so much of my graduate training. Mike and Danny, it has been such a pleasure getting to know and work with you both over the last couple of years and I wish you both the best with your own projects. To all the undergrads I have worked with in the lab, Dana, Anna, Abi, and Arad, you have all been amazing and I thank you for your enthusiasm, hard work, and most of all your patience with me.

Next, I would like to thank my thesis committee who has gone above and beyond to support and guide me through both my research and my career. This dissertation shares almost no resemblance with my original proposal, and the success of my project has a great deal to do with the advice from all of you on new avenues to pursue when my original plans were met with failure. All of you have been critical to either my funding applications or my career development, or both and I am extremely grateful for the support all of you have shown me and for always being so generous with your time.

I would also like to thank all of our collaborators who have either helped us directly in the lab or given excellent advice. BJ and Laryssa, we could not have asked for better collaborators on the DGK project. Ira, Mohan, and Irina, without help from all three of you I would no doubt still be troubleshooting my chromatin IPs. An extra thank you to Ira for all of the protocols you shared, both your scientific and career advice, and always asking the critical questions. To Alex (Young and Kadl), I may have never ended up pursuing the cardiovascular aspects of my project, but your unending patience and expertise in helping me to figure out the intubation and surgery techniques was always appreciated.

I have had a number of other mentors throughout my career who I would also like to take the time to thank here. During my time at the CDC, I would like to thank all those who gave me my first opportunities to develop as a scientist. Kamile, Valerie, Sigrid, Brandon, Johannetsy, and David, it was wonderful working with all of you and you have all been such amazing mentors to me. I would also like to thank Gordon Laurie for being an excellent director of the Biotech Training Program. You always made the extra effort to assist BTP trainees and I am especially grateful for your assistance in networking and obtaining my externship with Pfizer.

Next, I would like to thank all of my friends for making my time in Virginia such a wonderful experience. From coffee runs, happy hours, and cook outs to biking, squash, and tubing there are too many of you and too many good experiences to name them all, but I know you will all be lifelong friends. Graduate school can be trying at times, and your support, and sometimes commiseration, through it all has meant so much to me. Thank you to all my friends from before graduate school as well for your awesome visits, all your support, especially coming out to Jennifer and I's wedding (twice for some of you), and for being such amazing people.

Finally, I want to thank my family for always believing in me and supporting me in everything I pursue. To my parents, Tim and Sharon, you have always made me feel I can accomplish anything I set out to do, and it is only with your love, encouragement, and the values you instilled in me that I have made it to this point. To my sisters, Rachel and Stephanie, thank you for always being there and listening to me, whether I was venting or droning on about science for far longer than you had bargained for. To all of my

grandparents, you are the most amazing grandparents anyone could ever ask for. You have given me so much over the years, and all your love and support has meant the world to me. To all my aunts, uncles, and cousins, you are the best family and I love and am so thankful for all of you.

I said finally, but I have to say a special thank you to my wife, Jennifer, and our dog, Poppy. Jennifer, you inspire me every day with your own tenacity and hard work. You make me a better person, you make my life richer, and you make every challenge more manageable. Behind everything I achieve is your love and support, and I am so excited to move onto the next chapter with you. To our dog, Poppy, thank you for always being there for a cuddle or nap after a hard day.

TABLE OF CONTENTS

CHAPTER 1

GENERAL INTRODUCTION (ADIPOSE TISSUE, LIPID METABOLISM, AND ADENOSINE RECEPTORS)

Adipose tissue is a major site of energy storage in the body, and an endocrine organ which plays an important role in regulating metabolism. The principal cell type of adipose tissue is the adipocyte, the hallmark of which is the uptake and generation of lipids, and their storage as triacylglycerol (TAG) within lipid droplets. Adipocytes are critical mediators of energy balance within the body through the storage of excess energy under fed, or anabolic, conditions and the subsequent release of those energy stores under fasted, or catabolic, conditions. The dysregulation of lipid metabolism within adipocytes can therefore have detrimental consequences for metabolism within the entire body. In this chapter, I will discuss the primary mechanisms which regulate adipocyte lipid metabolism as well as the general anatomy and physiology of the various adipose tissue depots. I will also discuss the effects of obesity on adipose tissue and its role in the development of insulin resistance. Finally, I will provide an overview on adenosine and the adenosine receptors, as well as the known role of adenosine receptors within adipose tissue.

Lipid metabolism in adipocytes

Lipid metabolism within adipocytes is primarily controlled through catecholaminergic action on β-adrenergic receptors driving lipolysis and insulin action on

the insulin receptor driving lipid uptake and esterification. During catabolic conditions, adipocyte lipolysis is the process by which TAGs stored within lipid droplets are broken down in a stepwise manner into their individual components of non-esterified fatty acids (NEFA) and glycerol. Under anabolic conditions, the reverse process occurs with the esterification of fatty-acyl chains onto a glycerol backbone to form TAGs for storage.

Both catecholamines and insulin have significant, and opposite, effects on lipolysis through influencing cyclic AMP (cAMP) levels in adipocytes (Fig 1.1). The β-adrenergic receptors are $G\alpha_s$-coupled receptors, and their activation stimulates adenylyl cyclase and the production and accumulation of cAMP. The increase in cAMP activates PKA, which results in the phosphorylation of perilipins and hormone sensitive lipase (HSL) [1]. The phosphorylation of perilipins induces the dissociation of the protein CGI-58 which is then able to bind and activate adipose triglyceride lipase (ATGL) [2]. ATGL catalyzes the first step in lipolysis by removing one of the fatty acyl chains to produce NEFA and diacylglycerol (DAG). Importantly, ATGL is the rate limiting enzyme in the process of lipolysis, and loss of this enzyme, such as in our adipocyte-specific ATGL knockout mice ($FATA^{-/-}$), severely limits the ability of adipocytes to undergo lipolysis [3,4]. The phosphorylation of HSL also activates this enzyme which primarily catalyzes the second step by removing a second fatty acyl chain to produce monoacylglycerol [5]. The removal of the final fatty acyl chain by MGL results in the final products of NEFA and glycerol which can be released into the circulation. Meanwhile, activation of the insulin receptor leads to the mobilization of Akt to cause the phosphorylation and activation of phosphodiesterase-3B (PDE-3B) [1]. This enzyme catalyzes the degradation of cAMP to

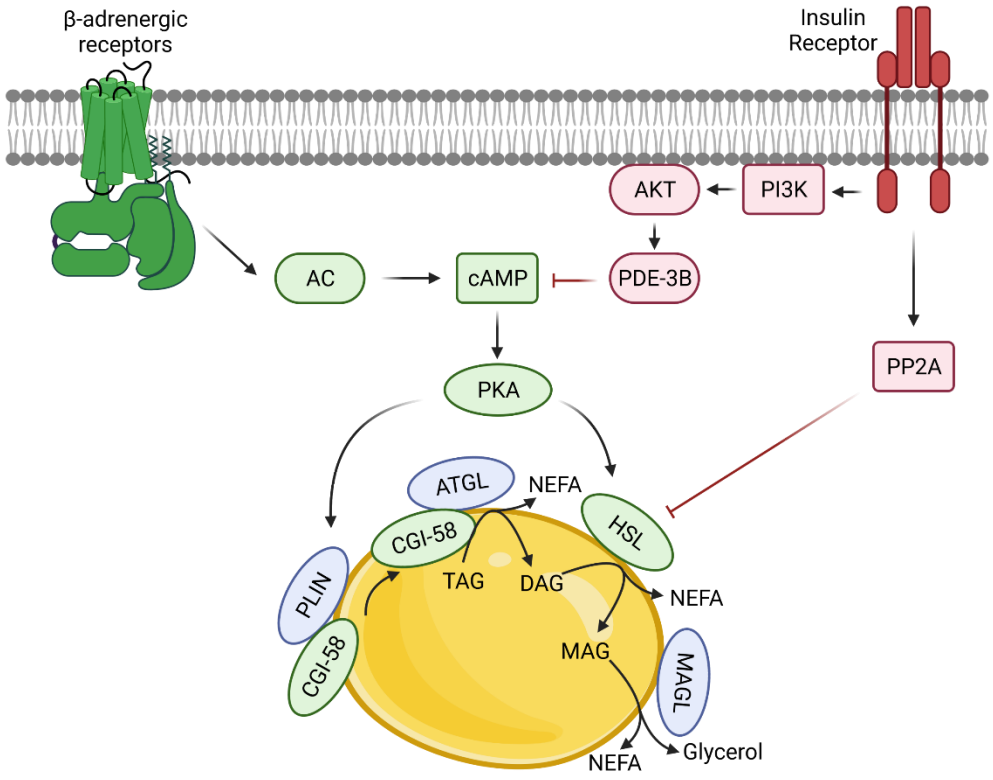

Figure 1.1: Regulation of lipolysis by catecholamines and insulin. Catecholamines act on β-adrenergic receptors in adipose tissue to activate lipolysis, while insulin acts on the insulin receptor to suppress lipolysis. Increased levels of cAMP downstream of β-adrenergic receptors activates PKA which phosphorylates perilipins and HSL. CGI-58 dissociates from perilipins and binds and activates ATGL while phosphorylation activates HSL. Insulin receptor activates PDE-3B downstream of Akt which degrades cAMP. Insulin receptor also activates PP2A which dephosphorylates HSL. Adenylyl cyclase (AC), protein kinase A (PKA), perilipin (PLIN), protein phosphatase-2A (PP2A).

counteract the effects of catabolic signals and reduce lipolysis. Insulin has also been reported to induce the dephosphorylation of HSL by activating protein phosphatase-2A, though the mechanisms underlying this response remain elusive [6]. Adipocyte lipolysis is the main source of circulating NEFA and glycerol, both of which can influence whole-body metabolism. It is therefore critical that we understand the factors that influence this catabolic process within adipocytes.

The signals which regulate esterification under anabolic conditions are significantly less well understood. Insulin increases the availability of substrates for TAG synthesis by activating lipoprotein lipase which breaks down circulating TAGs to supply NEFA, and by inducing glucose uptake through GLUT4 translocation which drives glyceroneogenesis in adipocytes [7]. Glucose is also used as a substrate for *de novo* lipogenesis, and elevated glucose activates the transcription factor ChREBP while insulin activates the transcription factor SREBP1 which target genes involved in lipogenesis and TAG storage [7,8]. The fatty acid transporters CD36 and FATP1 may also be involved in the stimulation of fatty acid uptake by insulin. It has long been established that catecholamines inhibit insulin signaling in adipocytes through the activation of β-adrenergic receptors [9,10]. Our lab has shown that the activation of lipolysis downstream of β-adrenergic receptors is required for this inhibition, and involves the dissociation of mTORC1 caused by oxidized fatty acids released during lipolysis, however many aspects of the mechanisms underlying this crosstalk remain unclear [11]. Because these processes are more difficult to investigate, in subsequent chapters we focus mostly on the regulatory processes and readouts related to adipocyte lipolysis.

Adipose tissue depots

There are three main types of adipose tissue within the body which have distinct roles, characteristics, and anatomical locations: subcutaneous, visceral, and brown adipose. Both subcutaneous and visceral adipose are known as white adipose tissue (WAT). These adipose depots are constituted mostly of white adipocytes, which store their TAGs within

a single, large, unilocular lipid droplet. Meanwhile, brown adipose tissue (BAT) consists mainly of brown adipocytes which store TAGs within multiple, smaller lipid droplets, have a high mitochondrial content giving them their distinctive brown coloration, and characteristically express the uncoupling protein UCP1.

Subcutaneous adipose tissue contains approximately 80% of all body fat present in lean, healthy individuals and serves as a buffer for excess energy intake through lipid storage [12]. During obesity, adipose depots expand either through hypertrophy of individual adipocytes or the increase in number of adipocytes known as hyperplasia. Excessive hypertrophy of adipocytes is associated with adipose tissue inflammation and insulin resistance, while the recruitment of preadipocytes and distribution of fat among increased adipocytes through hyperplasia is not [12]. Subcutaneous adipose tissue has a greater capacity for adipogenesis, and expansion of these depots has a much lower association with adipose tissue inflammation and insulin resistance, and may even be protective [13,14]. When the storage capacity of subcutaneous adipose tissue through hypertrophy is exceeded, excess energy is deposited in ectopic sites such as visceral adipose tissue, liver and skeletal muscle. It is this ectopic lipid deposition outside of subcutaneous adipose tissue that appears to lead to visceral adipose tissue inflammation, insulin resistance, fatty liver disease, and other features of metabolic syndrome [15].

Visceral and gonadal adipose tissue depots are located around internal organs within the intraperitoneal space. Visceral fat has a much lower capacity for hyperplasia, and thus expansion of these depots involves significantly more hypertrophy and is associated with inflammation and the development of insulin resistance and type 2 diabetes

in obese individuals [13,15]. Visceral adipose tissue also expresses higher levels of β-adrenergic receptors and exhibits a higher rate of lipolysis, or the breakdown of TAG stores, in response to adrenergic stimuli [13]. In addition, visceral adipose tissue is less sensitive to the antilipolytic effects of insulin relative to subcutaneous adipose tissue [16,17]. Critically, high levels of circulating NEFA are well known to induce insulin resistance [18].

BAT is known primarily for its high mitochondrial content, and ability to facilitate non-shivering thermogenesis through the uncoupling protein UCP1 [15]. Through oxidative phosphorylation, mitochondria produce an enormous proton gradient across the inner mitochondrial membrane which can be used to drive the production of ATP. UCP1 enables the shuttling of protons down this gradient across the inner mitochondrial membrane without the production of ATP resulting in the production of heat. In mice, the major site of BAT is located in the intrascapular region and is highly metabolically active. Differences in BAT metabolism can have drastic effects on whole-body metabolism. Increased metabolic activity of BAT can result in improved insulin sensitivity and glucose tolerance, resistance to high-fat diet-induced weight gain, and increased thermogenesis, while reduced metabolic activity can have opposite effects [19–21]. In humans, BAT depots were initially thought to only be present in neonates, however smaller depots have since been identified in adults which remain highly thermogenic and respond to cold and sympathetic activation [22]. The concept of beige adipocytes also describes white adipocytes identified in humans which display some characteristics of brown adipocytes, such as increased mitochondria and expression of UCP1 [15]. Still, the BAT depots found

in adult humans are significantly smaller than those found in mice and the physiological relevance of these depots in humans is still under investigation.

Obesity, adipose tissue, and insulin resistance

Rates of obesity have been rapidly rising for decades, and currently over 60% of the US population is considered either overweight or obese [12]. Obesity is associated with significant co-morbidities such as stroke, cardiovascular disease, and diabetes, and it is projected that by 2025 type 2 diabetes (T2D) will affect over 300 million people globally due to rising incidence of obesity [23,24]. Despite the significance of these pathologies, only a few therapeutic options exist to treat obesity, such as metformin, orlistat, and GLP-1 agonists, and the effects are very modest [25–27]. Understanding the underlying pathology by which obesity leads to these co-morbidities is therefore critical to treating these patients.

Obesity is associated with insulin resistance which leads to the development of T2D. Importantly, adipose tissue is one of the first tissues to become insulin resistant in obesity, and the induction of insulin resistance in adipose tissue alone using genetic manipulation leads to whole-body insulin resistance [28,29]. Obesity results in adipocytes which display impaired glucose uptake and elevated basal lipolysis [10,30]. Glucose uptake by adipose tissue is proportionally small compared with skeletal muscle and liver, and impaired glucose uptake in adipose tissue in itself is not believed to be a significant contributor to glucose intolerance in obesity [6]. However, increased circulating NEFA due

to elevated lipolysis is associated with insulin resistance in both obesity and T2D [18]. Further, the suppression of adipocyte lipolysis by insulin is a significant mechanism by which insulin reduces hepatic glucose production. Impaired suppression of lipolysis in insulin resistance can therefore lead to increased hepatic glucose production and hyperglycemia [31,32].

The expansion of visceral adipose tissue which is both more lipolytic and less responsive to insulin is one mechanism believed to contribute to increased rates of basal lipolysis and elevated circulating NEFA levels in obesity [15]. At the same time, adipocytes from obese individuals display a reduced maximal lipolytic response to adrenergic stimulation [6]. Thus, obese individuals are less able to modulate lipolysis and corresponding NEFA levels in response to changing nutrient conditions during fasting and feeding.

Adenosine, adenosine receptors, and adenosine signaling in adipose

Adenosine is a nucleoside which is believed to function as an extracellular signaling molecule in the body's response to stress conditions [33]. Elevations in extracellular adenosine can act to reduce imbalances between the supply and demand of energy, oxygen, and nutrients. In the hypoxic heart, for instance, adenosine will act to both reduce heart rate and increase coronary blood flow, thus reducing the energetic and oxygen demand by the heart and improving oxygen and nutrient delivery [34]. Due to the ubiquitous presence of equilibrative nucleoside transporters and the necessary maintenance of intracellular

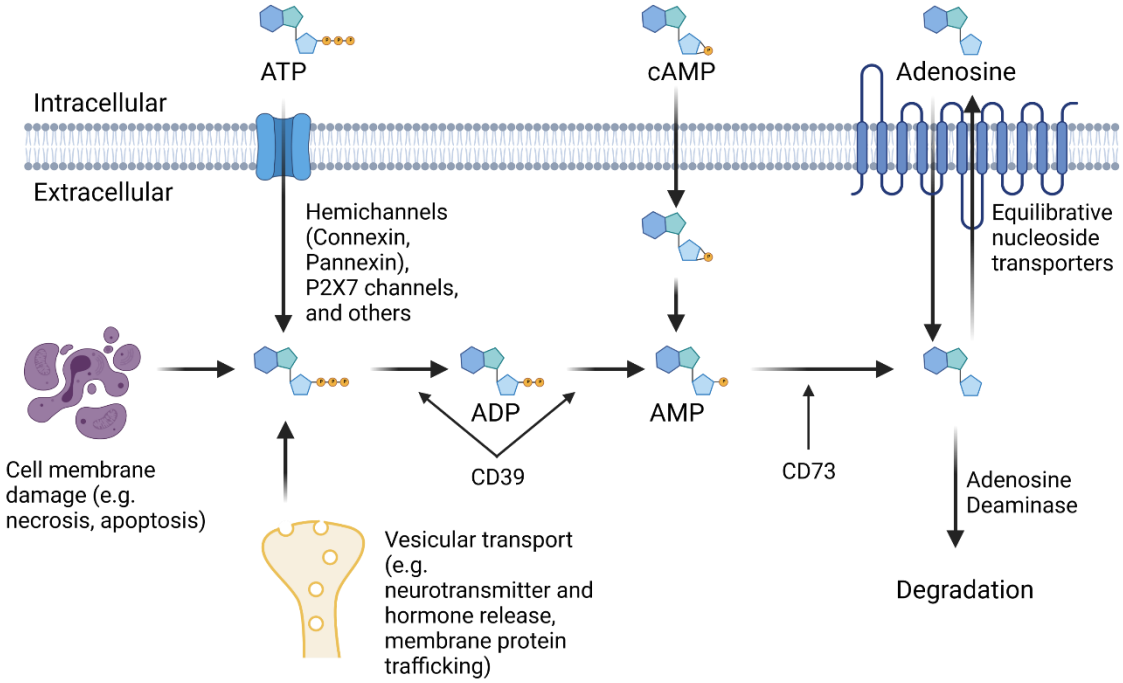

Figure 1.2: Sources of extracellular adenosine. Extracellular adenosine is always present due to the continuous maintenance of intracellular adenosine levels and the ubiquitous action of equilibrative nucleoside transporters. Elevations in intracellular adenosine will also elevate extracellular adenosine. Increases in intracellular AMP during energetic stress or as a result of cAMP degradation will also result in increased degradation of AMP and production of adenosine. Adenosine is also produced extracellularly through the degradation of ATP, cyclic AMP, and AMP by the actions of CD39, phosphodiesterases, and CD73 respectively. Extracellular ATP can be increased through release via channels (connexins, pannexins, P2X7) through vesicular transport such as neurotransmitter and hormone release, and during cell damage such as necrosis and apoptosis. Extracellular adenosine is rapidly degraded by adenosine deaminase.

adenosine levels for various metabolic pathways, extracellular adenosine is present even under basal conditions (Fig 1.2) [35]. The basal level of extracellular adenosine is estimated to be in the range of 30 – 200 nM and can vary depending on the tissue type. Extracellular adenosine levels are increased either when intracellular adenosine levels rise, or can be produced extracellularly through the degradation of other nucleosides such as ATP which occurs rapidly due to the presence of CD39 and CD73 [35,36]. Intracellular adenosine levels appear to rise primarily due to increased energetic demand, where a small percentage decrease in ATP levels can result in a large percentage increase in adenosine [36]. Elevated

cAMP levels may also contribute to rising adenosine levels through their degradation to AMP and adenosine intracellularly, or the export and subsequent degradation extracellularly [37]. Extracellular ATP levels can rise through several mechanisms, including damage to cell membranes such as in necrosis or apoptosis, release by channels such as pannexins, and protein transport vesicles [35]. ATP is also an important neurotransmitter that is co-released with noradrenaline by sympathetic neurons [38]. In all cases, adenosine levels are increased in response to clear stressors related to damage or a metabolic imbalance. Importantly, adenosine is rapidly degraded by extracellular adenosine deaminase and has a half-life of less than 2 seconds [39]. The extraordinarily high capacity of this system in endothelial cells ensures that circulating adenosine levels are virtually non-existent [35]. Adenosine is thus a highly localized signal with tissue specific effects, which when applied globally can appear contradictory.

Extracellular adenosine exerts its effects through four G-protein-coupled receptors: A_1, A_{2A}, A_{2B}, and A_3 [35]. The A_1 and A_3 receptors are coupled to $G\alpha_i$-proteins and act to suppress cAMP, while the A_{2A} and A_{2B} receptors couple to $G\alpha_s$-proteins and act to increase cAMP. A_{2B} also couples to $G\alpha_q$-proteins, and all of the adenosine receptors appear capable of activating phospholipase C through various mechanisms in a tissue-specific manner [40,41]. In addition, the A_1 and A_{2A} receptors display a high affinity for adenosine (10 nM and 30 nM respectively), while the affinity of A_{2B} and A_3 is significantly lower (1 µM and 100 nM) [42]. The deletion of all four of these receptors in mice is non-lethal, which suggested that adenosine mainly adapts the body to stress and is not necessary for maintaining homeostasis [43]. However, these mice displayed reduced lifespan which

implies that adenosine is important for responding to normal, everyday stressors, and the loss of this functionality is maladaptive.

Adenosine has been identified as a significant regulator of adipose tissue function. The main receptor involved in the regulation of mature white adipocytes is the A_1 receptor which counteracts the adrenergic stimulation of lipolysis, enhances insulin signaling, and promotes adipogenesis [44–46]. The A_{2A} receptor is involved in the activation of thermogenesis in BAT, where it is far more highly expressed compared with WAT [47]. Agonism of the A_{2A} receptor induces beiging in white adipocytes, however the high expression of A_1 receptors appears to block this effect by adenosine at physiological concentrations. The A_{2B} receptor has also been reported to activate thermogenesis in BAT, although its lower affinity for adenosine compared with A_{2A} and its role in supporting adenosine/A_{2A} signaling make it unclear how significant this effect is in the absence of exogenous agonism [48]. The A_{2B} receptor is also highly expressed in preadipocytes where it inhibits adipogenesis [44]. No clear role has been defined for the A_3 receptor in adipose tissue, despite its high expression in both white and brown adipocytes [47]. While both the A_1 and A_3 receptors are Gai-coupled and expressed in white adipocytes, the ablation of the A_1 receptors completely attenuates the antilipolytic activity of adenosine, perhaps due to the lower affinity of A_3 receptors for adenosine [49].

CHAPTER 2

LOSS OF A1 RECEPTOR IN ADIPOSE TISSUE

ABSTRACT

Adipose tissue is a critical regulator of energy balance, and alterations in adipose lipid metabolism in particular can influence peripheral insulin sensitivity and glucose production. Adenosine has been characterized as an important regulator of adipocyte lipid metabolism primarily through its actions on A_1 adenosine receptors (A1R). The actions of A1R have been well characterized in isolated adipocytes where it opposes catecholaminergic actions by suppressing cyclic AMP levels and inhibiting lipolysis, as well as augments insulin signaling to suppress lipolysis and drive esterification, glucose uptake, and lipogenesis. However, how A1R regulates adipose tissue and subsequent whole-body metabolism *in vivo* has been more difficult to ascertain, as global A1R knockout mice display several confounding phenotypes which appear unrelated to A1R signaling in adipose tissue. We sought to understand the role A1R plays in adipocytes to regulate lipid metabolism in response to both catabolic and anabolic stimuli *in vivo* by using an inducible, adiponectin-Cre with *Adora1* floxed mice (FAdora1$^{-/-}$), where F designates a fat-specific deletion. FAdora1$^{-/-}$ mice were overall metabolically normal, but had impairments in the suppression of lipolysis by insulin. On high-fat diet, male FAdora1$^{-/-}$ mice developed impaired glucose tolerance with no changes in insulin sensitivity. Male FAdora1$^{-/-}$ mice also exhibited a higher lipolytic response to isoproterenol and during a

cold tolerance test than WT controls. Meanwhile, female FAdora1-/- mice did not show any significant differences in lipid or glucose metabolism. Taken together, these data confirm a role for adipose A1R in limiting lipolysis during stress and augmenting insulin signaling to suppress lipolysis *in vivo*, though these actions appear to be dispensable in females.

INTRODUCTION

Adipose tissue serves as both a site for energy storage and an endocrine organ and can effect significant control over whole-body glucose and lipid metabolism [12]. During fasting, adipocytes undergo lipolysis to provide NEFA and glycerol for energy, while during feeding, adipocytes increase fatty acid and glucose uptake, as well as fatty acid esterification and *de novo* lipogenesis to facilitate adequate energy storage [6]. These processes are primarily regulated by catabolic hormones, such as catecholamines, driving lipolysis, and anabolic hormones, such as insulin, suppressing lipolysis and driving fatty acid uptake and esterification [50]. Defects in adipocyte function can result in impairments in whole-body insulin sensitivity and glucose tolerance [29,51]. Elevated levels of serum NEFA can also cause insulin resistance, and adipocyte lipolysis drives insulin resistance and hyperglycemia under acute stress conditions [52,53]. A deep knowledge of the signals which regulate adipocyte metabolism is therefore essential to our understanding of whole-body glucose and lipid metabolism and the disruptions which occur during pathological conditions such as obesity-induced insulin-resistance.

Adenosine is a nucleoside with a role in extracellular signaling that opposes catecholamine signaling and enhances insulin signaling in adipocytes [45]. Adenosine signals through four G protein-coupled receptors: A_1, A_{2A}, A_{2B}, and A_3 [35]. In adipocytes, adenosine has been found to act primarily through the $G\alpha_i$-coupled A1R [54]. Adenosine is typically regarded as a stress response signal, as interstitial levels of adenosine increase drastically in response to adrenergic stress in adipose as well as other tissues [34,55]. It is important to note, however, that adipose tissue maintains basal levels of adenosine that are

considered sufficient to provide tonic activation of A1R [46,56–59]. With this in mind, adenosine has been shown to regulate adipocytes in a few key contexts. Adenosine limits the lipolytic response of adipocytes to stress, as the degradation of adenosine with exogenous adenosine deaminase or inhibition with an A1R antagonist enhances the stimulation of adipocyte lipolysis by adrenergic signals such as norepinephrine or the β-adrenergic receptor agonist isoproterenol [46,58–60]. Additionally, adenosine signaling via A1R has been shown to augment insulin stimulated glucose uptake, lipogenesis, and suppression of lipolysis in adipocytes [61–63].

These roles for adenosine signaling in adipocytes have been well characterized in vitro, however, the effects of A1R signaling in adipocytes on whole-body metabolism have been more difficult to ascertain due to the broad expression of A1R across numerous tissues [64]. In both rats and humans, A1R agonism reduces serum NEFA, and yields improved insulin sensitivity in obese rats [65–67]. Further, reduced A1R expression in adipocytes due to obesity, hypertension, or prolonged pharmacological stimulation is associated with insulin resistance [54,68,69]. Despite this, mice with global A1R knock out display relatively normal systemic NEFA levels [49,70]. Global A1R knockout mice have also given conflicting results with glucose metabolism, where they have been shown to display impaired glucose tolerance [70], improved glucose tolerance [71], and no change to glucose tolerance [72]. However, these phenotypes were concomitant with significant confounding factors such as differences in body weight, food intake, insulin and glucagon secretion, and survival [43,49,70–72]. Dong and colleagues provided good evidence that adipose A1R improves glucose tolerance and insulin sensitivity by overexpressing A1R

using the aP2 promoter [73]. These mice did not display changes in body weight or insulin secretion; however, overexpression clearly enhanced the tonic activity of A1R resulting in suppression of basal lipolysis and reduced serum NEFA levels. It therefore remains unclear how endogenous adenosine and A1R regulate adipocyte metabolism *in vivo*, and whether endogenous A1R signaling in adipocytes impacts whole-body glucose and lipid metabolism.

To address this gap in knowledge, we generated for the first time an adipocyte-specific knockout of A1R and utilized a tamoxifen-inducible Cre system to eliminate any potential compensation that might arise during development. We sought to determine the impacts of A1R deletion in adipose on lipid and glucose metabolism in lean and obese mice, as well as the lipolytic response to stress. In this chapter, we find that adipose A1R augments insulin action to suppress lipolysis in the transition from the fasted to the fed state and limits the stimulation of lipolysis by adrenergic stimuli. We also find that the loss of adipose A1R leads to overt glucose intolerance in obese mice. These data agree with previous literature studying A1R action in isolated adipocytes and provide further evidence for the role of adipose A1R *in vivo* without the confounds of global deletion or overexpression.

RESULTS

Loss of A1R inhibition of lipolysis in adipocyte-specific A1R knockout mice

Several groups have previously evaluated the role of A1R in adipose tissue and fatty acid metabolism using mice with a global knockout of A1R, however these mice exhibit increased body weight and food intake [49,70], increased insulin and glucagon secretion [71,72], and decreased survival [43,74] which make it difficult to interpret the role of A1R specifically in adipose. To avoid these complications, we crossed mice with a tamoxifen-inducible Cre driven by the adiponectin promoter (Jax #025124) with an *Adora1*$^{loxP/loxP}$ strain [75] in which the terminal 3' exon of the *Adora1* gene, which encodes A1R, is flanked by loxP sites. Both Cre negative *Adora1*$^{loxP/loxP}$ control mice (WT) and Cre positive *Adora1*$^{loxP/loxP}$;AdipoQ-Cre-ERT2 knockout mice (FAdora1$^{-/-}$), where F indicates a fat-specific deletion, were treated with tamoxifen for 10 days at 8-weeks of age to induce knockout, followed by a 2-week washout period. Following tamoxifen treatment, FAdora1$^{-/-}$ mice exhibited an ~88% knockdown in A1R mRNA in isolated white adipocytes from gonadal fat pads and a ~95% knockdown in brown adipose tissue (Fig. 2.1 A,E). This resulted in an ~80% reduction in protein levels within isolated white adipocytes (Fig. 2.1 I). The FAdora1$^{-/-}$ mice did not display any compensatory changes in the other adenosine receptors A_{2A}, A_{2B}, or A_3 in white adipocytes (Fig. 2.1 B-D) or brown adipose tissue (Fig. 2.1 F-H). Meanwhile, A1R is also highly expressed in cardiac tissue and no reduction in A1R protein levels was observed within whole-heart lysates (Fig. 2.1 J) [34].

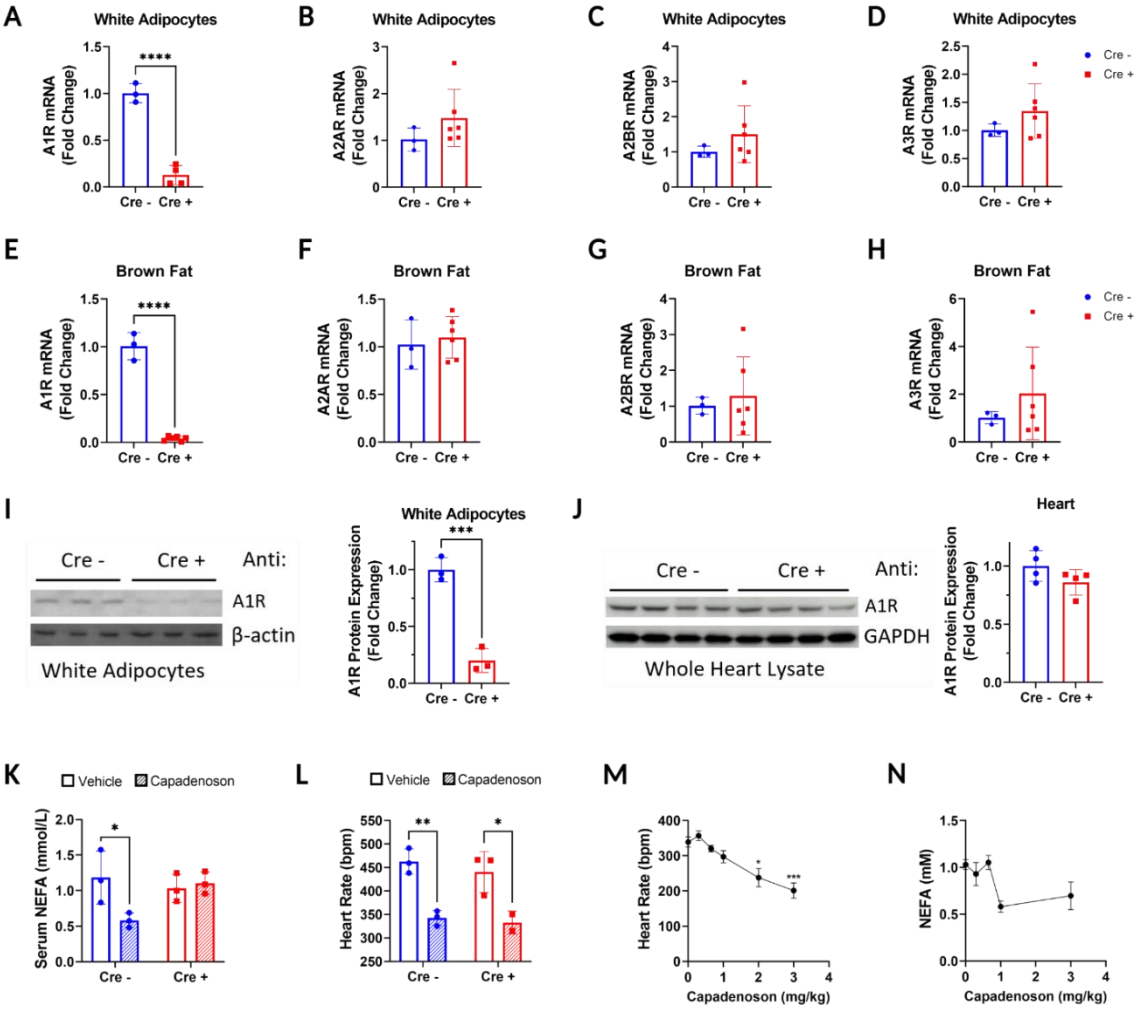

Figure 2.1: Tamoxifen induces a functional knockout of adipose A1R in FAdora1$^{-/-}$ mice. (A-D) mRNA levels in Cre negative WT (blue) and Cre positive FAdora1$^{-/-}$ mice (red) in isolated epididymal white adipocytes for A1 (A), A2A (B), A2B (C), and A3 (D) adenosine receptors. (E-H) mRNA levels in WT and FAdora1$^{-/-}$ mice in brown adipose tissue for A1 (E), A2A (F), A2B (G), and A3 (H) adenosine receptors. (I) Protein levels of A1R in isolated gonadal white adipocytes from WT and FAdora1$^{-/-}$ mice assessed and quantified by western blot normalized to β-actin loading control. (J) Protein levels of A1R in whole heart lysates from WT and FAdora1$^{-/-}$ mice assessed and quantified by western blot normalized to GAPDH loading control. (K and L) Serum NEFA levels (E) and heart rate (F) in WT and FAdora1$^{-/-}$ mice fasted overnight and treated for 2 hours with vehicle or 1 mg/kg capadenoson. (M and N) Heart rate (M) and serum NEFA levels (N) in WT and FAdora1$^{-/-}$ mice fasted overnight and treated for 2 hours with vehicle or indicated concentration of capadenoson. Error bars represent SD. *p<0.05, **p<0.01, ***p<0.001, ****p<0.0001, t-test or two-way ANOVA.

Agonism of A1R in adipocytes results in lower levels of NEFA within the blood stream [76]. Partial agonists of A1R such as capadenoson have previously been shown to reduce serum NEFA levels as well as cause modest reductions in heart rate through A1 receptors in the SA node [34,66]. We subjected WT and FAdora1$^{-/-}$ mice to an overnight fast and treated with either vehicle or capadenoson for 2 hours. Capadenoson significantly reduced serum NEFA in WT mice, but not FAdora1$^{-/-}$ mice (Fig. 2.1 K). Consistent with adipocyte-specific loss of A1R in our system, capadenoson treatment reduced heart rate in both WT and FAdora1$^{-/-}$ mice (Fig. 2.1 L).

Serum NEFA and heart rate display similar sensitivity to A1R agonism in mice

It has been previously reported in rats that partial agonists of A1R could suppress lipolysis without having significant effects on heart rate. Contrary to these reports, we were not able to separate these two effects. We administered increasing doses of capadenoson to overnight fasted WT mice and measured heart rate (Fig. 2.1 M) and serum NEFA (Fig. 2.1 N) 2 hours after administration. We found that capadenoson reduced heart rate at doses as low as 0.65 mg/kg. While the reduction in heart rate at 0.65 mg/kg was not statistically significant in this dose response experiment, subsequent experiments at this dose consistently produced a statistically significant reduction in heart rate (not shown). Meanwhile, capadenoson produced no detectable suppression of serum NEFA levels at doses below 1 mg/kg.

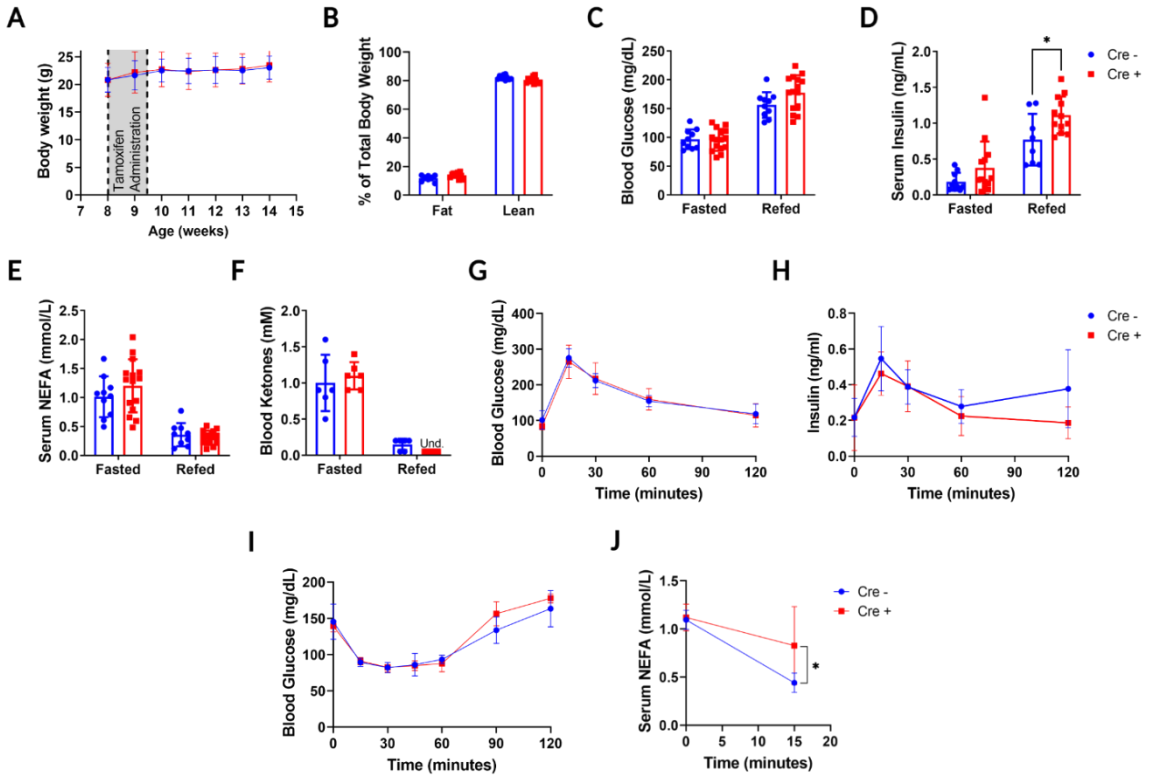

Figure 2.2: Induced loss of A1R in adipose impairs insulin suppression of lipolysis in male mice. (A) Body weight of male Cre negative WT (blue) and Cre positive FAdora1$^{-/-}$ mice (red) starting at the time of tamoxifen administration at 8 weeks. Gray box indicates timing of tamoxifen. (B) Fat and lean mass distribution in male WT and FAdora1$^{-/-}$ mice 6 weeks after the start of tamoxifen administration measured by EchoMRI. (C-F) Blood glucose (C), serum insulin (D), serum NEFA (E), and blood ketone (F) levels in male WT and FAdora1$^{-/-}$ mice after an overnight fast (fasted) and 4-hour refeeding period (refed). (G and H) Blood glucose (G) and serum insulin (H) in male WT and FAdora1$^{-/-}$ mice during an i.p. glucose tolerance test with 1 g/kg glucose. (I) Blood glucose in male WT and FAdora1$^{-/-}$ mice during an i.p. insulin tolerance test with 0.75 IU/kg insulin. (J) Serum NEFA in overnight fasted male WT and FAdora1$^{-/-}$ mice at 0 and 15 minutes after administration of 0.75 IU/kg insulin. Error bars represent SD. *p<0.05, t-test or two-way ANOVA.

Impaired insulin suppression of lipolysis in male FAdora1$^{-/-}$ mice

In contrast to global A1R knockout mice, FAdora1$^{-/-}$ male mice did not develop changes in body weight or fat and lean mass distribution following tamoxifen administration (Fig. 2.2 A,B). There were no differences between WT and FAdora1$^{-/-}$ male mice in blood glucose or serum insulin when fasted overnight, and only minor increases in glucose and insulin levels following a 4-hour refeeding period (Fig. 2.2 C,D). There were

also no differences in fasted or refed NEFA levels (Fig. 2.2 E), ketone levels (Fig. 2.2 F), glucose (Fig. 2.2 G) or insulin secretion (Fig. 2.2 H) during a glucose tolerance test (GTT), or insulin tolerance (Fig. 2.2 I). Overall, FAdora1$^{-/-}$ mice were relatively metabolically normal. However, when we treated fasted WT and FAdora1$^{-/-}$ male mice with insulin for 15 minutes, serum NEFA was significantly reduced in WT but not FAdora1$^{-/-}$ mice (Fig 2.2 J). This suggests that the loss of A1R in adipocytes impairs insulin action to suppress lipolysis. Throughout our characterization of the FAdora1$^{-/-}$ mice, female mice consistently lacked a distinct phenotype as compared with male mice. Female FAdora1$^{-/-}$ mice did not display significant differences in body weight (Fig. 2.3 A), body mass distribution (Fig. 2.3 B), fasting and refed values for glucose (Fig. 2.3 C), insulin (Fig. 2.3 D), NEFA (Fig. 2.3 E), and ketones (Fig. 2.3 F), glucose tolerance (Fig. 2.3 G), insulin secretion (Fig. 2.3 H), or insulin tolerance (Fig. 2.3 I). Female FAdora1-/- mice did display impairment in the suppression of lipolysis by insulin which reached statistical significance, however the difference was minor and likely does not represent a biologically significant difference (Fig. 2.3 J). In previously published studies, differences in body weight between WT and global A1R knockout mice were not apparent until approximately 5 months of age [49,70]. Both male and female FAdora1$^{-/-}$ mice continued to show no differences in body weight or body mass distribution ~7 months after tamoxifen injection (Fig. 2.4). It is worth noting, however, that the efficiency of A1R knockout in adipose tissue was not checked at this later time point.

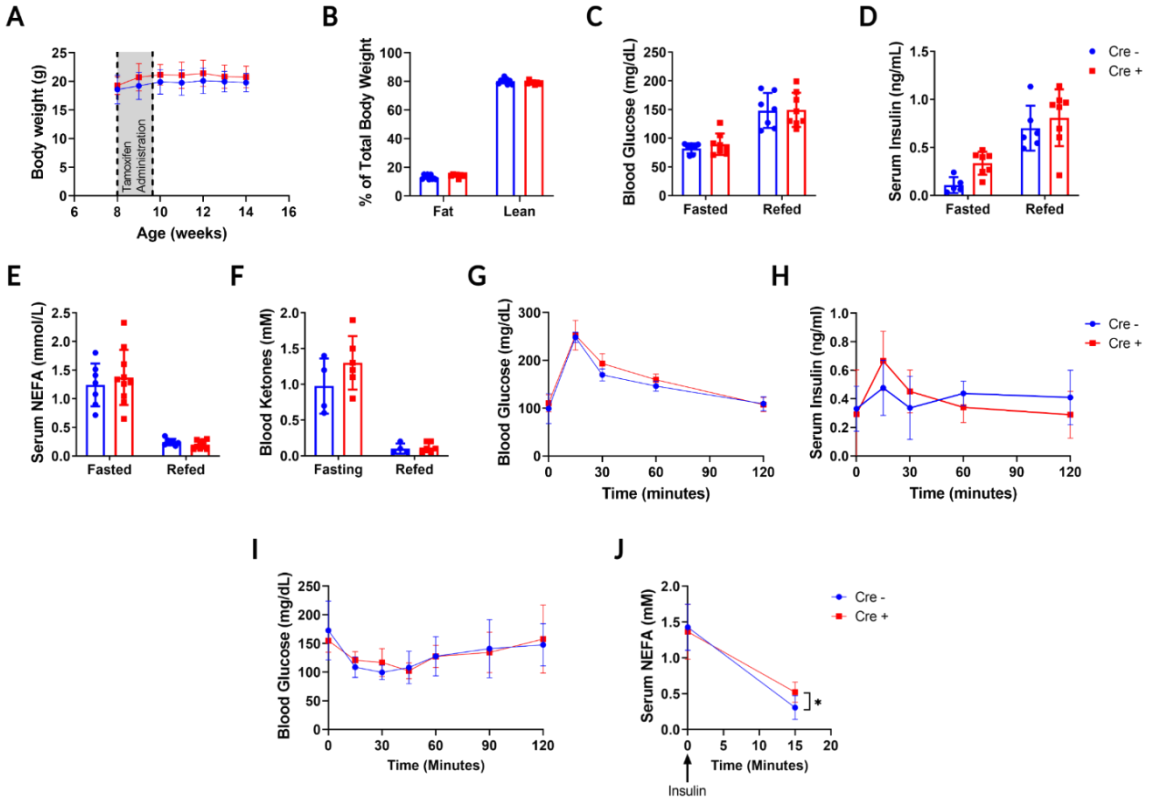

Figure 2.3: Female chow fed FAdora1$^{-/-}$ mice do not display alterations in basal metabolic parameters. (A) Body weight of female Cre negative WT (blue) and Cre positive FAdora1$^{-/-}$ mice (red) starting at the time of tamoxifen administration at 8 weeks. Gray box indicates timing of tamoxifen. (B) Fat and lean mass distribution in female WT and FAdora1$^{-/-}$ mice 6 weeks after the start of tamoxifen administration measured by EchoMRI. (C-F) Blood glucose (C), serum insulin (D), serum NEFA (E), and blood ketone (F) levels in female WT and FAdora1-/- mice after an overnight fast (fasted) and 4-hour refeeding period (refed). (G and H) Blood glucose (G) and serum insulin (H) in female WT and FAdora1$^{-/-}$ mice during an i.p. glucose tolerance test with 1 g/kg glucose. (I) Blood glucose in female WT and FAdora1$^{-/-}$ mice during an i.p. insulin tolerance test with 0.75 IU/kg insulin. (J) Serum NEFA in overnight fasted female WT and FAdora1$^{-/-}$ mice at 0 and 15 minutes after administration of 0.75 IU/kg insulin. Error bars represent SD. *p<0.05, t-test.

High fat diet results in overt glucose intolerance within male FAdora1$^{-/-}$ mice

To further explore the impacts of A1R knockout on adipose insulin sensitivity, we placed WT and FAdora1$^{-/-}$ mice on high fat diet (HFD) for 12 weeks. Tamoxifen was administered beginning after 7 weeks of HFD feeding to allow sufficient time for

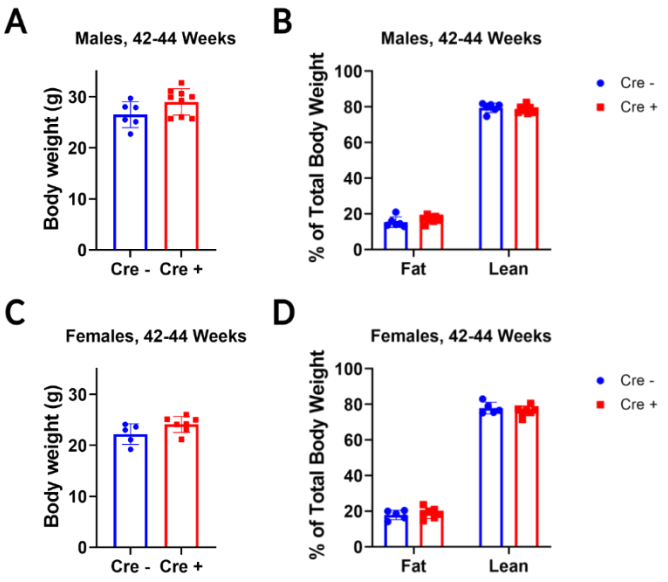

Figure 2.4: Inducible knockout of adipose A1R does not affect body weight or body mass distribution in aged mice. (A-D) Cre negative WT (blue) and Cre positive FAdora1$^{-/-}$ (red) mice were administered tamoxifen at 8 weeks of age. At approximately 42-44 weeks of age, body weight was measured for male (A) and female (C) mice, and body mass distribution was measured by EchoMRI for male (B) and female (D) mice.

tamoxifen washout and recovery. While tamoxifen had a clear secondary impact on weight gain, there were no differences between WT and FAdora1$^{-/-}$ male mice in body weight or body mass distribution (Fig. 2.5 A,B). In addition, FAdora1$^{-/-}$ male mice did not have any differences in activity or respiratory exchange ratio (Fig. 2.5 C,D). There also continued to be no differences in fasting or refed glucose (Fig. 2.5 E), insulin (Fig. 2.5 F), and NEFA levels (Fig. 2.5 G). However, while there were also no differences in insulin tolerance (Fig. 2.5 H), male FAdora1$^{-/-}$ mice on HFD displayed clear glucose intolerance during an i.p. GTT with no change in insulin secretion (Fig. 2.5 I,J). To explain the differences in glucose tolerance, we attempted to assess endogenous glucose production using a pyruvate tolerance test and observed no differences (not shown). However, it has been previously

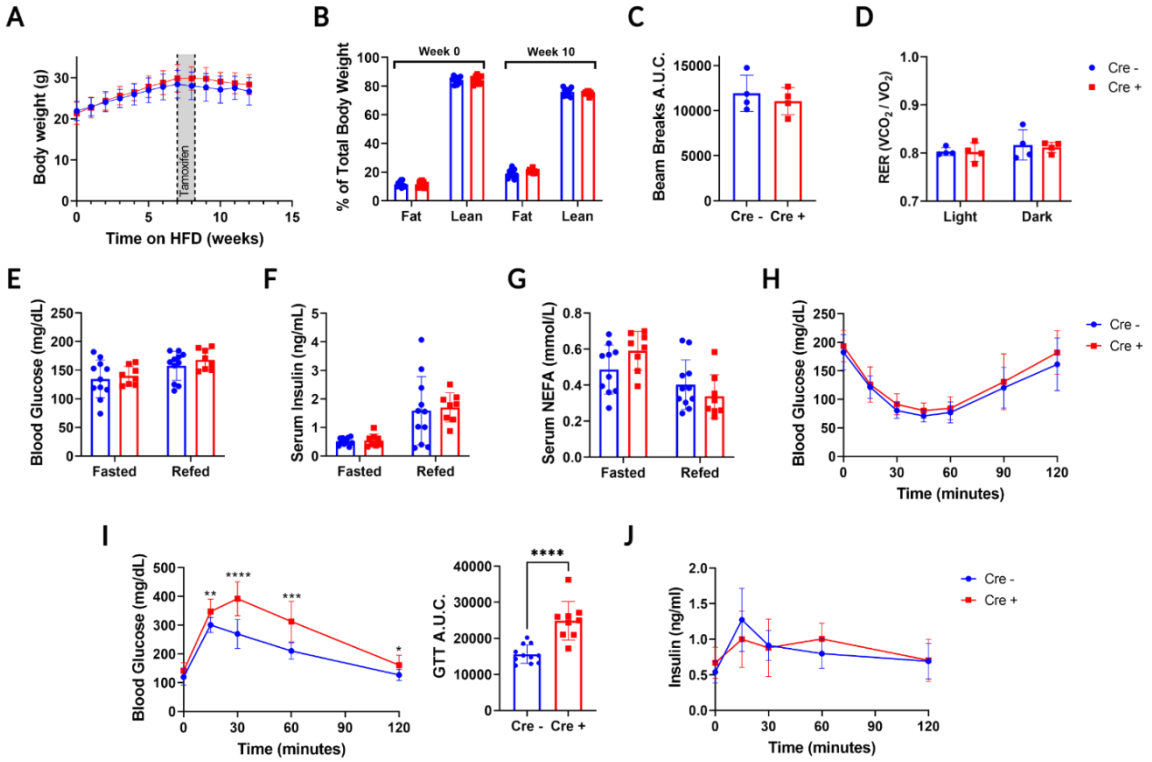

Figure 2.5: FAdora1$^{-/-}$ mice are more susceptible to high-fat diet-induced glucose intolerance. (A) Body weight of male Cre negative WT (blue) and Cre positive FAdora1$^{-/-}$ mice (red) starting at the beginning of high-fat diet feeding at 8 weeks. Gray box indicates timing of tamoxifen administration. (B) Fat and lean mass distribution in male WT and FAdora1$^{-/-}$ mice before and after 10 weeks of high-fat diet feeding measured by EchoMRI. (C-J) Data were collected for male WT and FAdora1$^{-/-}$ mice after 12-15 weeks of high-fat diet feeding. (C) Ambulatory activity for one full day/night cycle measured as area under the curve for total x-axis beam breaks in metabolic cages. (D) Respiratory exchange ratio (RER) in one full light and dark cycle. (E-G) Blood glucose (E), serum insulin (F), and serum NEFA (G) following an overnight fast (fasted) and 4-hour feeding period (refed). (H) Blood glucose during an i.p. insulin tolerance test with 0.75 IU/kg insulin. (I,J) Blood glucose and area under the curve (I), and serum insulin (J) during an i.p. glucose tolerance test with 1 g/kg glucose. Error bars represent SD. ****p<0.0001, t-test.

published that pyruvate administration induces torpor in obese, but not lean, mice [77]. Indeed, all of our HFD mice treated with pyruvate exhibited symptoms of torpor which is a significant confounding factor when using a pyruvate tolerance test as a readout for endogenous glucose production. There continued to be no significant differences in metabolic parameters between WT and FAdora1$^{-/-}$ among HFD fed female mice (Fig. 2.6).

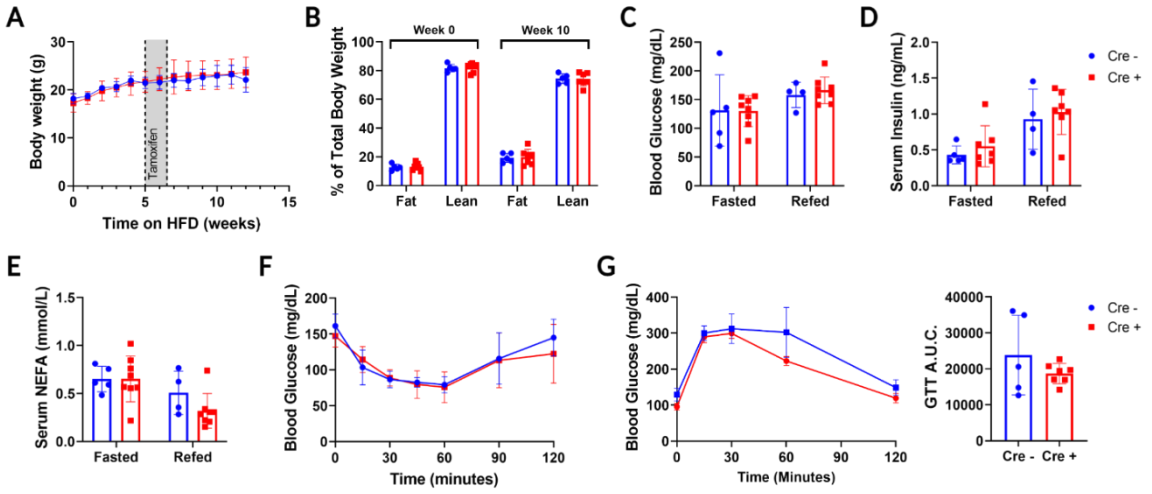

Figure 2.6: Female high-fat diet fed Fadora1$^{-/-}$ mice are not different from WT mice in basal metabolic parameters. (A) Body weight of female Cre negative WT (blue) and Cre positive FAdora1$^{-/-}$ mice (red) starting at the beginning of high-fat diet feeding at 8 weeks. Gray box indicates timing of tamoxifen administration. (B) Fat and lean mass distribution in female WT and FAdora1$^{-/-}$ mice before and after 10 weeks of high-fat diet feeding measured by EchoMRI. (C-G) Data were collected for female WT and FAdora1$^{-/-}$ mice after 12-15 weeks of high-fat diet feeding. (C-E) Blood glucose (C), serum insulin (D), and serum NEFA (E) following an overnight fast (fasted) and 4-hour feeding period (refed). (F) Blood glucose during an i.p. insulin tolerance test with 0.75 IU/kg insulin. (G) Blood glucose and area under the curve during an i.p. glucose tolerance test with 1 g/kg glucose. Error bars represent SD.

A1R limits the lipolytic response to adrenergic stress

Adenosine levels are known to rise during stress, and adenosine signaling provides numerous protective benefits during stress responses [34,55,78]. Stress-induced adrenergic stimulation activates lipolysis within adipose tissue, and exposure to high levels of NEFA during stress is associated with insulin resistance and lipotoxicity [52,53]. We hypothesized that adenosine provides a protective limit on lipolysis in adipose tissue and that the loss of adipose A1R would result in a stronger lipolytic response to adrenergic stimulation and higher serum NEFA levels. To test this, we subjected male WT and FAdora1$^{-/-}$ mice to an isoproterenol tolerance test. After a short 6-hour fast to normalize serum NEFA levels, we administered 10 mg/kg isoproterenol by i.p. injection to stimulate adipocyte lipolysis. In

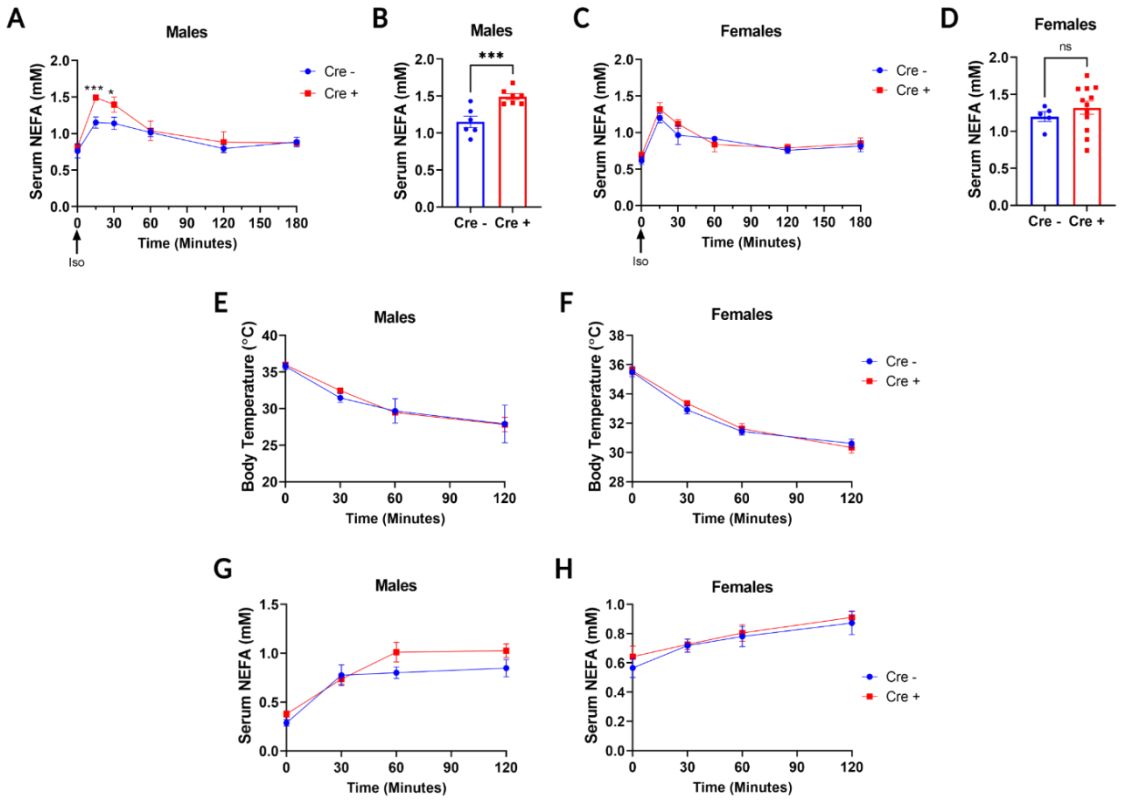

Figure 2.7: Male, but not female, FAdora1$^{-/-}$ mice are more lipolytically responsive. (A,B) Serum NEFA in 6-hour fasted male Cre negative WT (blue) and Cre positive FAdora1$^{-/-}$ (red) mice at the indicated time points after i.p. injection of 10 mg/kg isoproterenol (A) or at 15 minutes after injection with isoproterenol (B). (C,D) Same as in (A,B) for female mice. (E-H) Cold tolerance test for WT and FAdora1$^{-/-}$ mice fasted for 4-6 hours and placed at 4C. Body temperature for male (E) and female (F) mice starting immediately prior to beginning of cold exposure. Serum NEFA for male (G) and female (H) mice starting immediately prior to beginning of cold exposure. Error bars represent SD. *p<0.05, ***p<0.001, t-test.

WT mice, this dose of isoproterenol induces a modest and rapid increase in serum NEFA levels that returns to baseline levels within 2 hours (Fig. 2.7 A). As we expected, treatment of male FAdora1$^{-/-}$ mice with isoproterenol resulted in a stronger stimulation of lipolysis achieving significantly higher NEFA levels, but also returning to baseline within 2 hours (Fig. 2.7 A). The lipolytic response peaked 15 minutes after isoproterenol stimulation, which is not surprising considering the rapid induction of lipolysis and short half-life (~2

min) of isoproterenol (Fig. 2.7 B). We also subjected female WT and FAdora1$^{-/-}$ mice to an isoproterenol tolerance test and saw no differences in the lipolytic response (Fig 2.7 C,D).

Isoproterenol is an effective way to activate lipolysis through stimulation of β-adrenergic receptors, however it does not represent the physiological pathways activated during stress. Importantly, ATP is co-released with norepinephrine from sympathetic neurons and is rapidly degraded, contributing to the elevated adenosine levels seen during stress [38]. We therefore subjected WT and FAdora1$^{-/-}$ mice to a cold tolerance test to increase sympathetic tone under more physiological conditions. We fasted WT and FAdora1$^{-/-}$ mice for 4-6 hours, placed them at 4°C, and monitored their body temperature and serum NEFA levels. Cold exposure reduced body temperature similarly for WT and FAdora1$^{-/-}$ mice in both males and females (Fig. 2.7 E,F). However, after 1 hour of cold exposure, male FAdora1$^{-/-}$ mice experienced consistently higher elevations in serum NEFA when compared with WT mice (Fig. 2.7 G). Meanwhile, female FAdora1$^{-/-}$ mice displayed no differences in serum NEFA levels (Fig. 2.7 H).

DISCUSSION

In this chapter, we investigated the role of the A_1 adenosine receptor in adipose tissue in the regulation of lipid and glucose metabolism. Our findings agree with previous studies in isolated adipocytes and show that A1R augments insulin suppression of lipolysis and limits the lipolytic response to adrenergic stress *in vivo*. Further, this study agrees with findings from mice with A1R overexpression using the aP2 promoter [73], and demonstrates that A1R action in adipose tissue serves to protect mice from obesity-induced glucose intolerance.

The role of A1R in adipocytes *in vitro* has been well characterized by many groups who have demonstrated that adenosine enhances insulin-stimulated glucose uptake and lipogenesis and suppresses basal and stimulated lipolysis within adipocytes [57,59,61–63,79]. Investigating the role of adipose A1R *in vivo*, however, has been challenging as A1R is also involved in the regulation of numerous other tissues such as the brain, heart, skeletal muscle, and pancreatic islet cells. As previously mentioned, this has led to conflicting reports on the impact of global A1R knockout on glucose metabolism[70–72] Because all three groups saw changes in body weight and the secretion of glucagon and insulin, the role of adipose tissue A1R in these contexts has remained unclear. In agreement with previous studies on mice overexpressing A1R in adipose tissue, we now show that endogenous A1R in adipose also promotes glucose tolerance and insulin sensitivity [73]. Our studies show that mice with an inducible, adipocyte-specific knockout of A1R are similarly devoid of the changes in body weight and insulin and glucagon secretion, while also lacking any changes to basal fasted and fed serum NEFA levels. Instead, we saw that

loss of adipose A1R impairs the kinetics of insulin-mediated suppression of lipolysis rather than the final homeostatic set points. FAdora1$^{-/-}$ mice also developed glucose intolerance when placed on HFD, without changes to insulin secretion or sensitivity. The suppression of hepatic glucose production by insulin has been shown to be dependent on the appropriate suppression of adipocyte lipolysis [31,32]. Therefore, it is likely this glucose intolerance is driven by increased endogenous glucose production within FAdora1$^{-/-}$ mice, consistent with their impaired ability to reduce serum NEFA in response to insulin. It is worth noting that while we did not see increased insulin secretion during an i.p. glucose tolerance test, chow fed FAdora1$^{-/-}$ male mice did display significantly increased insulin levels under refed conditions. It is also possible that this increase in insulin is able to account for a reduced suppression of NEFA and maintain glucose tolerance under chow conditions. Following HFD feeding however, refed insulin levels are higher in both WT and FAdora1$^{-/-}$ male mice relative to chow conditions, but not different from each other. After HFD, it is possible that FAdora1-/- mice cannot further increase insulin secretion to compensate for the loss of adipose A1R resulting in glucose intolerance.

Acute stress results in a 10-100-fold increase in adenosine levels, and adenosine action on adipose A1R suppresses the stimulation of lipolysis by catecholamines [46,55,79]. High circulating NEFA levels during acute stress responses can have detrimental effects such as lipotoxicity and insulin resistance [53,80]. That FAdora1$^{-/-}$ mice exhibited a significantly stronger lipolytic response to adrenergic stimulation therefore suggests that A1R serves an important protective role to limit lipolysis during stress.

Finally, it remains unclear why female FAdora1-/- mice did not display any significant phenotypes. Gender-specific differences related to adipose A1R have not been previously reported, though the vast majority of studies have used only males. Publicly available tissue expression databases do not suggest any differences in adipose A1R expression exist between male and female mice. In addition, data from mixed male/female cohorts does not suggest any differences in the effectiveness of our inducible knockout approach between males and females. Regardless, we are currently working to perform a more in-depth comparison between males and females in terms of A1R expression and effectiveness of tamoxifen-induced knockout.

METHODS

Materials

All pharmacological compounds were obtained from Cayman Chemical (Ann Arbor, MI) unless otherwise stated. Capadenoson was obtained from MedChemExpress (Monmouth Junction, NJ). Peanut oil was obtained from Sigma-Aldrich (St. Louis, MO). Regular human insulin (Humulin R) was obtained from Eli Lilly (Indianapolis, IN). Adora1 antibody (PA1-041a) was obtained from ThermoFisher (Waltham, MA). β-actin antibody (A2228) was obtained from Sigma-Aldrich (St. Louis, MO). GAPDH (5174) antibody was obtained from Cell Signaling (Danvers, MA).

Animals

All animals were bred and maintained in accordance with the University of Virginia Animal Care and Use Committee regulations and the study was approved by the ACUC ethics committee. 12- to 16-week-old male and female mice were used for studies unless otherwise indicated. *Adora1*$^{loxP/loxP}$ mice were generously shared with us by Dr. Stanislav Zakharenko [75]. AdipoQ-cre-ERT2 (C57BL/6-Tg(Adipoq-cre/ERT2)1Soff/J, Jax #025124) mice were from the Jackson Laboratory. Inducible, fat-specific *Adora1* knockout mice were generated by crossing *Adora1*$^{loxP/loxP}$ with AdipoQ-Cre-ERT2 mice resulting in wildtype *Adora1*$^{loxP/loxP}$ (WT) mice and knockout *Adora1*$^{loxP/loxP}$;AdipoQ-Cre-ERT2 (FAdora1$^{-/-}$) littermates on a mixed C57BL/6J and C57BL/6N background. In FAdora1$^{-/-}$ mice, knockout was induced at 8-weeks by daily injection of tamoxifen (50 mg/kg) dissolved in peanut oil for 10 days, followed by a 14-day washout period prior to

experimentation. Cre-negative wild-type control mice were age and sex-matched littermates that received the same tamoxifen treatment protocol. For high-fat diet (HFD) studies in WT and FAdora1$^{-/-}$ mice, animals were placed on diet for 12 weeks starting at 8 weeks of age (BioServ, F1850). Tamoxifen injections were begun after 7 weeks of HFD.

General animal measurements

Body weight was measured in *ad lib* fed mice once weekly at the same time of day for both normal chow and HFD mice. Fat and lean mass distribution were determined in *ad lib* fed mice using Echo-MRI at the same time of day as body weights were collected. For fasted and refed measurements, mice were either fasted overnight (fasted) or then given access to chow and softened food for 4 hours (refed) as indicated. Under each condition, blood was collected from the tail vein and serum prepared for further analysis of NEFA or insulin concentrations. Blood glucose and ketone levels were measured using a One-touch Ultra glucometer and a Nova Max Plus ketone meter respectively. Ambulatory activity, carbon dioxide production (VCO_2), and oxygen consumption (VO_2) were measured using an Oxymax metabolic chamber system (Comprehensive Laboratory Animal Monitoring System) from Columbus Instruments (Columbus, OH). One full day and night was allowed for acclimation. For tissue harvesting, mice were euthanized by cervical dislocation, and tissues were flash frozen in liquid nitrogen.

Capadenoson effects on heart rate and lipolysis

To measure the effects of capadenoson on heart rate and lipolysis within WT and FAdora1-/- mice, we fasted mice overnight for approximately 16 hours. Capadenoson solution was made up in 0.9% saline. Capadenoson or vehicle was then administered via i.p. injection at a dose of 1 mg/kg. After 2 hours, blood was collected from the tail vein and serum was prepared and frozen at -80°C for further analysis of NEFA concentrations. Mice were then anesthetized with 2% isoflurane and heart rate was measured by echocardiogram. To assess the dose-responsive effects of capadenoson on heart rate and NEFA, the same overnight fasting and 2-hour administration procedure was used with WT mice that were administered either vehicle or the indicated dose of capadenoson.

Glucose tolerance test

Mice were fasted overnight, and baseline (time 0) blood glucose was measured, and serum prepared for further analysis of serum insulin concentrations. Mice were then administered 1 g/kg glucose via i.p. injection with a 20% glucose solution. At each indicated time point after glucose injection, blood glucose was measured, and serum was prepared for analysis of serum insulin levels.

Insulin tolerance test

Baseline (time 0) blood glucose was measured for a*d lib* fed mice immediately prior to the administration of 0.75 IU/kg human insulin (Humulin) via i.p. injection. Blood glucose was measured at each of the indicated time points following insulin administration.

Insulin suppression of NEFA

To measure the suppression of lipolysis by insulin, mice were fasted overnight and administered human insulin (Humulin) via i.p. injection (0.75 IU/kg). Serum was collected at 0 and 15 minutes after insulin administration. Mice were monitored for an additional 1 hour for hypoglycemia and administered glucose via i.p. injection as needed.

Isoproterenol tolerance test

WT and FAdora1-/- mice were fasted for 6 hours, and serum was prepared to measure basal (time 0) NEFA levels. Mice were then administered with 10 mg/kg isoproterenol via i.p. injection. Serum was prepared at the indicated time points for further analysis of NEFA concentrations. Isoproterenol was always prepared fresh as a 2 mg/mL solution in 0.9% saline.

Cold tolerance test

WT and FAdora1-/- mice were fasted for 6 hours, serum was prepared to measure basal (time 0) NEFA levels, and body temperature was measured using a rectal probe. Mice were then housed individually in chip bedding cages without food and placed without a lid at 4°C. Serum was collected and body temperature measured at the indicated time points following the initial housing at 4°C. Following the final time point, mice were placed back in their original cages under a heat lamp and monitored for 1 hour.

Measurement of serum NEFA and insulin

NEFA levels were measured in serum samples using the HR series NEFA-HR(2) Kit (Wako Diagnostics) according to the manufacturer's protocol. Insulin levels were measured in serum samples using the Ultra-Sensitive Mouse Insulin ELISA Kit (Crystal Chem) according to the manufacturer's protocol for the wide-range assay.

Adipocyte isolation

Adipocytes were isolated as previously described [11,29]. Epididymal fat pads were minced in low phosphate buffer (145 mmol/L NaCl, 5.4 mmol/L KCl, 1.4 mmol/L $CaCl_2$, 1.4 mmol/L $MgSO_4$, 0.2 mmol/L NaH_2PO_4, 5 mmol/L glucose, 10 mmol/L HEPES, pH 7.4) containing 2.5% bovine serum albumin (BSA, Sigma-Aldrich, St. Louis, MO), 3 mg/mL collagenase type I (Worthington, Lakewood, NJ), and 100 nmol/L adenosine, and

digested for 45 minutes in a 37°C water bath with mild agitation. For protein and RNA extraction, adipocytes were washed twice with buffer containing 0.1% BSA, and once with buffer without BSA.

RNA extraction and real-time qPCR

Total RNA was isolated using the PureLink RNA Mini Kit (Invitrogen) according to the manufacturer's protocol. White adipocytes were lysed with the provided lysis buffer. For brown adipose tissue, RNA was first extracted using Trizol Reagent (Invitrogen). The aqueous fraction from the trizol extraction was diluted 1:2 with 70% ethanol and loaded onto the PureLink RNA isolation columns. cDNA was synthesized from 500 ng RNA with the High-Capacity RNA-to-cDNA Synthesis Kit (Applied Biosystems). Real-time qPCR was performed with the iQ SYBR Green Supermix (Bio-Rad) in duplicate and analyzed with a CFX96 Real-Time PCR Detection System (Bio-Rad). Data were normalized to *Ppia* cDNA using the delta-delta-Ct method. Primers for *Adora2A*, *Adora2B*, and *Adora3* were sourced from the PrimerBank of the Center for Computational and Integrative Biology of Massachusetts General Hospital and Harvard University [81–83]. Primers targeting the 3' terminal exon for *Adora1* (exon 3) were designed using Primer3, and were used to determine the efficiency of the tamoxifen-induced knockout in FAdora1$^{-/-}$ mice [84,85].

Target	Forward Primer	Reverse Primer
Ppia	CGATGACGAGCCCTTGG	TCTGCTGTCTTTGGAACTTTGTC
Adora1 (exon 3)	ACTTCTTCGTCTGGGTGCTG	TCCCGTAGTACTTCTGGGGG
Adora2A	GCCATCCCATTCGCCATCA	GCAATAGCCAAGAGGCTGAAGA
Adora2B	AGCTAGAGACGCAAGACGC	GTGGGGGTCTGTAATGCACT
Adora3	AAGGTGAAATCAGGTGTTGAGC	AGGCAATAATGTTGCACGAGT

Sample preparation for western blots

Adipocytes were lysed with cell lysis buffer (10 mmol/L Na_2HPO_4, 50 mmol/L β-glycerophosphate disodium salt hydrate, 50 mmol/L NaF, 1 mmol/L EDTA, 1 mmol/L EGTA, pH 7.4) supplemented with protease inhibitors and 0.5 mmol/L dithiothreitol, homogenized by shearing through a 22G needle, and cleared by centrifugation at 17,000 x *g* for 10 minutes at 4°C. Tissues were homogenized by Potter-Elvehjem tissue grinder in Tissue Protein Extraction Reagent (ThermoFisher) supplemented with protease inhibitors and 0.5 mmol/L dithiothreitol and cleared by centrifugation at 17,000 x *g* for 10 minutes at 4°C. Protein concentrations were determined using BCA assay (Pierce).

Western blot and quantitative analysis

Equal amounts of proteins were separated by SDS-PAGE and transferred to PVDF. Membranes were blocked with 10% dry milk in TBST, and western blotting was carried

out with appropriate primary and secondary antibodies. Blots were imaged by detecting horseradish peroxidase conjugated chemiluminescence on an Amersham ImageQuant 800. For assessing differences in protein signal, membranes were stripped and reprobed with β-actin, or GAPDH loading controls as appropriate and as indicated. Blots were quantified using densitometry with ImageQuant software.

CHAPTER 3

REGULATION OF A_1 AND A_{2B} ADENOSINE RECEPTORS IN ADIPOSE BY FEEDING

ABSTRACT

Adenosine is believed to act primarily through A1R in adipose tissue to augment insulin action and suppress lipolysis. The A_{2B} adenosine receptor (A2BR) meanwhile is reported to have low expression in adipose tissue. However, A2BR is known to be highly regulated through transcriptional mechanisms, and data from the lab of Dr. Joel Linden indicated that serum can strongly induce A2BR expression in cultured adipocytes and that A2BR contributes to glucose intolerance in obesity. While A1R has a much higher affinity for adenosine, the adenosine response in a given tissue is determined by both the affinities and expression profiles of the four adenosine receptors. We investigated the regulation of both A1R and A2BR in adipose tissue under fasted and fed conditions and found that the expression profile of A1R and A2BR is rapidly switched by feeding. Insulin suppresses A1R expression in adipocytes by suppressing FOXO1 which binds to the *Adora1* promoter. Meanwhile, an undetermined factor in serum drives A2BR expression through activation of the NF-κB pathway. This regulation led to a desensitization of adipocytes to signaling through A1R and increased sensitivity to signaling through A2BR in the fed condition. Obesity also drives reduced A1R expression and increased A2BR expression, and disrupts this feeding-induced regulatory mechanism. These data provide new insights into the

regulation of adipose tissue lipid metabolism by adenosine and suggest that the dysregulation of these pathways may contribute to obesity-induced insulin resistance.

INTRODUCTION

As previously discussed, adenosine can signal through four G protein-coupled receptors: A_1 and A_3 which are $G\alpha_i$-coupled, and A_{2A} and A_{2B} which are $G\alpha_s$-coupled. The resulting downstream signal from adenosine in a given tissue is therefore a consequence of both the expression profile and affinity of these receptors. In white adipocytes, adenosine has been primarily characterized as signaling through A1R which causes a significant suppression of lipolysis. Indeed, in chapter 2 we demonstrated that the loss of A1R specifically in adipocytes leads to impaired suppression of lipolysis by insulin and a stronger lipolytic response to adrenergic stimuli. However, most metabolic studies, including the relevant data presented in chapter 2, are performed in fasted animals in order to reduce error introduced by varied feeding times. In communication with our collaborator, Dr. Joel Linden, we learned that the expression profiles of adenosine receptors in adipose tissue may shift between fasted and fed conditions, potentially altering the downstream signaling effects of adenosine.

Similar to A1R, discerning the role of A2BR in metabolism is difficult because it is expressed in numerous tissues, particularly immune cells, endothelial cells, epithelial cells, myocardial cells, and hepatocytes [86,87]. In young and lean mice, global A2BR knockout improves insulin sensitivity and glucose tolerance, while acute A2BR agonism drives hepatic glucose production and glucose intolerance [88–91]. A2BR antagonism also improves glucose uptake in KKA^Y diabetic mice [90]. On the other hand, global A2BR knockout worsens insulin sensitivity, glucose tolerance, and liver lipid metabolism in aged and HFD-fed mice, while chronic agonism of A2BR improves metabolic phenotypes in

HFD mice [89,92,93]. The improvements in metabolism with chronic A2BR agonism in these studies were attributed to reduced SREBP-1c activation in the liver and alternative activation of macrophages to reduce inflammation in adipose tissue [88,89,92,93]. All of these studies, however, reported significantly increased bodyweight and fat mass in global A2BR knockout mice, which is a significant contributor to metabolic syndrome. Historically A2BR has not been strongly associated with adipocytes, however recent evidence points to a role for A2BR in regulating adipocyte metabolism. Alexander Pfeifer's lab reported that A2BR drives thermogenic activation of brown adipocytes and increased energy expenditure, and thus the loss of brown adipose A2BR would be expected to contribute to increased body weight and fat accumulation [48]. In addition, while much of the glucose intolerance caused by acute A2BR agonism is associated with a direct effect in the liver inducing hepatic glucose production [87], our collaborator Dr. Joel Linden found that deleting A2BR in adipocytes using an aP2-driven Cre reduced the glucose excursion effect of A2BR agonism in mice (personal communication). Interestingly, this effect was greater following 5 weeks of HFD, and, in humans, obesity is associated with higher A2BR expression in adipose tissue [92]. These data suggest a role for adipose A2BR in reducing glucose tolerance which is aggravated by obesity. Further, adipose A2BR acts in contrast with signaling through A1R which promotes insulin sensitivity, which is unsurprising given its opposite effects on cAMP.

Adipocytes are believed to express very low levels of A2BR, however A2BR is known to be highly transcriptionally regulated through transcription factors such as HIF-1α, NF-κB, and Nkx2.5 [94,95]. Dr. Linden also found that when 3T3-L1 adipocytes were

supplemented with 10% FBS in the media, A2BR was significantly upregulated within 4 hours compared to serum-starved adipocytes (personal communication). Further, while agonism of A2BR with either the A_{2B}-specific agonist LUF6210 or the non-specific adenosine agonist NECA had no effect on cAMP levels in serum-starved 3T3-L1 adipocytes, both compounds induced a profound increase in cAMP levels in 3T3-L1 adipocytes supplemented with 10% FBS which could be blocked with the A_{2B}-specific antagonist ATL801.

These data suggested that under nutrient replete or obese conditions, adipocytes may switch their response to adenosine from an A1R-mediated to an A2BR-mediated signal. We therefore sought to explore how both A1R and A2BR were regulated in adipocytes between catabolic and anabolic conditions, as well as in obesity, in order to better understand this shift in adenosine signaling. In this chapter, we show that anabolic conditions induced by serum and insulin cause a rapid downregulation in A1R as well as upregulation in A2BR within adipocytes to shift adenosine signaling from the $G\alpha_i$-coupled pathway under fasted conditions to the $G\alpha_s$-coupled pathway under fed conditions. We show that feeding results in A1R downregulation and A2BR upregulation *in vivo* specifically within adipocytes. The downregulation of A1R was dependent on the action of insulin to suppress FOXO1 transcriptional activity, and we found that FOXO1 binds to the *Adora1* promoter in adipocytes. The upregulation of A2BR was dependent on the activation of the NF-κB pathway by an as yet undefined factor present in serum. This regulation led to a desensitization of adipocytes to signaling through A1R and increased sensitivity to signaling through A2BR in the fed condition. Similar to humans, obese mice

exhibited reduced A1R expression and increased A2BR expression in adipose tissue and a shift in adenosine signaling towards A2BR which resembled the fed condition. Further, obese mice no longer exhibited acute changes in A1R and A2BR expression with fasting and feeding.

RESULTS

Adenosine receptor expression switches to low A1R and high A2BR in adipocytes under anabolic conditions

In order to explore A1R and A2BR expression in adipocytes under fasted and fed conditions, we used 3T3-L1 adipocytes that were serum-starved overnight to approximate fasting, catabolic conditions, and used serum-starved adipocytes with the addition of 10% FBS and 1 nM insulin to the media for 4 hours to approximate fed, anabolic conditions. Following the addition of FBS and insulin to the media, we tracked changes in the expression of both A1R and A2BR over time and found that A1R was rapidly suppressed while A2BR was induced, and the maximal effect for both receptors was reached within 2 hours (Fig 3.1 A). We found that the expression of A1R was strongly regulated by insulin, and that a 4-hour treatment with insulin significantly suppressed A1R expression in a dose-responsive manner with an EC_{50} of ~150 pM (~0.25 μU/mL), which is well within the physiological range (Fig 3.1 B). Meanwhile, the addition of 10% FBS alone had no effect on A1R expression (Fig 3.1 C). In contrast, insulin was not a strong regulator of A2BR expression. A 4-hour treatment with insulin resulted in only a modest induction in A2BR expression, and only at an extremely supra-physiological concentration of 1 μM (Fig 3.1D). A 4-hour treatment with 10% FBS, however, was still able to induce a significant increase in A2BR expression without the addition of insulin (Fig 3.1 E). The induction of A2BR expression was similarly regulated by serum in a dose-responsive manner and achieved a near-maximal effect with 10% FBS (Fig 3.1 F). These data suggest that while A1R expression is regulated in adipocytes directly by insulin, A2BR expression is regulated by

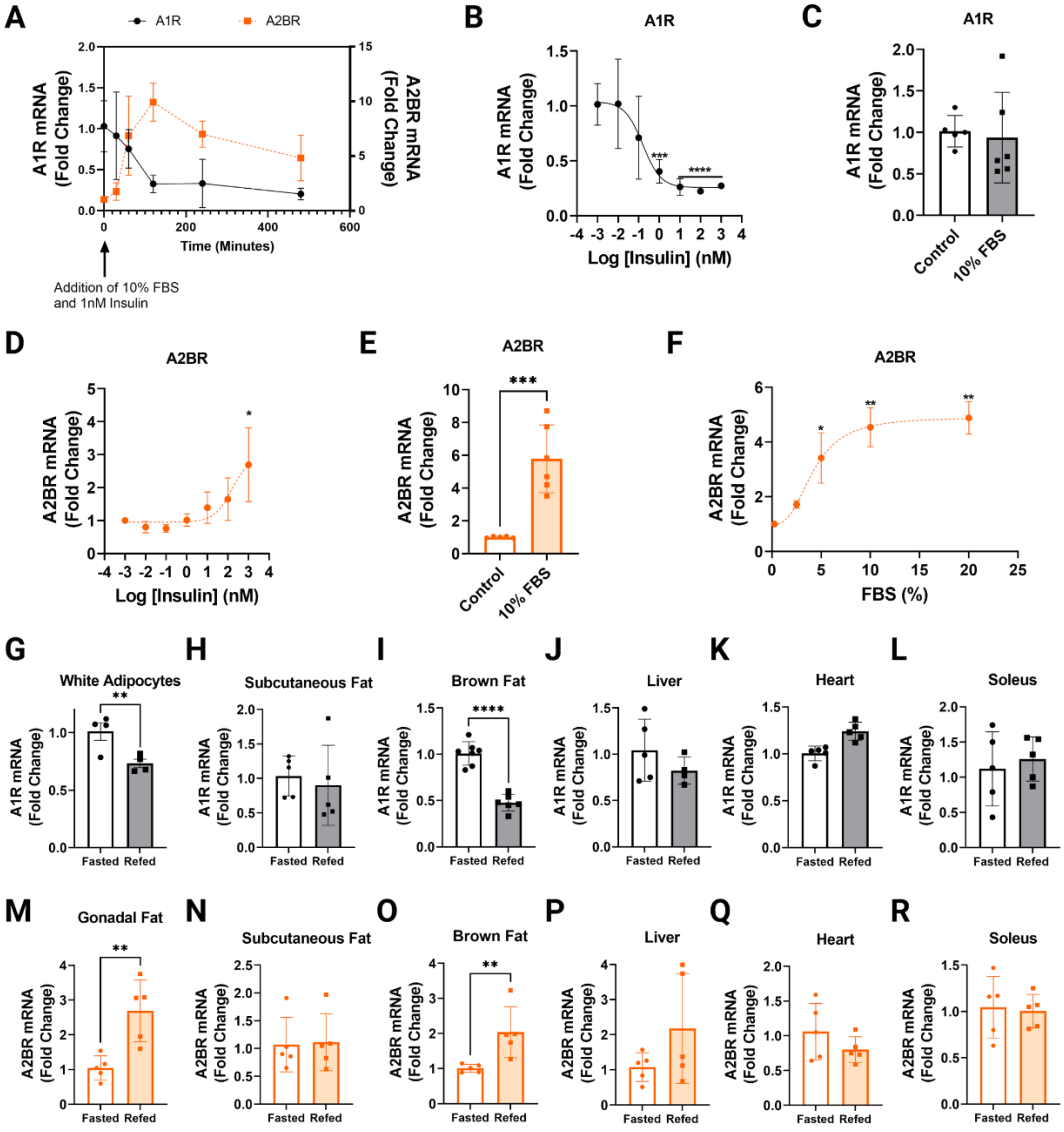

Figure 3.1: A1R and A2BR are reciprocally regulated by feeding in adipocytes through insulin and a serum factor respectively. (A-F) 3T3-L1 adipocytes 10-12 days after differentiation were serum starved overnight and treated with insulin or FBS as indicated. (A) Time course for the suppression of A1R mRNA (black, left axis) and induction of A2BR mRNA (orange, right axis) by the addition of 1 nmol/L insulin and 10% FBS. (B) Dose response of insulin effects on A1R expression after 4 hours. (C) Effect of a 4-hour treatment with 10% FBS on A1R mRNA expression. (D) Dose response of insulin effects on A2BR expression after 4 hours. (E) Effect of a 4-hour treatment with 10% FBS on A2BR mRNA expression. (D) Dose response of FBS effects on A2BR expression after 4 hours. (G-R) Adipocytes and tissues from wild-type male C57BL/6J mice were harvested after either an overnight fast (white) or following a 4-hour refeeding period (shaded). mRNA expression of A1R was measured in epididymal white adipocytes (G), subcutaneous adipose tissue (H), brown adipose tissue (I), liver (J), heart (K), and soleus muscle (L). mRNA expression of A2BR was likewise measured in epididymal white adipose tissue (M), subcutaneous adipose tissue (N), brown adipose tissue (O), liver (P), heart (Q), and soleus muscle (R). Error bars represent SD. *p<0.05, **p<0.01, ***p<0.001, ****p<0.0001, t-test or one-way ANOVA.

a factor other than insulin which is present in serum and is both dose-responsive and saturable.

Feeding suppresses A1R expression and induces A2BR expression specifically in epididymal and brown adipose depots

To test whether this regulation of A1R and A2BR occurs in response to feeding *in vivo*, we subjected 12-week-old wildtype C57Bl/6J mice to either an overnight fast alone (fasted), or followed up with a 4-hour refeeding period (refed). We found that refeeding suppressed A1R expression in white adipocytes isolated from epididymal fat pads, as well as in brown fat, but curiously this suppression was not seen in subcutaneous fat pads (Fig 3.1 G-I). Further, no changes in A1R expression were seen in other highly insulin-responsive tissues such as liver, heart, and soleus (Fig 3.1 J-L). Similarly, we saw that feeding induced a significant increase in A2BR expression in gonadal and brown fat, but not in subcutaneous fat (Fig 3.1 M-O). However, while no changes in A2BR expression were seen in heart and soleus, there was a modest, albeit not statistically significant, increase in A2BR expression within the liver (Fig 3.1 P-R).

Insulin regulates A1R transcription in adipocytes via the PI3K-Akt pathway

We next sought to determine the signaling mechanisms downstream of insulin that are responsible for A1R downregulation. The insulin receptor signaling pathway has numerous effectors but can be simplified to two immediate primary effectors:

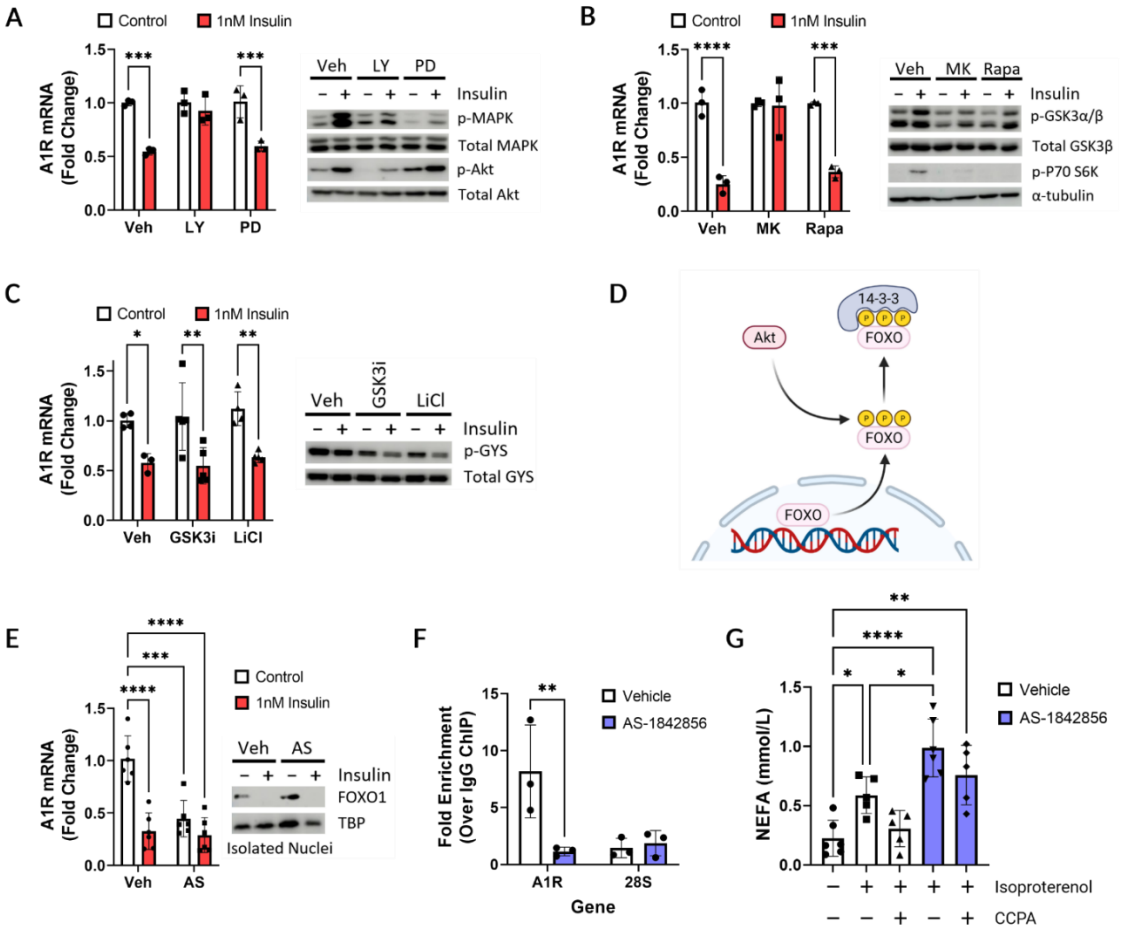

Figure 3.2: The insulin-Akt-FOXO1 pathway acutely regulates A1R expression to modulate adenosine signaling in adipocytes. (A-C, E) 3T3-L1 adipocytes 10-12 days after differentiation were serum starved overnight and treated with insulin as indicated for either 4 hours (mRNA analysis) or 15 minutes (phospho-protein western blot analysis). (A) Effect of untreated control (white) or 1 nmol/L insulin treatment (red) on A1R mRNA expression, phospho-MAPK (T202/Y204), and phospho-Akt (S473) after 15-minute pre-treatment with vehicle (Veh), 50 μmol/L LY294002 (LY), or 25 μmol/L PD98059 (PD). (B) Effect of 1 nmol/L insulin on A1R mRNA expression, phospho-GSK3α/β (S21/S9), and phospho-P70 S6K (T389) after 15-minute pre-treatment with vehicle (Veh), 25 μmol/L MK-2206 (MK), or 250 nmol/L rapamycin (Rapa). (C) Effect of 1 nmol/L insulin on A1R mRNA expression and phospho-GYS (S641) after 15-minute pre-treatment with vehicle (Veh), 1.4 μmol/L GSK3 inhibitor IX (GSK3i), or 30 mmol/L LiCl. (D) Diagram for the control of FOXO subcellular localization by Akt. Phosphorylation of FOXO by Akt facilitates the interaction of FOXOs with 14-3-3 proteins resulting in the cytoplasmic retention of FOXOs and reduced transcriptional activity. (E) Effect of 1 nmol/L insulin on A1R mRNA expression and nuclear localization of FOXO1 after 15-minute pre-treatment with vehicle (Veh) or 1 μmol/L AS-1842856 (AS). (F) Fold-enrichment by ChIP with FOXO1 over normal rabbit IgG of A1R promoter region (A1R) or 28S rDNA control region (28S) after 4-hour treatment of 3T3-L1 adipocytes with vehicle (white) or 1 μmol/L AS1842856 (blue). (G) NEFA released into the media by isolated adipocytes that were treated with vehicle or 1 μmol/L AS-1842856 for 4 hours, followed by vehicle or 100 nmol/L CCPA for 15 minutes in the presence of adenosine deaminase and a subsequent 30-minute treatment with vehicle or 30 nmol/L isoproterenol. Error bars represent SD. *p<0.05, **p<0.01, ***p<0.001, ****p<0.0001, one-way or two-way ANOVA.

phosphoinositide 3-kinase (PI3K) and mitogen activated protein kinase kinase (MAP2K). To interrogate these pathways, we utilized the pharmacological inhibitors LY294002 and PD98059 to inhibit PI3K and MAP2K respectively. While a 4-hour treatment with insulin alone suppressed A1R transcription and strongly activated the PI3K pathway as seen with phosphorylation of Akt at S473, a 30-minute pretreatment with LY294002 prevented both effects (Fig. 3.2 A). Meanwhile, inhibition of MAP2K with PD98059 significantly blunted insulin-induced phosphorylation of P42/44 MAPK at T202/Y204 but did not prevent the suppression of A1R transcription.

Downstream of PI3K, the protein kinase Akt is an important intermediary effector that phosphorylates proteins important for insulin signaling in adipocytes, such as mTORC1 and GSK3β. MK-2206 is a specific inhibitor of Akt1/2/3 which was able to prevent both insulin-induced phosphorylation of GSK3α/β at S21/9 and suppression of A1R (Fig. 3.2 B). Treatment with rapamycin, a specific inhibitor of mTORC1, blocked phosphorylation of the downstream target P70 S6 kinase (S6K) at T389, however there was no impact to the suppression of A1R by insulin (Fig. 3.2 B). We also inhibited the action of GSK3 with the GSK3 inhibitor IX, and with LiCl. Both treatments significantly impaired the phosphorylation of glycogen synthase (GYS) at S641, but neither had any impact on the suppression of A1R (Fig. 3.2 C). Thus, A1R transcription is suppressed by insulin via the PI3K-Akt pathway but is not dependent on mTORC1 or GSK3β.

A1R transcription is regulated by FOXO1

The forkhead box proteins within the FOXO family are transcription factors with known sensitivity to nutrient status. Phosphorylation of forkhead box proteins by Akt inhibits their transcriptional activity by promoting the interaction of FOXOs with 14-3-3 proteins and their retention within the cytoplasm (Fig. 3.2 D) [96]. FOXO1 is highly expressed in insulin sensitive tissues such as adipose and liver, and contains 3 known phosphorylation sites that are targets of Akt [97]. Further, both FOXO1 and A1R are involved in adipocyte differentiation and adipogenesis and show a similar pattern of upregulation as adipocyte differentiation progresses [44,98]. We therefore hypothesized that FOXO1 may be directly regulating A1R transcription in adipocytes. To explore this hypothesis, we utilized the pharmacological inhibitor AS-1842856 which competitively inhibits the DNA binding of FOXO1 [99]. Treatment of 3T3-L1 adipocytes with insulin both suppressed A1R transcription and induced the translocation of FOXO1 out of the nucleus as determined by western blot of isolated nuclei (Fig. 3.2 E). Treatment with AS-1842856 alone resulted in the suppression of A1R transcription to a similar level as insulin treatment but did not affect FOXO1 localization. Finally, treatment with both insulin and AS-1842856 did not result in any further suppression of A1R, suggesting that insulin and AS-1842856 suppress A1R transcription through a similar mechanism.

We next wanted to confirm that FOXO1 directly binds to the promoter of A1R to regulate its transcription. We used the LASAGNA-search 2.0 tool to identify sites containing the consensus motif for FOXO1 binding within the A1R promoter [100]. We identified a region within the first intron of the A1R gene locus containing 4 consensus

motifs within a span of 50 bp. We next used chromatin immunoprecipitation (ChIP) to enrich for FOXO1 binding sites, followed by qPCR and found this region within the A1R locus was significantly enriched compared with a normal IgG control ChIP (Fig. 3.2 F). There was no enrichment in the control region within 28S rDNA.

Inhibition of FOXO1 in adipocytes induces A1R insensitivity

Thus far, we have shown that feeding suppresses A1R transcription in adipocytes, and that insulin is capable of suppressing A1R transcription through the phosphorylation and inactivation of FOXO1. We therefore wondered what the effects of direct FOXO1 inhibition would be on adipocyte lipolysis and A1R sensitivity. We isolated adipocytes from the epididymal fat pads of overnight fasted male C57BL/6J mice and treated them with either vehicle or the FOXO1 inhibitor AS-1842856 for 4 hours. We then treated the cells with vehicle or the A1R agonist CCPA in the presence of adenosine deaminase for 15 minutes followed by a 30-minute treatment with vehicle or isoproterenol and measured NEFA release into the media. In the absence of FOXO1 inhibition, isoproterenol strongly increased the concentration of NEFA within the media and the addition of CCPA suppressed NEFA back to control levels as expected (Fig. 3.2 G). While the inhibition of FOXO1 alone had no effect on NEFA release (not shown), the addition of isoproterenol in these adipocytes resulted in a significantly higher induction in lipolysis which CCPA was not able to suppress (Fig. 3.2 G). Taken together, these data demonstrate that A1R transcription is acutely regulated via the insulin-Akt-FOXO1 signaling axis within

adipocytes, and that insulin stimulation results in a rapid downregulation of A1R transcription and reduced sensitivity to A1R signaling.

The induction of A2BR in adipocytes is dependent on the activation of the NF-κB pathway

We took a similar approach to determine the signaling mechanisms responsible for the induction of A2BR by serum in 3T3-L1 adipocytes by utilizing pharmacological inhibitors of major cellular signaling pathways. Since the factor in serum which induces A2BR expression is unknown, we first utilized pharmacological inhibitors of a wide variety of major cellular signaling pathways to better facilitate the future characterization of the exact signaling mechanisms and identification of the unknown factor. Neither inhibition of PI3K with LY294002, nor inhibition of MAP2K with PD98059 was able to prevent the induction of A2BR expression by serum (Fig 3.3 A). A2BR induction was also unaffected by adenosine levels or GPCR-related pathways, as the removal of endogenous adenosine with adenosine deaminase, the inhibition of $G\alpha_q$ subunits, and the stimulation of the $G\alpha_s$-coupled β-adrenergic receptors with isoproterenol all had no effect (Fig 3.3 B). Further, the inhibition of JAK/STAT signaling with JAK inhibitor I (JAKi), as well as the inhibition of JNK signaling with the JNK inhibitor SP600125 (SP) were also unable to prevent the induction of A2BR by serum (Fig 3.3 C). Meanwhile, activation of PPAR-γ with pioglitazone added during adipocyte differentiation significantly suppressed A2BR (not shown) but did not affect its induction by serum (Fig 3.3 D). Presumably this effect was due to improved differentiation of fibroblasts into adipocytes since fibroblasts express higher levels of A2BR and treatment of 3T3-L1 adipocytes with pioglitazone for 4 hours

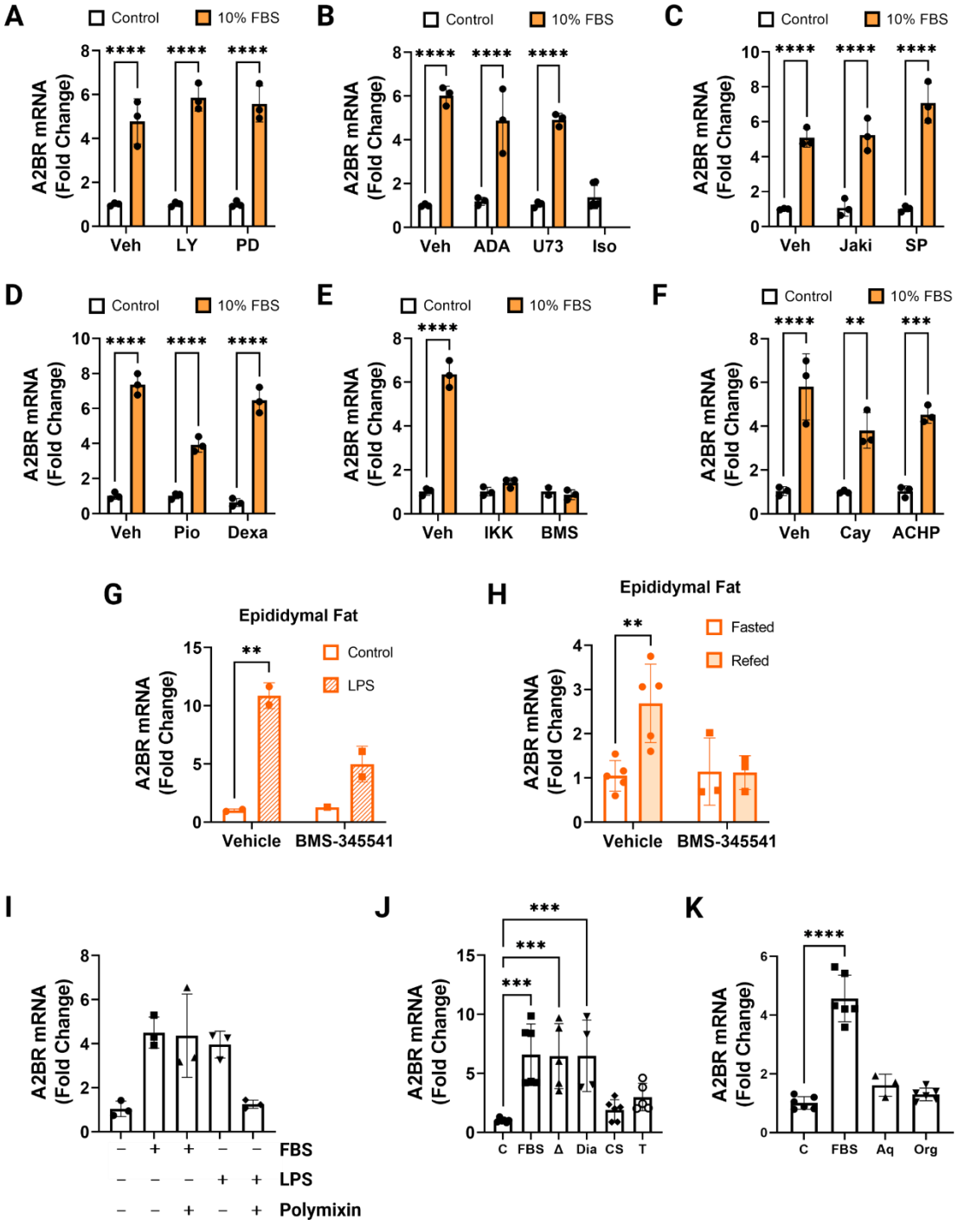
A
Control
10% FBS
A2BR mRNA (Fold Change)
Veh
LY
PD
B
Veh
ADA
U73
Iso
C
Veh
Jaki
SP
D
Veh
Pio
Dexa
E
Veh
IKK
BMS
F
Veh
Cay
ACHP
G
Epididymal Fat
Control
LPS
Vehicle
BMS-345541
H
Epididymal Fat
Fasted
Refed
Vehicle
BMS-345541
I
FBS
LPS
Polymixin
J
C
FBS
Δ
Dia
CS
T
K
C
FBS
Aq
Org

Figure 3.3: Serum and feeding induced upregulation of A2BR in adipocytes requires activation of the NF-κB pathway. (A-F) 3T3-L1 adipocytes 10-12 days after differentiation were serum starved overnight and treated with 10% FBS as indicated for 4 hours. (A) Effect of untreated control (white) or 10% FBS treatment (orange) on A2BR mRNA expression after 15-minute pre-treatment with vehicle (Veh), 50 μmol/L LY294002 (LY), or 25 μmol/L PD98059 (PD). (B) Effect of 10% FBS treatment on A2BR mRNA expression after 15-minute pre-treatment with vehicle (Veh), 1 U/mL adenosine deaminase (ADA), 5 μmol/L U73122 (U73), or 30 nmol/L isoproterenol (Iso). (C) Effect of 10% FBS treatment on A2BR mRNA expression after 15-minute pre-treatment with vehicle (Veh), 1 μmol/L JAK inhibitor I (Jaki), or 10 μmol/L SP600125 (SP). (D) Effect of 10% FBS treatment on A2BR mRNA expression after 15-minute pre-treatment with vehicle (Veh), on 3T3-L1 adipocytes differentiated in the presence of 10 μmol/L pioglitazone (Pio), or 100ng/mL dexamethasone (Dexa). (E) Effect of 10% FBS treatment on A2BR mRNA expression after 15-minute pre-treatment with vehicle (Veh), 20 μmol/L IKK-16 (IKK), or 25 μmol/L BMS-345541 (BMS). (F) Effect of 10% FBS treatment on A2BR mRNA expression after 15-minute pre-treatment with vehicle (Veh), 1 μmol/L CAY-10576 (Cay), 10 μmol/L ACHP. (G) Effect of a 4-hour treatment with control PBS or 100 μg/kg LPS in overnight fasted mice pre-treated with either vehicle or 30 mg/kg BMS-345541 for 1 hour on A2BR mRNA expression in epididymal adipose tissue. (H) A2BR mRNA expression in epididymal adipose tissue from fasted and refed mice treated with either vehicle or 30 mg/kg BMS-345541 1-hour prior to feeding. (I-K) 3T3-L1 adipocytes 10-12 days after differentiation were serum starved overnight and treated as indicated for 4 hours. (I) Effect of 10% FBS or 100 ng/mL LPS with or without pre-treatment with 50 μg/mL polymyxin B on A2BR mRNA. (J) Effect of 10% FBS with various treatments on A2BR mRNA. Control untreated FBS (FBS), heat inactivation (Δ), 10 kDa molecular weight cutoff dialysis (Dia), charcoal stripped (CS), and trypsin digested (T). (K) An organic extraction was performed on FBS, the aqueous and organic fractions were dried down under N_2 gas, and resuspended to the original volume in DMEM + 1% BSA. Effect of 10% FBS, aqueous fraction (Aq), or organic fraction (Org) on A2BR mRNA. Error bars represent SD. *p<0.05, **p<0.01, ***p<0.001, ****p<0.0001, one-way or two-way ANOVA.

did not affect A2BR expression (not shown). Activation of glucocorticoid receptors with dexamethasone also had no effect on A2BR expression.

The NF-κB pathway has been previously identified as a key regulator of A2BR expression whereby active NF-κB drives higher A2BR expression [94]. While NF-κB can be activated by a diverse range of stimuli, there are three main pathways through which different NF-κB complexes with distinct target genes become activated [101]. The canonical NF-κB pathway which critically involves the activation of inhibitor of NF-κB kinase (IKK) α and β. The non-canonical pathway involves the activation of only IKKα. Finally, there is a poorly characterized pathway which involves IKKε [102]. We found that IKK-16 and BMS-345541, which are inhibitors of IKKα/β, were both able to prevent the induction of A2BR by serum (Fig 3.3 E). Meanwhile, inhibition of IKKε with CAY-

10576 did not prevent the induction of A2BR (Fig 3.3 F). Interestingly, pre-treatment with ACHP, which is a less specific inhibitor of IKKα/β, also did not prevent the induction of A2BR for reasons that are unclear, and this experiment was not repeated to confirm. Thus, the induction of A2BR by serum is dependent on IKKα/β activity, suggesting that a factor which is present in serum regulates A2BR expression through either the canonical or non-canonical pathway for NF-κB.

We next wanted to know if the NF-κB pathway was also required for the induction of A2BR expression by feeding *in vivo*. As a control, we first administered 30 mg/kg BMS-345541 into 12-week old C57Bl/6J mice one-hour prior to injection with LPS to confirm that this dose was able to partially block the NF-κB pathway and subsequent induction of A2BR in epididymal fat (Fig 3.3 G). We next similarly administered BMS-345541 one-hour prior to refeeding and found that this was able to fully block the induction of A2BR caused by refeeding (Fig 3.3 H). Thus, the induction of A2BR by both serum and refeeding is dependent on IKKα/β activity, and the activation of NF-κB pathway through either the canonical or non-canonical pathway.

The A2BR inducing factor in serum is susceptible to both charcoal stripping and trypsin digestion

We next wanted to identify what factor in serum was responsible for the induction in A2BR expression. Given the stronger association of serum-starvation with NF-κB activation, we first wanted to ensure that the A2BR induction by serum was not the result

of endotoxin contamination within the serum. We therefore pre-treated 3T3-L1 adipocytes with polymyxin B prior to treatment with either FBS or lipopolysaccharide (LPS) in order to neutralize endotoxins which may be present in the serum. Pre-treatment with polymyxin B was able to prevent the induction of A2BR cause by LPS, but not by FBS (Fig 3.3 I). We then proceeded to treat 3T3-L1 adipocytes with differentially treated sera, including heat inactivation (Δ), 10 kDa molecular weight cutoff dialysis (Dia), charcoal stripping (CS), and trypsin digestion (T). We found that the factor in serum responsible for A2BR induction was retained by 10 kDa dialysis, and is susceptible to both charcoal stripping and trypsin digestion (Fig 3.3 J). Finally, we used a modified Bligh-Dyer extraction method to separate the aqueous and organic fractions in serum and dried each fraction under N_2 gas. These fractions were separately resuspended in DMEM containing 1% BSA and added to 3T3-L1 adipocytes at a concentration equivalent to 10% FBS. Neither the aqueous, nor the organic fraction were able to stimulate A2BR expression, suggesting that either a factor is destroyed during the organic extraction process or factors present in both fractions are required for activity (Fig 3.3 K). Further studies are needed to characterize which aspects of the NF-κB pathway are involved in the induction of A2BR and identify the factor(s) in serum responsible for this induction.

Feeding desensitizes adipocytes to A1R signaling in vivo

We next wanted to determine how this regulation of A1R and A2BR by feeding impacts adenosine signaling in adipocytes *in vivo*. We hypothesized that a downregulation in A1R expression following feeding would lead to a desensitization of adipocytes to

signaling through A1R. To investigate this possibility, we first re-evaluated our approach to the isoproterenol tolerance test which we performed in WT and FAdora1$^{-/-}$. As discussed in Chapter 2, we subjected WT and FAdora1$^{-/-}$ mice to a short 6-hour fast to normalize serum NEFA levels, administered 10 mg/kg isoproterenol by i.p. injection to stimulate adipocyte lipolysis, and followed serum NEFA levels over time. We found that FAdora1$^{-/-}$ mice exhibited a stronger stimulation of lipolysis and achieved significantly higher NEFA levels, particularly at 15 minutes after isoproterenol administration, when compared with WT mice (Fig 2.7 A,B and Fig 3.4 A,B). With the insulin-induced downregulation of A1R in mind, we next conducted these experiments under refed conditions by fasting mice overnight followed by a 4-hour refeeding period prior to stimulation with isoproterenol. As expected, both WT and FAdora1$^{-/-}$ mice had significantly lower levels of serum NEFA following refeeding. However, there was no longer any difference in the elevation of NEFA following isoproterenol stimulation (Fig. 3.4 C,D). Both WT and FAdora1$^{-/-}$ mice reached a similar peak in serum NEFA at 15 minutes (Fig. 3.5D) and returned to baseline within 2 hours. Presumably this is due to a downregulation of A1R within adipocytes in WT mice which diminishes the effects of the loss of adipose A1R in FAdora1$^{-/-}$ mice.

To confirm that this was due to a loss in adipose A1R sensitivity within WT mice under refed conditions, we next subjected 12-week-old WT C57BL/6J mice to an isoproterenol tolerance test using the same experimental setup; lipolysis was stimulated using isoproterenol in C57BL/6J mice that were either fasted for 6 hours or fasted overnight and refed for 4-hours. We first administered a 30-minute pre-treatment with the A1R antagonist 8-cyclopentyl-1,3-dipropylxanthine (DPCPX) and collected serum to assess

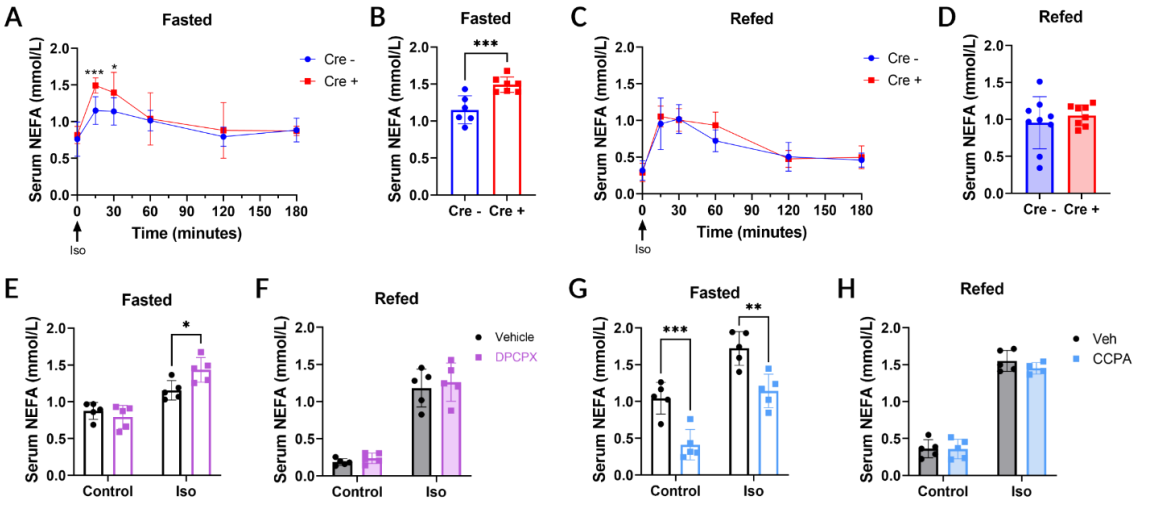

Figure 3.4: Feeding induces desensitization of adipose A1R. (A,B) Serum NEFA in 6-hour fasted male Cre negative WT (blue) and Cre positive FAdora1$^{-/-}$ (red) mice at the indicated time points after i.p. injection of 10 mg/kg isoproterenol (A) or at 15 minutes after injection with isoproterenol (B). (C,D) Same as in (A,B) for mice that were fasted overnight and refed for 4 hours. (E) Serum NEFA in 6-hour fasted wild-type male C57BL/6J mice treated with vehicle (black) or 0.1 mg/kg DPCPX (purple) for 30 minutes both before (control) and 15 minutes after (iso) i.p. injection with 10 mg/kg isoproterenol. (F) Same as in (E) for mice that were fasted overnight and refed for 4 hours. (G,H) Same as in (E) and (F) except mice were treated with vehicle (black) or 0.5 mg/kg CCPA (light blue) for 30 minutes before isoproterenol injection. Error bars represent SD. *p<0.05, **p<0.01, ***p<0.001, t-test or two-way ANOVA.

NEFA levels under control conditions before subsequent induction of lipolysis with isoproterenol for 15 minutes. Treatment with DPCPX alone did not alter NEFA levels, however DPCPX-treated mice exhibited a stronger lipolytic response to isoproterenol compared with vehicle-treated mice under fasted conditions (Fig. 3.4 E). This difference in lipolytic response was not present in refed mice, consistent with the results seen in FAdora1$^{-/-}$ mice (Fig. 3.4 F).

While these data alongside the results obtained with FAdora1$^{-/-}$ mice suggest a loss of sensitivity to A1R signaling in response to feeding, it is possible the discrepancy in these phenotypes between the fasted and refed conditions could be explained by differences in endogenous adenosine levels. A substantial reduction in extracellular adenosine following

refeeding would also produce a lack of any phenotype with both genetic knockout and antagonism of A1R. Therefore, we subjected fasted and refed C57BL/6J mice to pre-treatment with the A1R agonist 2-chloro-N^6-cyclopentyladenosine (CCPA) and isoproterenol stimulation. Under fasted conditions, agonism of A1R with CCPA produced a significant decrease in serum NEFA in both the control and isoproterenol stimulated states (Fig. 3.4 G). Strikingly, all effects of A1R agonism on serum NEFA were eliminated under refed conditions, even with isoproterenol stimulation (Fig. 3.4 H). These data confirmed that adipocytes are indeed desensitized to A1R signaling in response to feeding, and that changes in extracellular adenosine are unlikely to be responsible for reduced signaling through A1R during the fed state.

A2BR agonism drives increased glucose excursion in the refed state, dependent on adipocyte lipolysis

As demonstrated by Dr. Joel Linden (personal communication), A2BR agonism drives glucose excursion in mice which is partially dependent on adipose A2BR. Given the induction of adipose A2BR caused by feeding, we wanted to compare this glucose excursion effect between fasted and refed mice. We modeled our initial experiments on the original paper from Dr. Linden's group demonstrating that adenosine receptor agonism induces severe glucose intolerance during a GTT dependent on A2BR [90]. We administered either vehicle or the A2BR agonist BAY 60-6583 (BAY) to 12-week-old WT C57Bl/6J mice 30 minutes prior to starting a GTT and monitored blood glucose levels. This experiment was performed in mice that were either fasted for 6 hours or were fasted

overnight followed by a 4-hour refeeding period. As expected, A2BR agonism caused significant glucose excursion in both fasted and refed mice (Fig 3.5 A). Further, the glucose excursion effect appeared to be larger within refed mice. While the area under the curve for refed mice was not significantly different from fasted mice receiving BAY, it is important to note that the limit of detection for the OneTouch Ultra Glucometer is 600 mg/dL. Two out of three mice in the fasted group surpassed this limit of detection for only a single time point (90 minutes), while at least three out of the five mice in the refed group were above the limit of detection for 4 of the time points (45, 60, 90, and 120 minutes).

To avoid this problem with the limit of detection, we next measured just the glucose excursion caused by A2BR agonism in the absence of any glucose injections. As in Figure 3.5 A, BAY was injected into either fasted or refed mice, blood glucose was measured at the indicated time points, and serum was collected to analyze changes in serum NEFA concentrations. While the basal glucose values for fasted mice were significantly lower than refed mice, which is to be expected, the glucose excursion caused by A2BR agonism in refed mice was significantly greater (Fig 3.5 B). Fasted mice had a mean basal glucose of 73.2 mg/dL and increased to 238.4 mg/dL at 120 minutes after injection with BAY, while refed mice had a basal value of 191 mg/dL which increased to a peak of 483.6 mg/dL. Intriguingly, A2BR agonism only induced lipolysis under refed conditions, seen as an increase in serum NEFA levels, while serum NEFA decreased in fasted mice injected with BAY (Fig 3.5 C). The differences in glucose excursion and lipolysis between fasted and refed mice can be more easily visualized by setting the basal values for both groups to 0 and observing changes in the raw value of glucose or NEFA (Fig 3.5 D,E). Note that these

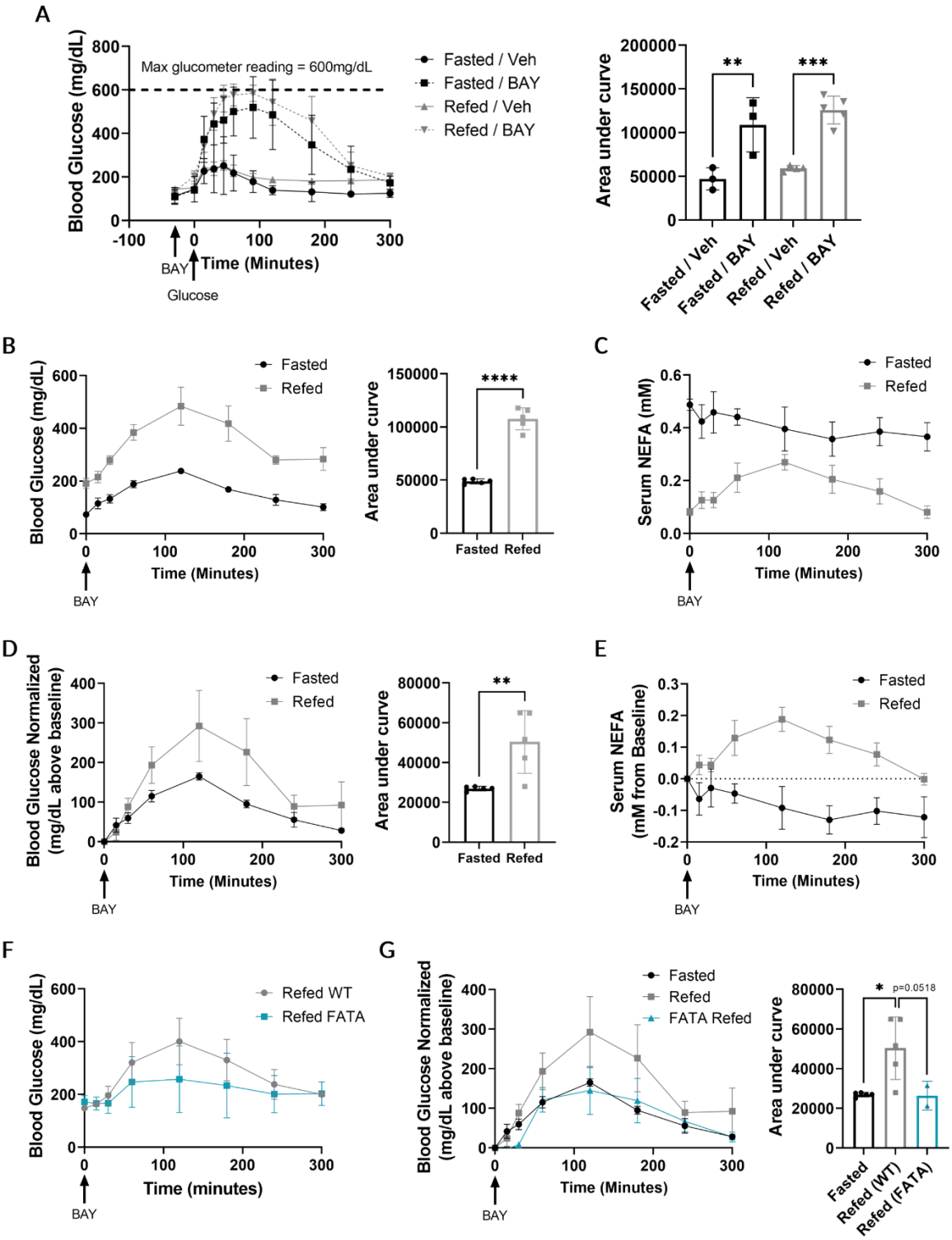
A
Blood Glucose (mg/dL)
Max glucometer reading = 600mg/dL
Fasted / Veh
Fasted / BAY
Refed / Veh
Refed / BAY
BAY
Glucose
Time (Minutes)
Area under curve
Fasted / Veh
Fasted / BAY
Refed / Veh
Refed / BAY
B
Blood Glucose (mg/dL)
Fasted
Refed
Time (Minutes)
Area under curve
Fasted
Refed
C
Serum NEFA (mM)
Fasted
Refed
Time (Minutes)
D
Blood Glucose Normalized (mg/dL above baseline)
Fasted
Refed
Time (Minutes)
Area under curve
E
Serum NEFA (mM from Baseline)
Fasted
Refed
Time (Minutes)
F
Blood Glucose (mg/dL)
Refed WT
Refed FATA
Time (minutes)
G
Blood Glucose Normalized (mg/dL above baseline)
Fasted
Refed
FATA Refed
Time (Minutes)
Area under curve
p=0.0518
Fasted
Refed (WT)
Refed (FATA)

Figure 3.5: Feeding enhances glucose excursion effects of A2BR agonism dependent on adipocyte lipolysis. 12–14-week-old C57BL6/J mice were either fasted overnight (fasted) or followed up with a 4-hour refeeding period (refed) and administered vehicle (Veh) or 0.75 mg/kg BAY 60-6583 (BAY) as indicated. (A) Fasted (black) and refed (gray) mice were administered Veh (solid lines) or BAY (dashed lines) 30 minutes prior to beginning a glucose tolerance test with 1 g/kg glucose as indicated by arrows. Blood glucose and corresponding area under the curve were measured over 5 hours. (B-E) Fasted (black) and refed (gray) mice were administered BAY as indicated by arrow and blood glucose (B) and serum NEFA (C) were measured over 5 hours. Blood glucose (D) and serum NEFA (E) were normalized to baseline by subtracting respective time 0 values from all time points. (F) Blood glucose over 5 hours for refed WT (gray) and $FATA^{-/-}$ (teal) mice administered BAY. (G) Refed $FATA^{-/-}$ blood glucose values and area under the curve with BAY administration were normalized to baseline and compared with blood glucose values from fasted (black) and refed (gray) WT mice. Error bars represent SD. *p<0.05, **p<0.01, ***p<0.001, ****p<0.0001, t-test or one-way ANOVA.

data are not normalized in any way but have been given the same starting value to better observe the differences in how these two groups respond to A2BR agonism.

The regulation of adipocyte lipolysis is an important component in the control of endogenous glucose production. NEFA and glycerol that are released from adipose tissue during lipolysis can drive increased uptake by the liver and subsequent gluconeogenesis and glucose excursion. We hypothesized that since A2BR agonism drives adipocyte lipolysis only in the refed state, the increased glucose excursion seen in refed mice was dependent on adipocyte lipolysis. To test this hypothesis, we utilized $FATA^{-/-}$ mice which have an adipocyte-specific deletion of ATGL, the enzyme which catalyzes the first and rate-limiting step in lipolysis. Adipocytes lacking ATGL are severely limited in their ability to undergo lipolysis, and we have previously published data using $FATA^{-/-}$ mice as an effective way to block adipocyte lipolysis [4,80]. Under refed conditions, the glucose excursion effects of A2BR agonism were significantly blunted in FATA mice compared with WT mice (Fig 3.5 F). Strikingly, when basal glucose values were again set to 0, the blunted glucose excursion in refed FATA-/- mice matched the glucose excursion seen in fasted WT mice. These data suggest that the increased glucose excursion in refed WT mice

is dependent on adipocyte lipolysis, and that A2BR agonism drives adipocyte lipolysis only in the refed condition (Fig 3.6).

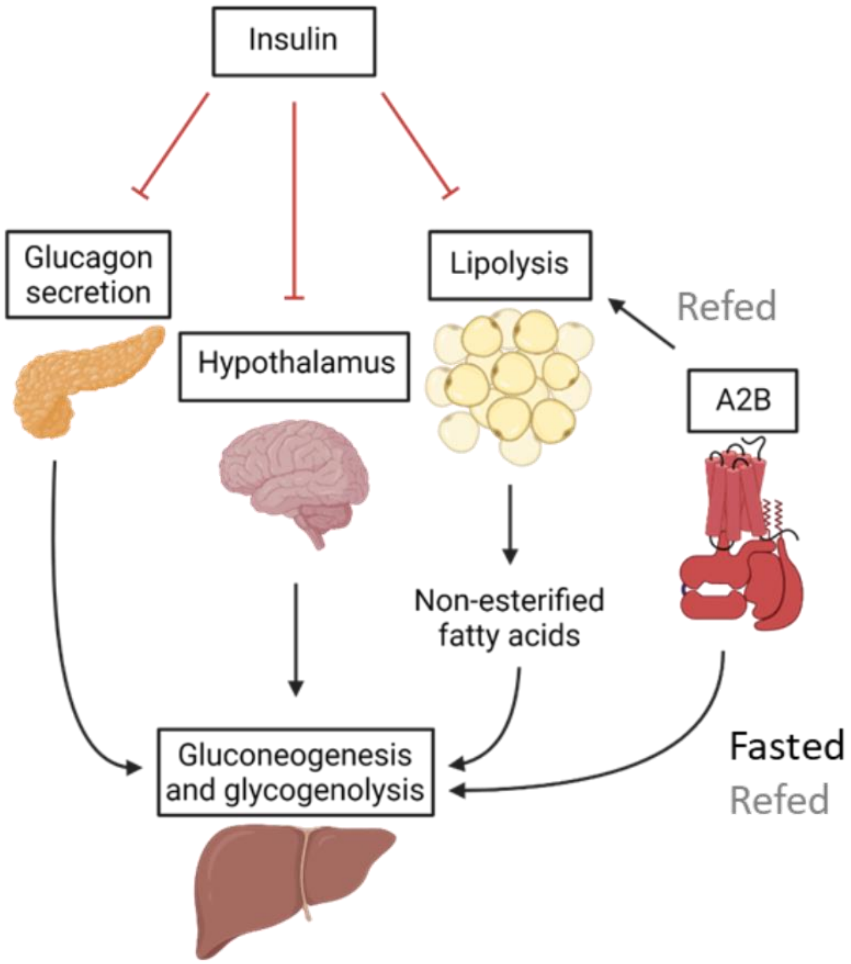

Figure 3.6: Schematic for proposed effects of A2BR agonism on hepatic glucose production. Insulin indirectly regulates hepatic glucose production through inhibiting pancreatic glucagon secretion, inhibiting activity of the hypothalamic-pituitary-adrenal-axis, and suppressing adipocyte lipolysis. As previously reported, A2BR activation directly drives hepatic glucose production by elevating cAMP levels in the liver. Our data suggest A2BR activation also drives hepatic glucose production by counteracting insulin suppression of lipolysis only under the refed condition. This figure was modified from Santoleri and Titchenell [229].

Obesity shifts adenosine signaling towards A2BR in adipose and disrupts regulation by feeding

Changes in adenosine signaling have been previously implicated in the development of insulin resistance in obesity. Multiple groups have demonstrated that obesity correlates with increased adenosine levels in human adipose tissue, yet reduced expression of A1R in adipose tissue in humans [68,103]. It has also been shown that obese humans have higher expression of A2BR in adipose tissue [92]. We wanted to know how obesity impacts not only A1R and A2BR signaling in adipocytes, but also the regulation of A1R and A2BR expression by feeding. We first placed C57BL/6J mice on either a normal chow or high fat diet (HFD) for 12 weeks, after which normal chow mice weighed on average 29.4 g ± 1.7 g and HFD mice weighed 46.5 g ± 3.2 g. We then compared A1R mRNA expression in isolated epididymal adipocytes from overnight fasted mice and confirmed that HFD also results in significantly reduced expression of A1R mRNA in mice (Fig. 3.7 A). We also isolated epididymal adipocytes from 4-hour refed mice and confirmed that HFD results in increased A2BR expression (Fig 3.7 B). When A1R expression between fasted and refed HFD mice is compared, we found that feeding no longer suppressed A1R transcription (Fig. 3.7 C). Similarly, feeding no longer induced A2BR expression in HFD mice (Fig 3.7 D).

To test how downregulation of A1R induced by HFD impacts adenosine signaling through A1R, we next repeated the experiments using the A1R antagonist DPCPX alongside isoproterenol stimulation of lipolysis with mice on HFD. We found that DPCPX did not result in an increased lipolytic response to isoproterenol under either fasted or refed

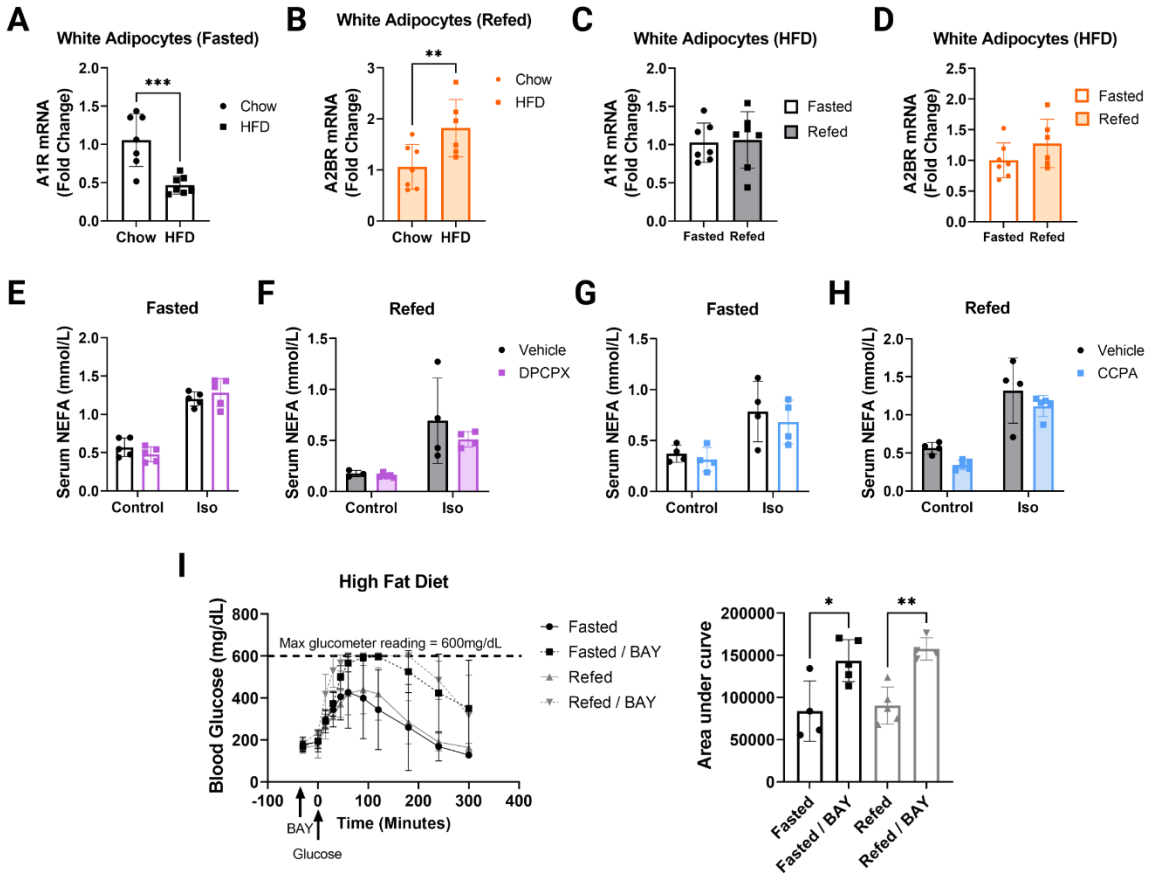

Figure 3.7: High-fat diet downregulates and desensitizes A1R in mouse adipocytes and disrupts regulation of A1R expression by feeding. (A-B) Epididymal white adipocytes were isolated from male wild-type C57BL/6J mice fed either normal chow control diet (Chow) or high-fat diet (HFD) for 12 weeks following an overnight fast. mRNA expression of A1R (A) and A2BR (B) was measured. (C-D) Epididymal white adipocytes were isolated from male wild-type C57BL/6J mice fed HFD for 12 weeks following either an overnight fast (fasted, white) or a 4-hour refeeding period (refed, shaded) and mRNA expression of A1R (C) and A2BR (D) was measured. (E-I) Male wild-type C57BL/6J mice were fed high-fat diet for 12 weeks before experimentation. (E) Serum NEFA in 6-hour fasted mice treated with 0.1 mg/kg DPCPX for 30 minutes both before (control) and 15 minutes after (iso) i.p. injection with 10 mg/kg isoproterenol. (F) Same as in (E) for mice that were fasted overnight and refed for 4 hours. (G,H) Same as in (E) and (F) except mice were treated with 0.5 mg/kg CCPA for 30 minutes before isoproterenol injection. (I) Following an overnight fast (fasted, black) or a subsequent 4-hour refeeding period (refed, gray), mice were administered Veh (solid lines) or 0.75 mg/kg BAY (dashed lines) 30 minutes prior to beginning a glucose tolerance test with 1 g/kg glucose as indicated by arrows. Blood glucose and corresponding area under the curve were measured over 5 hours. Error bars represent SD. *p<0.05, **p<0.01, ***p<0.001, t-test or one-way ANOVA.

conditions in these mice (Fig. 3.7 E,F). Further, administration of the A1R agonist CCPA was also unable to suppress lipolysis under either fasted or refed conditions in HFD mice (Fig. 3.7 G,H). These results demonstrate that, in addition to suppressing A1R

transcription, obesity disrupts the regulation of A1R transcription by fasting and feeding and the regulation of lipolysis by A1R signaling.

Finally, we wanted to know how the induction of A2BR resulting from HFD impacts signaling through A2BR. Similar to the experiment shown in Fig 3.5 A, we administered vehicle or BAY to fasted or refed HFD mice 30 minutes prior to glucose administration as part of a GTT. Once again, BAY induced profound glucose excursion in both fasted and refed mice, and on HFD, a majority of mice in both groups exhibited blood glucose levels above the limit of detection during the timepoints where this effect peaked (Fig 3.7 I). While this data is difficult to interpret due to these peak values being above the limit of detection, blood glucose values at the earlier time points (15, 30, and 45 minutes) and at later time points (180 and 240 minutes) indicate that refed mice on HFD retain an increased glucose excursion effect in response to A2BR agonism over fasted mice.

DISCUSSION

In this chapter, we investigated the regulation of the A_1 and A_{2B} adenosine receptors by feeding in adipose tissue, as well as the implications of this regulatory mechanism on the control of lipid metabolism by adenosine. We found that A1R and A2BR are reciprocally regulated at the transcriptional level by feeding in adipose tissue which desensitizes adipose tissue to adenosine signaling through A1R and enhances sensitivity to A2BR. The downregulation of A1R was mediated by insulin action to shut down the transcriptional activity of FOXO1 which binds to the promoter region of A1R. The upregulation of A2BR was mediated by an as yet undetermined factor present in serum which activates the NF-κB pathway. We further found that obesity also induces a downregulation of A1R and an upregulation of A2BR in adipose tissue and disrupts the regulation of these receptors by feeding. Since reduced A1R signaling and increased A2BR signaling are both associated with insulin resistance, the chronic shift in expression of these receptors in obesity which mimics the expression profile of the fed condition may contribute to obesity-induced insulin resistance.

This reciprocal regulation of A1R and A2BR initially presents as counterintuitive since FOXO1 drives high expression of the anabolic A1R in the fasted state when conditions are primarily catabolic, while NF-κB drives high expression of the catabolic A2BR in the fed state when conditions are primarily anabolic. However, this view of these receptors in steady state misses a critical component of this regulation, which is the lag between stimulation by insulin and serum and the observed shift in A1R and A2BR mRNA. Considering the data presented here and in Chapter 2, we propose the following model for

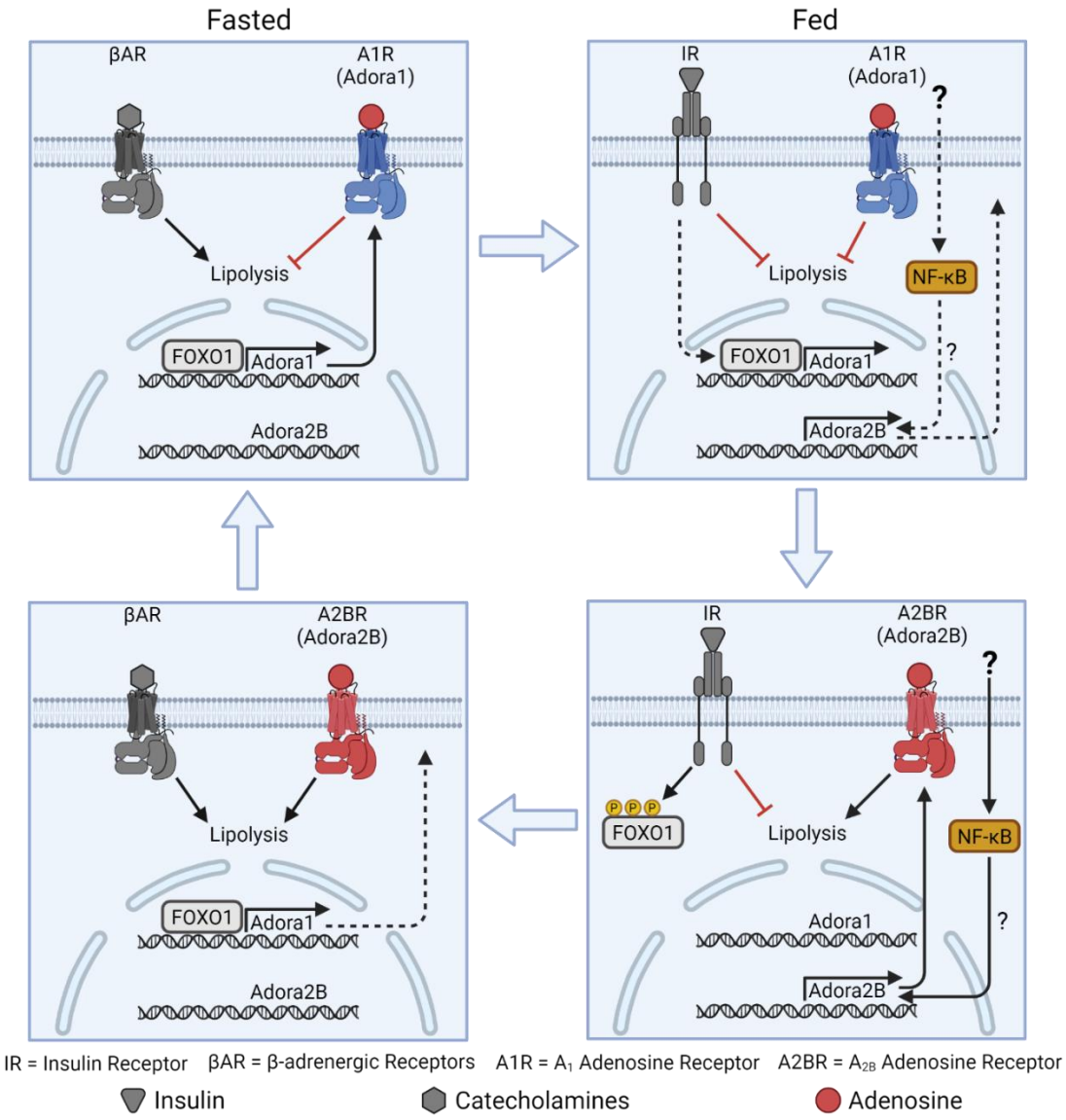

Figure 3.8: Proposed mechanism for the modulation of adenosine signaling in adipocytes during fasting and feeding. Under fasted conditions, active FOXO1 drives high expression of A1R which serves to limit lipolysis stimulated by catecholamines during stress (top left). Upon feeding, catecholamine levels decrease while insulin levels increase. Insulin acts to suppress lipolysis and induce the phosphorylation and inactivation of FOXO1, decreasing transcription of A1R. Simultaneously, an unknown serum factor activates signaling through NF-κB which enhances transcription of A2BR. Initially, A1R expression persists at high levels while A2BR remains low and adenosine signaling through A1R augments the suppression of lipolysis by insulin (top right). Inactive FOXO1 and activated NF-κB under fed conditions eventually leads to reduced A1R expression and increased A2BR expression, resulting in adenosine signaling through A2BR which counteracts insulin suppression of lipolysis to preserve low levels of circulating NEFA (bottom right). Reduced nutrient levels brought on by fasting lead to decreased insulin and increased catecholamines. Adenosine signaling through A2BR facilitates the initial induction of lipolysis by catecholamines upon fasting (bottom left). Decreased insulin levels lead to active FOXO1 simultaneously with reduced activation of NF-κB which switches adenosine signaling back towards A1R to reengage its limitation on lipolysis in the fasted state.

this regulatory mechanism. First, we propose that active FOXO1 drives high A1R in the fasted state to limit deleterious effects such as lipotoxicity resulting from the overstimulation of lipolysis by catabolic signals (Fig. 3.8, top left). Upon feeding, A1R initially remains high to augment insulin action to suppress lipolysis and promote a switch in adipocytes to the anabolic state (Fig. 3.8, top right). However, a postprandial decline in A1R levels mediated through reduced FOXO1 transcriptional activity with a simultaneous increase in A2BR levels mediated through NF-κB regulated transcriptional activity switches adenosine to a catabolic signal in adipose (Fig. 3.8, bottom right). We posit that high A2BR under fed conditions can act to limit the suppression of lipolysis by insulin, perhaps to preserve low levels of circulating NEFA for tissues such as the heart which rely heavily on fatty acids as an energetic substrate. Finally, we propose that a switch in adenosine signaling to A2BR facilitates the reentrance of adipocytes into the catabolic state by augmenting catecholaminergic signaling to drive lipolysis and hepatic glucose production upon fasting (Fig. 3.8, bottom left). Homeostasis posits that an organism responds to changing conditions to maintain the internal milieu constant, while allostasis suggests that organisms alter the internal milieu in order to meet anticipated demands through neuronal mechanisms [104,105]. It has been suggested that adenosine plays a more significant role in allostasis than in homeostasis, and the switch in A1R and A2BR expression appears to be an allostatic adaptation to the predicted eventual shift from anabolism to catabolism [106].

The significant reduction in A1R mRNA following feeding which appears to be mediated by the insulin-Akt-FOXO1 signaling axis may explain a central shift in adenosine

receptors that occurs during adipogenesis. Gharibi et. al. demonstrated that A1R promotes adipogenesis, and that A1R expression is dramatically increased several days into the adipocyte differentiation process before falling to a level that is still significantly elevated over preadipocytes [44]. Interestingly, Nakae and colleagues demonstrated that FOXO1 also promotes adipogenesis, and FOXO1 expression follows a strikingly similar pattern and timing during adipocyte differentiation [98]. It follows that increased expression of A1R during the differentiation process is driven by FOXO1, although further work is needed to demonstrate this mechanism.

Adenosine levels are increased in response to adrenergic stress, and adenosine action on A1R suppresses adrenergic stimulation of lipolysis in adipocytes [46,55,79]. A1R agonists have been clearly demonstrated to suppress basal and ß-adrenergic-stimulated lipolysis *in vivo*, however these experiments were performed in fasted subjects, even in human patients, as is typical for most metabolic studies [65–67,107]. While we found that both genetic loss of adipose A1R (Chapter 2) and general antagonism of A1R resulted in a stronger lipolytic response to adrenergic stimuli in fasted conditions, this effect was not present in refed mice. We did not measure the effects of feeding on interstitial or local plasma adenosine levels, however the desensitization of adipose A1R under refed conditions was independent of any potential reduction in adenosine as lipolysis in WT refed mice was also unaffected by a high dose (0.5 mg/kg) of the full A1R agonist CCPA. It is also unlikely that alternative pathways influencing cAMP levels, such as insulin activation of phosphodiesterases, are confounding our results, as isoproterenol still produced a clear induction in lipolysis within refed mice which was not suppressed by A1R agonism.

Instead, the loss of A1R sensitivity correlated with reduced A1R mRNA expression mediated through FOXO1, however we would like to note that the reductions in mRNA measured *in vivo* may not be large enough to account for the full loss of A1R sensitivity observed. Other mechanisms such as post-translational modifications or changes in $G\alpha_i$ proteins may be involved. Indeed, phosphorylation of A1R has been implicated in the process of its desensitization, internalization, and coupling to G-proteins [108,109]. It may also be interesting to investigate the sensitivity of adipocytes to other $G\alpha_i$-coupled antilipolytic agents, such as nicotinic acid or prostaglandin E_2, under refed conditions. Further, A1R has been reported as having a slower turnover relative to the other adenosine receptors with desensitization occurring in a range between 4 and 24 hours [110]. This places the acute effects we observed in adipocytes within a plausible range, albeit at the shortest extreme. It is therefore worth mentioning that the suppression of A1R in 3T3-L1 adipocytes by insulin was sustained for up to 6 hours after the removal of insulin which would allow sufficient time for desensitization through receptor turnover (not shown).

The induction of A2BR, while surprising for its adipocyte specificity and dependence on feeding, is consistent with previous reports on the regulation of this receptor through transcription. A2BR is strongly induced through transcriptional mechanisms in multiple tissues by hypoxia and inflammation through HIF-1α and NF-κB [86,94]. Further, A2BR is known to have a rapid turnover of less than 1 hour, suggesting persistent transcription is required to maintain high receptor expression [110]. The activation of NF-κB by feeding and by serum, however, is unexpected and even contrasts with data in COS cells where serum starvation activates NF-κB [111]. At the same time, we do not see

consistent upregulation of other NF-κB targets in adipocytes by serum such as Tnf. In this chapter we only present evidence for the involvement of NF-κB using two pharmacological inhibitors, both of which target IKKα/β. Additional data is needed looking at NF-κB activation through induced nuclear localization of downstream effectors (RelA, RelB, c-Rel, p50/p105, and p52) as well as utilizing pharmacological or genetic targeting at other points in this pathway to confirm its involvement in upregulating A2BR. It is worth mentioning that the C-terminal domain of A2BR plays a role in inhibiting NF-κB activation which could serve as an important mechanism for negative-feedback regulation in this process [112].

Another significant shortcoming is the lack of an identified factor in serum which is regulated by feeding and activates NF-κB in adipocytes to induce A2BR expression. The contrasting effects of serum to activate NF-κB in adipocytes while suppressing it in COS cells, as well as the adipocyte-specific induction of A2BR by feeding suggests a ligand/receptor interaction which provides adipocyte specificity. Further work is needed, perhaps using size-exclusion, ion exchange, ammonium sulfate precipitation, or other methods of separation to identify the factor in serum which is sufficient to cause this induction of A2BR.

In characterizing the effects of A2BR agonism during fasting and feeding, we used the A2BR agonist BAY 60-6583 rather than the non-specific agonist NECA used by Figler et al. in order to provide additional specificity and avoid some of the undesirable effects of A_1 receptors on the cardiovascular system [90]. However, BAY 60-6583 is only a partial agonist of A2BR and does not stimulate the $G\alpha_q$-coupled responses of A2BR, thus a

significant portion of A2BR activity is missing in this model [113]. Despite this, adipose tissue clearly exhibited enhanced sensitivity to A2BR agonism under refed conditions as observed through the increase in circulating NEFA levels following BAY 60-6583 agonism.

The ability of adipocytes to respond to A2BR agonism under refed or high-fat diet conditions may explain some of the contrasting effects of A2BR observed in metabolic syndrome. Acutely, A2BR activation drives hepatic glucose production and glucose intolerance, while antagonism improves glucose tolerance and global A2BR knockout improves both insulin sensitivity and glucose tolerance in young and lean mice [88–91]. Chronically, A2BR activation improves metabolic syndrome in HFD mice, while A2BR global knockout reduces insulin sensitivity and glucose tolerance and leads to dysregulated lipid metabolism in the liver [89,92,93]. The role of A2BR in adipose tissue described herein, and recently by Dr. Alexander Pfeifer's lab, may therefore explain these discrepancies between acute vs. long term impacts of A2BR on metabolism [47,48]. Under refed conditions, A2BR can drive adipocyte lipolysis and hepatic glucose production, and acutely this effect would appear as adipose insulin resistance and whole-body glucose intolerance. It therefore follows that antagonism of A2BR, or the genetic deletion of A2BR in young, lean mice could improve insulin sensitivity and glucose tolerance. With chronic antagonism or genetic loss of A2BR, however, the loss of this feeding induced mechanism could lead to increased lipid storage and fat mass expansion over time. This effect would become exacerbated by HFD where A2BR is chronically upregulated under both fasted and refed conditions. Further, A2BR was recently discovered to drive thermogenic

activation of brown adipocytes and increased energy expenditure, and thus the loss of brown adipose A2BR would also be expected to contribute to increased body weight and fat accumulation [48].

Obesity has been shown to reduce responsiveness to inhibitors of cyclic AMP accumulation such as adenosine [103]. This has been associated with reduced expression of A1R in adipocytes isolated from obese human patients as compared to lean patients [68,103]. We observed that A1R expression is also reduced in adipocytes isolated from obese mice and confirmed that this leads to a lack of A1R sensitivity in obese mice under both fasted and refed conditions. At the same time, obesity has also been associated with an increased expression of A2BR in human adipose tissue which correlates strongly with reduced expression of IRS-2 and insulin sensitivity [92]. We likewise observed a significant induction in A2BR expression in HFD-fed mice. Together, these shifts resemble an adipocyte which has become stuck mimicking the fed state in terms of the adenosine response, which our data suggest would produce a more insulin resistant and lipolytic phenotype. It is possible that both this shift in adenosine receptor expression and the loss of cyclical fluctuations in expression between fasting and feeding may contribute to insulin resistance and glucose intolerance and the overall metabolic inflexibility seen in obesity.

Finally, there are two very important questions which the work presented in this chapter does not address. First, we were unable to produce consistent and reliable western blots to properly assess changes in receptor protein expression with fasting and feeding. To address this question, we are currently establishing radioligand binding assays which will enable us to interrogate membrane receptor density which is also more indicative of

receptor sensitivity than total receptor protein expression. We also do not know if the changes in A1R and A2BR expression with feeding are sufficient to switch the response to endogenous adenosine towards an A2BR-mediated response. It is possible that the induction of A2BR acts to counteract the remaining signal through A1R to, in effect, produce a full desensitization A1R, rather than mediate an adenosine-induced increase in cAMP.

In summary, adipose A1R and A2BR are acutely regulated by feeding to modulate the adenosine response and allow adipose tissue to adequately adapt to changing nutrient conditions. High expression of adipose A1R under fasted conditions is necessary to limit adrenergic-driven lipolysis and enhance insulin-mediated suppression of lipolysis. High expression of A2BR under fed conditions may act to preserve low levels of circulating NEFA and facilitate the induction of lipolysis upon fasting, though further work is needed to confirm this.

METHODS

Materials

All pharmacological compounds were obtained from Cayman Chemical (Ann Arbor, MI) unless otherwise stated. 3-isobutyl-1-methylxanthine (IBMX), dexamethasone, GSK3 inhibitor IX, formaldehyde, polymyxin B sulfate, sequencing grade trypsin, and peanut oil were obtained from Sigma-Aldrich (St. Louis, MO). LPS-B5 (*E. coli* 055:B5) was from Invivogen (San Diego, CA). Regular human insulin (Humulin R) was obtained from Eli Lilly (Indianapolis, IN). Control treated FBS, heat inactivated FBS, 10 kDa molecular weight cutoff dialyzed FBS, and charcoal stripped FBS were from Sigma-Aldrich (St. Louis, MO). All antibodies were obtained from Cell Signaling (Danvers, MA) unless otherwise specified. Adora1 antibody (PA1-041a) was obtained from ThermoFisher (Waltham, MA). The FOXO1 antibody (18592-1-AP) used for ChIP-qPCR was obtained from ProteinTech (Rosemont, IL).

Animals

All animals were bred and maintained in accordance with the University of Virginia Animal Care and Use Committee regulations and the study was approved by the ACUC ethics committee. 12- to 16-week-old C57BL6/J male mice were used for studies unless otherwise indicated. Details on the Fadora1$^{-/-}$ mice can be found in Chapter 2. For diet studies in wild-type animals, C57BL/6J mice at Jackson Labs were put on HFD beginning at 6 weeks of age (#380050) and were shipped to the University of Virginia vivarium at 14

weeks of age. The mice were then maintained on HFD (Research Diets, D12492) for another four weeks before experiments, for a total of 12 weeks of HFD.

Animal Procedures and Measurements

Details on measuring glucose and NEFA may be found in Chapter 2. All pharmacological compounds were administered via i.p. injection in 0.9% NaCl, except for BAY 60-6583 which was administered in 50% PEG-400/50% physiological saline and glucose which was administered as a 20% glucose solution. Mice were either fasted overnight (fasted) or then given access to chow and softened food for 4 hours (refed) as indicated, with exception of the fasted condition for the isoproterenol tolerance tests where mice were fasted for 6 hours. For tissue harvesting, mice were euthanized by cervical dislocation, and tissues were flash frozen in liquid nitrogen.

Adipocyte isolation

Adipocytes were isolated as described in Chapter 2. For protein and RNA extraction, adipocytes were washed twice with buffer containing 0.1% BSA, and once with buffer without BSA. For lipolysis assays, adipocytes were washed three times with buffer containing 2.5% BSA.

Lipolysis assays

Isolated adipocytes were treated with vehicle or 1 Mm AS-1842856 for 4 hours in lipolysis assay buffer (145 mmol/L NaCl, 5.4 mmol/L KCl, 1.4 mmol/L $CaCl_2$, 1.4 mmol/L $MgSO_4$, 0.2 mmol/L NaH_2PO_4, 5 mmol/L glucose, 2.5% BSA, 100 nmol/L adenosine, 10 mmol/L HEPES, Ph 7.4) in a 37°C water bath with mild agitation. Adipocytes were washed twice with assay buffer without adenosine and separated into assay tubes with ~100,000 cells per assay in a total assay volume of 200 Ml. Adipocytes were treated with vehicle or 100 nmol/L CCPA followed by the addition of 1 U/Ml adenosine deaminase to all lipolysis assays and incubation at 37°C with mild agitation for 15 minutes. Adipocytes were then treated with vehicle or 30 nmol/L isoproterenol and incubated for an additional 30 minutes. Assays were centrifuged for 1 minute at 200 x *g*, adipocytes were aspirated off, and assay buffer was collected and assessed for NEFA concentration. All assays were performed in triplicate, and each N represents independently isolated adipocytes.

RNA extraction and real-time qPCR

Details for RNA extraction and qPCR, as well as primers may be found in Chapter 2.

2.7 Culture and treatment of 3T3-L1 adipocytes

3T3-L1 fibroblasts and adipocytes (ATCC) were cultured and differentiated as previously reported [11]. Briefly, 3T3-L1 fibroblasts were maintained and grown to confluency in DMEM (Gibco, 11965-092) with 10% newborn calf serum (Gibco, 16010-159), 1% fetal bovine serum (FBS, Gemini Bio Products, Lot #A15H74K), and 1% antibiotic-antimycotic (AA, Gibco). Cells were differentiated 3 days after becoming confluent in DMEM with 10% FBS, 1% AA, and containing 0.25 IU/Ml insulin, 0.5 mmol/L IBMX, 0.25 µmol/L dexamethasone, and 10 µmol/L pioglitazone. After 4 days, adipocytes were maintained in DMEM with 10% FBS.

Experiments were performed with 3T3-L1 adipocytes 10 – 12 days after differentiation. Adipocytes were serum starved overnight in DMEM with 0.25% FBS and 0.25% BSA and treated with the indicated inhibitors at the concentrations described in figure legends 30 minutes prior to the addition of insulin or FBS. For qPCR analysis and FOXO1 translocation western blots, cells were treated with 1 nmol/L insulin or 10% FBS for 4 hours unless otherwise indicated. For western blot analysis of phospho-proteins, cells were treated with 1 nmol/L insulin for 15 minutes.

2.8 Nuclear isolation

3T3-L1 adipocytes were washed twice with cold PBS and lysed in sucrose buffer (250 mmol/L sucrose, 50 mmol/L NaF, 1 mmol/L EDTA, 50 mmol/L Tris, Ph 7.4) with Dounce homogenization. Lysates were incubated on ice for 5 minutes, and then centrifuged

at 17,000 x G for 10 minutes at 4°C. Supernatant was removed and frozen at -80°C as the cytosolic fraction. Pellets were resuspended with cell lysis buffer, briefly sonicated on ice with a probe tip sonicator, and frozen at -80°C as the crude nuclear fraction.

Western blot analysis

Details for sample preparation may be found in Chapter 2. Western blots were probed as indicated with β-actin (#A228, Sigma), α-tubulin (T9026, Sigma), GAPDH (#5174), TBP (#8515), A1R (#PA1-041a, ThermoFisher), phospho-Akt (S473, #9271), phospho-MAPK (T202/Y204, #9101), phospho-GSK3α/β (S21/S9, #9331), phospho-P70 S6K (T389, #9205), phospho-GYS (S641, #3891), total Akt (#2920), total P42/P44 MAPK (#4696), total GSK3β (#9315), total GYS (#3893), and FOXO1 (#2880). For assessing differences in protein or phospho-protein signal, membranes were stripped and reprobed with β-tubulin, α-actin, or TBP loading controls as appropriate and as indicated, and phospho-protein blots were additionally reprobed with the corresponding total antibody.

2.11 Chromatin immunoprecipitation

Chromatin immunoprecipitation (ChIP) was performed as previously described with modifications [114]. Briefly, 3T3-L1 adipocytes were serum starved overnight in DMEM with 0.25% FBS and 0.25% BSA and treated with vehicle or 1 μmol/L AS-1842856 for 4 hours. Cells were fixed in 1% formaldehyde for 10 minutes, and fixation was quenched with 125 mmol/L glycine for 5 minutes. Cells were washed twice with cold

PBS, lysed in hypotonic lysis buffer (10 mmol/L Tris-HCl, Ph 8.0, 10 mmol/L NaCl, 3 mmol/L $MgCl_2$, 0.5% NP-40) supplemented with protease inhibitors by Dounce homogenization, and incubated on ice for 5 minutes. Nuclei were pelleted by centrifugation at 17,000 x *g* for 5 minutes at 4°C. Pellets were resuspended with SDS lysis buffer (50 mmol/L Tris-HCl, Ph 8.0, 10 mmol/L EDTA, 1% SDS) and chromatin was sheared by sonication using a Diagenode BioRuptor Pico with 30 sec on and 30 sec off for 12 cycles. ChIP was performed using 3 μg of FOXO1 rabbit-antibody (ProteinTech) or normal rabbit IgG (Cell Signaling), and antibodies were pulled down with protein A agarose (Roche). Chromatin pulldown of the *Adora1* promoter region or 28S Rdna control region was assessed by Qpcr using the following primers: *Adora1* promoter: 5'-TGACCCTTGAAACCATGTGA-3' and 5'-CCCAGAGTACCCAACACACA-3', 28S Rdna: 5'-CTGGGTATAGGGGCGAAAGAC-3' and 5'-GGCCCCAAGACCTCTAATCAT-3'. FOXO1 binding was measured as enrichment over normal rabbit IgG ChIP.

CHAPTER 4

DISCUSSION AND FUTURE DIRECTIONS

The discovery that adenosine signaling in adipocytes occurs through dynamic rather than static pathways has wide-reaching implications for the role of adenosine in metabolism and related pathologies. There are a number of open questions in a direct vein from this research regarding the role of adenosine in adipocyte biology, the effects of this system on whole-body lipid and glucose metabolism, and the dysfunction of this dynamic regulation of adenosine receptors that occurs in obesity. There is also the interesting possibility that this feeding-induced switch in adenosine receptors could be an important mechanism by which postprandial thermogenesis occurs. More broadly, shifts in adipose responses to adenosine could play a role in circadian control of metabolism, cardiovascular disease, or cachexia.

Pharmacology of adenosine in adipocytes

As mentioned in Chapter 3, it remains unclear whether the changes in A1R and A2BR expression during feeding mediate a complete switch in adipose adenosine signaling from one that is dominated by A1R to one that is dominated by A2BR. The transcriptional changes induced by feeding for A1R and A2BR that we observed correspond with decreased and increased functional potency of A1R and A2BR respectively. The A1R has been reported as having a high binding affinity for adenosine and A2BR as having a low

binding affinity, however it is worth noting that the ligand binding affinity of G-protein-coupled receptors is significantly influenced by the current coupling state of the receptor with G-proteins [115]. The accurate determination of the true binding affinities under the coupled vs. uncoupled state is immensely difficult, and measuring comparative affinities for the adenosine receptors is additionally complicated by the lability of the native ligand requiring the use of adenosine analogs. Further, the functional potency of these receptors is determined by the ligand binding affinity and the receptor density at the plasma membrane. Importantly, adipocytes are known to possess a spare reserve capacity of A1R receptors, meaning that full receptor occupancy by the ligand is not required to exert a maximal effect (as measured by the suppression of cAMP) [57,107]. Therefore, a downregulation of A1R would likely not result in a reduced maximal response to adenosine, but would reduce the functional potency of adenosine at the A1R and a rightward shift of the dose-response curve for an A1R agonist. In other words, despite a reduction in A1R density, adipocytes are still very likely to retain sufficient A1R density for adenosine to elicit a maximal response, however a greater percentage of receptors would need to be occupied to elicit this response and thus the functional potency of adenosine at A1R in adipocytes is reduced. Meanwhile, because A2BR is not well expressed on adipocytes and does not exhibit spare receptors, the upregulation of A2BR would result in an increased maximal response and perhaps a leftward shift of the dose-response curve for an agonist if the induction in A2BR is strong enough to produce spare receptors. The signaling effects of adenosine in adipocytes will therefore depend on whether the functional potency of adenosine favors A1R or A2BR. The use of a non-specific agonist such as NECA as opposed to specific agonists in cultured primary

adipocytes may provide an answer to this question. Quantifying the changes in the functional potency of agonists at A1R and the maximal response of A2BR may also give additional insight into the magnitude of these shifts.

Adenosine control of adipose tissue and whole-body metabolism

The dynamic change in adenosine receptors between fasting and fed states suggests that adenosine is important in modulating adipocyte metabolism and function under these conditions. While global knockouts of both A1R and A2BR have significant changes that make it difficult to assess the role of these receptors in adipose, in both scenarios circulating NEFA levels are minimally affected. Our data in FAdora1$^{-/-}$ mice provide evidence that A1R enables adipocytes to rapidly suppress lipolysis in response to food intake, but is not important for establishing the final homeostatic set point in circulating NEFA levels. We hypothesized that A2BR may function in the opposite direction to facilitate an increase in lipolysis during the initial phases of fasting. To test these hypotheses, we are currently generating inducible, adipocyte-specific A2BR knockout mice, and A1R/A2BR double knockout mice in addition to our FAdora1$^{-/-}$ mice. These three mouse models will be useful for investigating the role of these adenosine receptors in the dynamics of adipose tissue metabolism during fasting and feeding cycles. Specifically, we would like to know the timing with which key metabolic parameters such as NEFA, glucose, insulin, and ketones shift upon feeding and fasting in the absence of these adenosine receptors. In regards to circulating NEFA, we hypothesize that FAdora1-/- mice would exhibit impaired kinetics in the suppression of lipolysis, though circulating NEFA would be reduced to the same

level over a longer time course (Fig 4.1 A). In adipocyte-specific A2BR knockout mice ($FA2B^{-/-}$), we predict that the stimulation of lipolysis and the elevation of circulating NEFA upon fasting would exhibit impaired kinetics and likewise result in a longer time course to achieve elevated fasting NEFA levels (Fig 4.1 B). In the complete absence of this system, we predict that adipocyte-specific A1R/A2BR double-knockout ($FAdKO^{-/-}$) mice would display impaired kinetics in both transitions (Fig 4.1 C). While these mice might be able to achieve normal fasted and fed circulating NEFA levels, we predict that they would exhibit a near chronic mismatch in metabolism due to impaired kinetics during these transitions between fasted and fed conditions. It is likely that this mismatch would contribute to the dyslipidemia and insulin resistance which often accompany adipocyte dysfunction.

Related to these experiments, an adipocyte-specific knockout of A2BR has been recently described, but with minimal metabolic phenotyping data [48]. In the $FAdora1^{-/-}$ mice, we found that in addition to augmenting insulin signaling to suppress lipolysis, adipose A1R also acted to limit the lipolytic response to adrenergic stimuli in the fasted state. Under fed conditions, insulin provides a strong anabolic stimulus to suppress lipolysis which must be overcome in order to elevate circulating NEFA during acute stress responses. It is possible that the upregulation of A2BR also serves the purpose of augmenting adrenergic action to stimulate lipolysis in the fed, but not fasted state. Thus, $FA2B^{-/-}$ mice may display an impaired lipolytic response to isoproterenol under fed conditions.

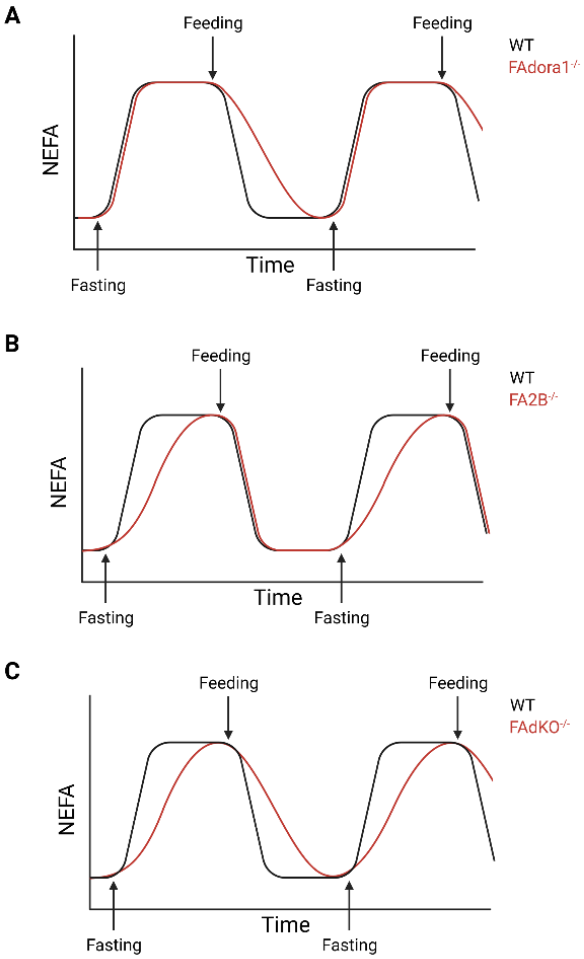

Figure 4.1: Proposed shifts in adipocyte metabolism with loss of A1R and A2BR. (A) Loss of adipose A1R in FAdora1-/- mice leads to slower kinetics in the suppression of lipolysis by insulin during feeding. Insulin still suppresses circulating NEFA to the same extent under fed conditions, but requires longer to achieve this effect. (B) Loss of adipose A2BR ($FA2B^{-/-}$) would lead to slower kinetics in the stimulation of lipolysis by catecholamines during fasting. Catecholamines would likewise result in elevation of circulating NEFA to the same extent but would require a longer time course. (C) Loss of adipose A1R/A2BR ($FAdKO^{-/-}$) would result in impaired kinetics in both transitions between fasting and feeding.

The $FAdKO^{-/-}$ mice will not only enable investigation of the purpose of A1R/A2BR signaling as a whole in adipose tissue, but also the purpose of the dynamic regulation of these receptors. In the context of this adipocyte-specific double-knockout model, a lox-stop-lox system could be used with *Adora1* or *Adora2B* inserted at the ROSA26 locus to

simultaneously induce constitutive, transgene expression of these receptors in adipose. Constitutive expression of A1R specifically in adipocytes in FAdKO$^{-/-}$ mice would therefore mimic adipocytes under fasted conditions without the ability to downregulate A1R transcription in response to feeding. On the other hand, constitutive expression of A2BR in adipocytes would mimic adipocytes under fed conditions with chronic upregulation of A2BR and downregulation of A1R, which is also the phenotype induced by obesity (Fig 4.2). In this instance, we would hypothesize that adipocytes would exhibit chronically elevated lipolysis and reduced response to the antilipolytic effects of insulin, highly similar to the defects in lipolysis that occur with obesity. The effects of chronically forcing adipocytes into an expression profile which emulates the fasted or fed condition on metabolism, adipogenesis, body weight and fat mass may give new insights into the role of this dynamic regulation of A1R and A2BR.

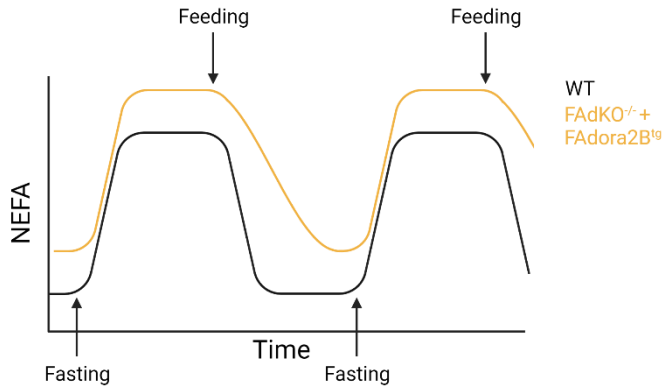

Figure 4.2: Proposed shifts in adipocyte metabolism with loss of A1R and chronic upregulation of A2BR. Representation of the proposed changes to fatty acid kinetics in a mouse model with adipocyte specific deletion of A1R and A2BR, and transgenic expression of A2BR in adipocytes to chronically mimic the low A1R/high A2BR expression profile seen in the refed state or in obesity. Loss of A1R would lead to slower kinetics in the suppression of lipolysis by insulin during feeding. The high expression of A2BR under both fasted and refed conditions would lead to a chronic elevation in lipolysis and circulating NEFA.

Dysregulation of adipose tissue by adenosine in obesity

More work is needed to determine how obesity dysregulates the pathways described herein which control A1R and A2BR expression. As we and others report, A1R is downregulated in adipose tissue with obesity. However, in obesity the FOXO1 transcription factor is typically more transcriptionally active. Due to insulin resistance, the phosphorylation status of FOXO1 is reduced, leading to nuclear translocation and higher transcriptional activity [97]. Therefore, other mechanisms must be involved during obesity which either disconnect or overcome the regulation of A1R by FOXO1. Meanwhile, low-grade chronic inflammation which occurs in adipose tissue during obesity would be expected to activate inflammatory pathways such as NF-κB and result in the upregulation of A2BR [6]. The cytokine/adipokine TNFα in particular has been shown to activate NF-κB and upregulate A2BR, and thus may play an important role in the dysregulation of A2BR in obesity [94]. It is also interesting to note that in our experiments with HFD-fed mice, BAY 60-6583 administration still appeared to produce an even higher glucose excursion in refed mice as compared with fasted mice, despite the lack of induction of adipose A2BR by feeding in these mice. In refed normal chow mice, we observed an induction of A2BR in liver which was not statistically significant, and we did not investigate immune cell populations. It may be worth further investigating this feeding-induced regulation of A2BR in these contexts where A2BR is already known to play a critical role.

It also remains unclear how rapidly the shifts in adipose adenosine receptors occurs with HFD feeding. It has been shown that HFD rapidly causes insulin resistance in adipose

tissue within 3 days, which is long before factors such as changes in inflammation begin to influence insulin sensitivity in adipose tissue [6]. Further, calorie restriction can also rapidly enhance insulin sensitivity in adipose tissue. Given the role of adenosine in adipose tissue insulin sensitivity, it seems plausible that changes in adenosine receptor expression could be involved in these rapid changes.

Potential role for adenosine receptors in postprandial thermogenesis

Adenosine has been shown to activate thermogenesis in brown adipocytes through both A_{2A} and A_{2B} receptors [47,48]. Further, A2BR has also been shown to support the activation of A_{2A} receptors as well as drive brown adipocyte thermogenesis through its own activation [48]. On the other hand, activation of A1R, either centrally or with broad administration of A1R agonists, is known to cause hypothermia [116,117]. Brown adipocytes have been shown to be significantly less responsive to A1R than white adipocytes, and the primary signal generated by adenosine was increased cAMP mediated through A_{2A} receptors [47]. However, these brown adipocytes were cultured in extremely high levels of insulin (20 nM – 750 nM) and do not appear to have been cultured in the absence of insulin and serum prior to these experiments. Our studies would indicate that brown adipocytes cultured under these conditions would have their expression of A1R significantly suppressed while also having elevated expression of A2BR relative to fasted levels. It is therefore possible that brown adipocytes are significantly more responsive to A1 receptors under fasted or hypoinsulinemic conditions.

Postprandial thermogenesis is a well-documented phenomenon in mice and humans where body temperature is elevated following feeding dependent on changes in both skeletal muscle and adipose tissues. In sheep, postprandial thermogenesis within fat pads reaches its peak approximately 4-hours after food intake [118]. Assuming the postprandial shifts in adenosine receptor expression and the kinetics of these changes are preserved across mice and sheep, it seems plausible that this change in adenosine signaling could play a role in mediating postprandial thermogenesis. In support of this hypothesis, we will be assessing the effects of A1R agonism on body temperature within WT and FAdora1$^{-/-}$ mice. We would expect that the hypothermic effects of A1R agonism would be partially attenuated in FAdora1$^{-/-}$ mice.

Potential for circadian regulation of adenosine signaling in adipose

Throughout our experiments, we aimed to perform our analyses at approximately the same time of day to avoid the effects of circadian regulation. However, numerous studies have clearly defined the importance of circadian regulation in metabolism, and disruptions in circadian rhythms are associated with the development of metabolic syndrome [119]. Adenosine receptors, particularly A_1 and A_{2A}, are heavily involved in circadian rhythms and sleep in the central nervous system [120]. Adipose tissues also contain their own circadian clocks which regulate significant aspects of adipose physiology through clock-controlled genes [121]. The role of adenosine in the circadian control of adipose tissue, however, has not been explored. In one study, human subjects switched onto a night shift displayed normal suppression of lipolysis following a meal, but a delayed

return to fasting NEFA levels [122]. Changes in adenosine receptor expression by circadian mechanisms, such as significantly elevated A1R or an inability to appropriately regulate A1R and A2BR expression in response to feeding, could provide one explanation for this delay. More studies are needed to determine how circadian rhythms affect adipose expression of adenosine receptors.

Adipose adenosine signaling in cardiovascular disease

We initially developed the FAdora1$^{-/-}$ mice to investigate the role of adipose A_1 adenosine receptors in the cardioprotection of A1R partial agonists in myocardial infarction and heart failure. Partial agonists of A1R, such as capadenoson, were reported to improve cardiac function in rat models of heart failure and myocardial infarction [34,123,124]. Unfortunately, neladenoson, an analog of capadenoson, failed to improve cardiac function in human patients with heart failure during clinical trials (Jürgen Schrader, personal communication). In rats, partial A1R agonists have been shown to suppress adipocyte lipolysis with minimal cardiac effects such as reduced heart rate [34,57,107]. Our lab has shown that inhibiting lipolysis during a myocardial infarction results in significant improvements to cardiac function [125]. We hypothesized that the beneficial effects of partial A1R agonists were at least partially due to the inhibition of lipolysis. In human patients, the administration of beta blockers would significantly mask this effect, and this polypharmacy may have been one contributing factor to the failure of Neladenoson in clinical trials.

While A1R agonism suppresses lipolysis in both mice and rats, mouse adipocytes are less sensitive to A1R agonism than rat adipocytes [126]. We discovered that the ability of partial A1R agonists to suppress lipolysis in mice cannot be separated from significant effects on heart rate (Figure 2.1). Since A1R partial agonists are still substantially effective at improving cardiac function in mouse models of myocardial infarction, the suppression of lipolysis is likely not a significant contributor to this effect. The failure of these compounds in clinical trials could still involve adipose adenosine receptors, however. Capadenoson and its analogs were discovered to also be A2BR partial agonists [127]. While we demonstrate that capadenoson suppresses lipolysis under fasted conditions, it is possible that it could activate lipolysis under refed conditions. Numerous studies suggest that increased adipocyte lipolysis is detrimental to cardiac function in the contexts of myocardial infarction and heart failure.

Adipose A2BR and cachexia

Cachexia is a wasting syndrome that results in uncontrolled loss of both adipose and skeletal muscle. Cachexia occurs with a number of chronic diseases such as chronic infection and heart failure, but it is most commonly associated with cancer. Fat catabolism has been implicated as an important contributor in cachexia, and deletion of ATGL attenuates weight loss in mice with cancer-associated cachexia [128]. These chronic diseases are also associated with chronic, low-grade inflammation which our work indicates is likely to mediate an upregulation of A2BR in adipose tissue. Future studies on

lipid metabolism in cachexia should consider the role of the adenosine system within adipose tissue.

Therapeutic potential of adenosine receptors for metabolism

The adenosine receptors have broad effects across numerous tissues, and whether or not they have therapeutic potential for metabolic diseases appears controversial. Many studies have argued the benefits of targeting the adenosine receptor system for various aspects of metabolic syndrome, however the results of global knockout mice and pharmacological manipulation have often been contradictory. The existing literature on adenosine supports a role in regulating cells under stress in a highly localized manner, rather than coordinating coherent, global responses in the body. For example, adenosine action in pancreatic β-cells to suppress insulin secretion and in adipocytes to suppress lipolysis. In both situations, adenosine alleviates stress (energetic stress from insulin secretion and adrenergic stress on lipolysis), yet these actions oppose one another in the context of whole-body lipid metabolism. For this reason, it remains unclear if pharmacological agents targeting A1R or A2BR will be effective in addressing metabolic diseases.

This work along with previous literature which has already been discussed provide a strong support for the role of A1R in adipose tissue as an insulin sensitizer. Several early studies, however, found that activation of A1R in skeletal muscle impairs insulin action [129,130]. It was also found that the administration of an A1R antagonist, BWA-1433,

resulted in improved glucose tolerance and insulin sensitivity, and increased glucose uptake in skeletal muscle [131,132]. In contrast, later studies supported a role for A1R in enhancing insulin-stimulated glucose uptake in skeletal muscle [133,134]. It was also discovered that BWA-1433 is not specific to A1R, but is also a potent antagonist of the A_{2B} adenosine receptor (A2BR) [40]. Further, A1R antagonism with the more specific antagonist DPCPX did not improve glucose uptake in skeletal muscle [135,136]. While partial A1R agonists have been used to reduce fasting serum NEFA levels in obese rats and humans, to date there remains no conclusive evidence on whether or not A1R agonism can improve whole-body insulin sensitivity and glycemic control [66,67].

As mentioned in Chapter 3, acute A2BR agonism drives lipolysis and glucose intolerance, and A2BR knockout improves glucose tolerance and insulin sensitivity in young mice. Older A2BR knockout mice, however, exhibit increased body weight and fat mass, and impaired glucose tolerance and insulin sensitivity. Chronic A2BR agonism may actually improve metabolic syndrome by decreasing body weight, increasing BAT activation and energy expenditure, reducing adipose tissue inflammation, and decreasing liver expression of lipogenic genes [48,88,89,92,93]. We hypothesized based on our data that upregulated A2BR in adipose tissue contributes to obesity-induced glucose intolerance and insulin resistance, however when considering the aggregate effect of A2BR across all tissues, it is possible A2BR agonism is more beneficial for treating metabolic syndrome than A2BR antagonism.

Currently, the most promising target in the adenosine system for treating metabolic syndrome is the A_{2A} adenosine receptor. Gnad et al demonstrated a profound induction in

energy expenditure in mice with A_{2A} adenosine receptor agonism which resulted in reduced body weight and improved glucose tolerance in obese mice [47]. The major caveat with this approach is that the physiological relevance of brown adipocytes in humans is still highly controversial. Only human clinical trials will be able to determine if this mechanism is a viable approach for improving metabolic syndrome in patients.

Conclusion

Overall, this work has uncovered the dynamic nature of adenosine signaling in adipose tissue and provides new insights into the regulation of adipocyte metabolism. The reciprocal regulation of A1R and A2BR in adipocytes during feeding has broad implications for the role of adenosine in metabolic syndrome, thermogenesis, and circadian rhythms. Significant work is still needed to characterize the regulatory pathways driving the postprandial upregulation of A2BR, as well as the importance of this shift in adenosine receptors to the cyclical regulation of adipocyte metabolism during fasting and feeding.

APPENDIX A

IDENTIFICATION OF RITANSERIN ANALOGS THAT DISPLAY DGK ISOFORM SPECIFICITY

PREFACE

The following appendix was published in Biochemical Pharmacology in collaboration with Dr. Benjamin Purow's lab [137]. Only minor changes have been made to the formatting. Credit is shared with all authors for the writing of this published work.

ABSTRACT

The diacylglycerol kinase (DGK) family of lipid enzymes catalyzes the conversion of diacylglycerol (DAG) to phosphatidic acid (PA). Both DAG and PA are lipid signaling molecules that are of notable importance in regulating cell processes such as proliferation, apoptosis, and migration. There are ten mammalian DGK enzymes that appear to have distinct biological functions. DGKα has emerged as a promising therapeutic target in numerous cancers including glioblastoma (GBM) and melanoma as treatment with small molecule DGKα inhibitors results in reduced tumor sizes and prolonged survival. Importantly, DGKα has also been identified as an immune checkpoint due to its promotion of T cell anergy, and its inhibition has been shown to improve T cell activation. There are few small molecule DGKα inhibitors currently available, and the application of existing compounds to clinical settings is hindered by species-dependent variability in potency, as well as concerns regarding isotype specificity particularly amongst other type I DGKs. In order to resolve these issues, we have screened a library of compounds structurally analogous to the DGKα inhibitor, ritanserin, in an effort to identify more potent and specific alternatives. We identified two compounds that more potently and selectively inhibit DGKα, one of which (JNJ-3790339) demonstrates similar cytotoxicity in GBM and melanoma cells as ritanserin. Consistent with its inhibitor profile towards DGKα, JNJ-3790339 also demonstrated improved activation of T cells compared with ritanserin. Together our data support efforts to identify DGK isoform-selective inhibitors as a mechanism to produce pharmacologically relevant cancer therapies.

INTRODUCTION

Diacylglycerol kinases (DGKs) are a family of enzymes that phosphorylate diacylglycerol (DAG) to form phosphatidic acid (PA) [138]. Both DAG and PA are active signaling molecules that are tightly regulated to influence central cell signals such as Protein Kinase C/D, Ras, mTOR, SHP1, and many others [139–142]. Importantly, the elimination of DAGs via DGKs is considered the main pathway by which DAG-related signaling is attenuated.[142] The mammalian family of DGK enzymes is characterized into 5 classes based on the presence of different functional domains, and is comprised of 10 unique isoforms.[141] While this large number of isoforms has made characterizing the biological function of these enzymes challenging, there is now mounting evidence for involvement of several of these isoforms in a variety of pathological states.

Recently, DGKα has become of particular interest in the cancer field for its dual role in both promoting cancer growth and metastasis and simultaneously suppressing T cell activation.[143] DGKα is a member of the type I isoform group that has been implicated in the progression of many types of cancers, including melanoma and glioblastoma (GBM).[144,145] DGKα has also been identified as an important checkpoint in T cell activation, and overactive DGKα leads to the induction of T cell anergy.[146–150] DGKα inhibition can rescue T cell activation, and DGKA knockout mice have hyperactive T cells that are resistant to anergy.[150,151] In keeping with this, there is now mounting evidence that DGKα inhibition may improve immunotherapies such as chimeric antigen receptor-modified T (CAR-T) cells.[152–154] It is important to note that there is substantial evidence to suggest that DGKζ may be stronger than DGKα in modulating T cells, and the

use of CRIPSR/Cas9 to knock out both DGKα and DGKζ resulted in significant improvements to antitumor activity by human CAR-T cells.[153] However, DGKζ has also been shown to be important for restraining immunosuppressive regulatory T (Treg) cells, as well as suppressing NF-κB activation, thus creating potential complications in targeting it for cancer therapy.[155,156]

Interestingly, there are differential effects on the Ras pathway of DGKα inhibition in cancer cells (decreased) versus in T cells (increased).[157,158] Additionally, DGKα has been shown to have different substrate specificity depending on membrane curvature.[159] This suggests that DGKα has context-dependent effects that vary across cells and tissues and even intracellular conditions. Further, there is evidence for the conversion of specific DAG species into PA in certain cell types that appears to depend on which DGK family member is predominantly expressed.[160–162] It is therefore likely that the biological roles of the various DGK members are distinguished by expression profiles, context of activation, and subcellular localization. This highlights the importance of developing inhibitors with a high degree of specificity for the purposes of cancer treatment.

There are two long-established inhibitors of DGKα that have been used extensively *in vitro* in the laboratory, R59022 and R59949. With the goal of identifying other DGKα inhibitors with higher clinical potential, as well as understanding the chemical features to enable the design of superior inhibitors, we recently characterized the structurally-similar serotonin receptor antagonist ritanserin as a DGKα inhibitor.[163] The primary advantage ritanserin holds over other DGKα inhibitors lies in its characterization in clinical trials as a serotonin receptor antagonist, and which have already demonstrated its safety and beneficial pharmacological properties in human patients.[164] These existing small-

molecule DGKα inhibitors have shown species-dependent variability in potency; ritanserin stimulates human but not mouse T cells, in direct contrast to the effects of R59949 on both. This context-dependent inconsistency may be better understood and addressed by the identification of novel and more potent and specific inhibitors for DGKα. Velnati and colleagues recently published AMB639752 as a minimal pharmacophoric structure for DGKα inhibition that lacks anti-serotonergic activity and demonstrated its selectivity over other DGK isoform types, yet its selectivity over the other type I isoforms has not been explored.[165] Additionally, Liu et al. reported on their compound CU-3, which displays a high degree of potency against DGKα and significant selectivity over other isoforms.[166] However, the *in vivo* safety and toxicity for CU-3 and its related structures remains unknown. Meanwhile, some studies have begun to localize the critical features required of ritanserin and related compounds for DGK inhibition and to identify the mechanism of action, but thus far no new ritanserin analogs have been identified.[167,168] In this study, we screened a compound library generated by Janssen Pharmaceuticals containing compounds structurally similar to ritanserin. We sought to identify ritanserin analogs that provide higher potency against DGKα, as well as selectivity versus other type I DGK isoforms, working toward the ultimate goal of improved DGKα inhibitors for immunotherapy and cancer treatment.

RESULTS

Ritanserin lacks specificity for DGKα over other type I DGK isoforms

The serotonin receptor antagonist ritanserin and the analogs R59022 and R59949 have shown antitumor efficacy both *in vitro* and *in vivo* in multiple cancers, with demonstrated mediation through DGKα.[145,169,170] In characterizing the inhibitory activity of ritanserin against the other type I DGK isoforms, DGKβ and DGKγ, we overexpressed FLAG-tagged DGK isoform constructs and confirmed their expression in HEK 293T cell lysates (Fig. A1 A). To validate subsequent kinase assays, the linear range of activity was identified for each enzyme (Fig. A1 B) alongside a GFP control to ensure that the intensity of enzyme activity would be proportional to the concentration of enzyme assayed.

At the chosen 5 μg of total protein, we determined the relative incorporation of [^{32}P] into our DAG liposomes with each DGK type I isoform (Fig. A1 C) and found that all three isoforms displayed similar levels of enzymatic activity (nmol/min/mg) when normalized to relative expression. With the introduction of the previously characterized DGKα inhibitors ritanserin and R59022 to determine the level of inhibition, we found that at 50 μM, both ritanserin and R59022 significantly inhibit the activity of all three isoforms relative to a DMSO control treatment (Fig. A1 D). While ritanserin and R59022 displayed significant efficacy against DGKα (~63% and ~72% respectively), both inhibitors showed similar activity against DGKγ (~63% and ~70%). Ritanserin and R59022 displayed lower but still significant inhibitory activity against DGKβ (~58% and ~63%). This lack of specificity amongst the type I isoforms lies in contrast to other DGK isoforms such as δ, θ, and ι, and suggests that structural features shared between the isoforms may contribute to

their potential for inhibition by ritanserin.[163]

Screen of a ritanserin analog library points to novel DGKα small-molecule inhibitors

To identify additional compounds with improved selectivity for DGKα over the other type I isoforms, we screened a selected library of 188 compounds with a potential for inhibition of DGKα. The structure of ritanserin consists of two -4-fluoro-benzene rings, a thiazolopyrimidine group, and a protonatable nitrogen which is contained within a piperidine (Fig. A2 A). Having been developed as a serotonin receptor antagonist, the central nitrogen of ritanserin is known to be key for its anti-serotonergic function, but has also been found to be necessary for inhibitory activity towards DGKα.[165] The library of compounds was provided to us by Janssen Pharmaceuticals and was assembled based on their structural similarity to ritanserin.

Using our radiolabeled kinase assay, we screened all 188 ritanserin analogs for inhibitory effects against DGKα enzyme activity, normalized to vehicle. To identify compounds of greatest interest, we established criteria based on the strictly standardized mean difference (SSMD, < -5) and log fold change (< -0.6), and identified 30 compounds that met the thresholds for these criteria (Fig. A2 B and Table A1). When select hits were rescreened alongside ritanserin, nine compounds demonstrated comparable or improved inhibition of DGKα; however, only seven of these compounds had available structural information and were thus chosen for further testing (Fig. A2 C, E-K). Notably, two of these compounds were more similar in structure to the DGKα inhibitor R59949 than ritanserin (Fig A2 D, H, K).

Specificity of ritanserin analogs for DGKα

Based on our initial two screens assessing the ritanserin analogs for potency against DGKα, we next set out to determine the specificity of these compounds for DGKα over the other type I DGK isoforms. We first performed dose-response experiments to determine the IC_{50} and IC_{90} values for the seven candidate compounds towards DGKα resulting from the screen (Table A2). We tested these compounds on DGKβ and DGKγ at their determined IC_{50} and IC_{90} values towards DGKα. Two were identified to have very limited inhibitory activity against the DGK type I isoforms β and γ. Thus, while ritanserin demonstrated a degree of inhibition of DGKβ/γ, compounds JNJ-3790339 and JNJ-3940447 at IC_{50} did not affect DGKβ/γ activity (Fig. A3), demonstrating greater specificity of these compounds towards DGKα.

We further sought to evaluate the specificity of these compounds by determining their inhibition of another DGK subtype. We chose the type IV DGKζ, due to its known role in the suppression of Treg cells and NF-κB activation.[155,156,171] Type IV DGKs are distinct from type I in that they lack the N-terminal RVH and EF Hand motifs which cooperate to control calcium-dependent enzyme activation.[160] They additionally have PDZ-binding and ankyrin domains involved in protein-protein interactions, as well as a MARCKS domain. After confirming expression of DGKζ in our HEK-293T cell lysates, we identified a protein concentration within the linear range of activity (Fig. A4 A, B) and measured activity following treatment with ritanserin, compound JNJ-3790339, and compound JNJ-3940447. Neither ritanserin nor its analogs showed any inhibitory effect on DGKζ at their respective DGKα IC_{50} values (Fig. A4 C).

For the sake of completeness, we tested all of our candidate compounds to assess

their inhibitory activity against DGKβ/γ/ζ at their respective IC_{50} and IC_{90} values against DGKα (IC_{50} in Table A3, IC_{90} not shown). Notably, even at its IC_{90}, JNJ-3790339 continued to show a high degree of selectivity for DGKα. Further, neither ritanserin nor any of the other candidate compounds shows inhibitory activity against DGKζ, lending further evidence for type I specificity of this class of compounds.

Cytotoxicity of ritanserin analogs in cancer cells

One of the potential applications for DGKα small-molecule inhibition is in the treatment of various cancers for which targeting DGKα has demonstrated cytotoxicity.[143–145,169] To determine if our newly identified inhibitors show the same cytotoxic effects against cancer cells *in vitro* and *in vivo* as DGKα inhibition has previously shown,[145] we performed dose response assays with the human melanoma cell line A375, the GBM cell line U251, and the human malignant Jurkat T cell line using ritanserin, ketanserin, JNJ-3790339, JNJ-3940447, and vehicle (Fig. A5 A). Ritanserin and JNJ-3790339 treatment resulted in significant loss in cell viability at 15 μM of compound in both the A375 and U251 cell lines, while none of the compounds had significant cytotoxicity against Jurkat T cells at this concentration (Fig. A5 B). Ritanserin and JNJ-3940447 had cytotoxicity in Jurkat T cells only at high concentrations (40 μM), while JNJ-3790339 was somewhat more potent (Fig. A5 A). A similar lack of potency was seen with JNJ-3940447 across all cell lines with no substantial induction of cytotoxicity until 40 μM.

Activation of primary WT and DGKα$^{-/-}$ T cells with DGKα inhibition

Given the demonstrated ability of the small molecule DGKα inhibitors to promote

T cell activation[172], we investigated whether the inhibitors identified by this screen might also possess this immune-stimulating ability. Human malignant Jurkat T cells were costimulated with functional CD3/CD28 antibodies alongside ritanserin, ketanserin, or the analogs identified by our screen. Treatment with all of the analogs and ritanserin resulted in increased mRNA expression of the early activation marker CD69 and the cytokine tumor necrosis factor alpha (TNFα) versus the DMSO vehicle control (Fig. A6 A). Further, the most potent inhibitor we identified, JNJ-3790339, also displayed the highest activation response with significantly increased CD69 and TNFα expression compared to activation in the presence of DMSO, and a trend towards increased expression of TNFα over activation in the presence of ritanserin. The negative control ketanserin was also included in the assay, as it is structurally similar to ritanserin and its analogs and functions as a serotonin inhibitor, but has no inhibitory activity against DGKα. As expected, ketanserin did not result in increased expression of CD69 or TNFα.

To confirm that the effects of these compounds were specific to their inhibitory activity against DGKα, we isolated and costimulated T cells from the spleens of WT and DGKα$^{-/-}$ mice and treated with three analogs from our initial screen identified as the most potent inhibitors of DGKα (Fig. A6 B). Both JNJ-3790339 and JNJ-3790892 resulted in enhanced activation of T cells from WT but not DGKα$^{-/-}$ mice, though only activation with JNJ-3790892 reached significance. JNJ-3790339 and JNJ-3790892 had among the lowest IC_{50}'s demonstrated by enzyme activity assay, while compound JNJ-3940447 with the second-lowest IC_{50} did not produce such an activating effect. The imperfect correlation between DGKα IC_{50} and T cell activation suggests that there may be additional specific properties of these drugs that modulate their T cell activation, such as differing cell

permeability and retention. Ritanserin was not used in experiments with primary murine T cells due to its previously demonstrated inability to activate murine T cells, but the DGKα inhibitor R59949 was used instead.[172] In these settings the two ritanserin analogs JNJ-3790339 and JNJ-3790892 possess greater potential to stimulate T cells than ritanserin and R59949 (Fig. A6 A-B).

DISCUSSION

The large number of mammalian DGK isoforms and their apparent lack of substrate specificity has made deciphering the individual roles of the different isoforms into an immensely complex task. Having access to selective and specific pharmacological compounds that modulate the activity of individual DGK isoforms is crucial to interrogating the physiological roles of these enzymes. DGKα is a member of the type I isoform group of DGKs that has been implicated in a number of pathological conditions, including glioblastoma and melanoma, and represents a promising therapeutic target.[143] The other type I DGKs, β and γ, possess the same structural domains as DGKα, most notably calcium-binding EF hand motifs which enhance their activity in the presence of calcium. Their structural and functional similarity highlight the importance for identifying specific and selective inhibitors for DGKα. The various isotypes tend to have different subcellular localizations[141], and therefore the unintended off-target effects of inhibiting the wrong DGK may prove to be detrimental. Liu et al have reported on a DGKα inhibitor, CU-3, with a novel scaffold that proved to be both potent and highly selective over all other DGK isoforms and was efficacious in improving the activation of malignant Jurkat T cells.[166] Velnati and colleagues recently identified a novel pharmacophoric structure for inhibiting DGKα with the compound AMB639752, which has improved selectivity for type I DGK isoforms and eliminates the anti-serotonergic activity that is a significant potential limitation of the ritanserin analogues.[165] However, the selectivity of AMB639752 for DGKα over other type I isoforms is unknown, and both compounds lack indications of *in*

vivo activity.

The identification of ritanserin as a DGKα inhibitor demonstrates the value in repurposing therapeutics, as previous clinical trial data have already shown that it is safe and well tolerated in human patients.[164] Initially designed as a serotonin receptor antagonist, its ability to inhibit DGKα suggested its potential for use in the treatment of certain cancers such as glioblastoma and melanoma.[144,145,169] While ritanserin was found to effectively inhibit DGKα and demonstrate cytotoxic effects in cancer cells, its potency was not a great improvement beyond those of the previously identified DGKα inhibitors R59022 and R59949. Furthermore, in this study we found that while ritanserin has a high degree of specificity for type I DGK isoforms[163], there is little specificity across the type I isoforms (Fig. A1). By screening a library of 188 ritanserin analogs initially created by Janssen Pharmaceuticals, we were able to identify 30 additional compounds with significant inhibitory activity against DGKα (Fig. A2, Table A1). We found that two of these compounds in particular, JNJ-3790339 and JNJ-3940447, demonstrated a high degree of selectivity for DGKα over the other type I DGKs (Fig. A3, Table A3). We also investigated the activity of these inhibitors on a DGK from an alternate subtype, the type IV DGKζ. We chose this isoform due to its known role in promoting T cell anergy, a function it shares with DGKα. We found that neither ritanserin nor the analogs JNJ-3970339 and JNJ-3940447 demonstrated any significant inhibitory activity against DGKζ (Fig. A4). While this limits their toxicity, it is possible a compound with dual inhibitory functions against DGKα and DGKζ may have higher therapeutic potential; thus, it may be worth further investigating the activity of these ritanserin analogs against DGKζ. Even when we tested these compounds at their IC_{90}, JNJ-3790339 maintained a

high specificity for DGKα and JNJ-3940447 demonstrated only moderate activity against DGKζ and a downward trend in DGKγ activity that was not statistically significant (~68% inhibition against DGKα vs ~31% against DGKs γ and ζ, not shown). Unfortunately, it remains unclear how the minor differences in the structures of these two compounds yield this higher selectivity. There are currently no crystal structures for any of the type I DGKs, and there was not enough accessible information on structures within this library to perform a structure-activity relationship analysis. Further, the compounds screened in this study were developed by Janssen Pharmaceuticals during a search for psychoactive compounds with antagonistic properties against the serotonin receptors. While we did not test for serotonin receptor antagonism in this study, it is highly likely that all of the compounds identified exhibit significant inhibitory activity against serotonin receptors which could be an important limitation with this class of compounds.

The enhanced potency and selectivity of JNJ-3790339 and JNJ-3940447 against DGKα, however, supported further investigation into their therapeutic potential. GBM is the most common primary cancer of the central nervous system and makes up >51% of all gliomas.[173] It is the most aggressive primary brain tumor with a median survival of 15 months and a 5-year survival rate of less than 5%.[174] GBM is extremely resistant to treatment, even with surgical resection followed by concurrent radiation and chemotherapy, highlighting the need for novel therapeutics. We have previously shown that the overexpression of DGKα found in GBM cells suppresses cAMP levels to drive the key oncogenic pathways mTOR and HIF-1α.[145] Melanoma is another notoriously aggressive and invasive cancer, and while the advent of immunotherapy has resulted in improved patient outcomes over the past decade, there has been demonstrated potential for

the efficacy of adjuvant DGKα inhibition.[145] Inhibition of DGKα with ritanserin or its analog R59022 results in toxicity to GBM cell lines that does not occur in non-cancer derived cell lines.[145,169] We tested JNJ-3790339 and JNJ-3940447 for their ability to induce cell death in the melanoma cell line A375, the GBM cell line U251, and the malignant Jurkat T cell line (Fig. A5). We found that JNJ-3790339 displayed a similar ability as ritanserin to induce cancer cell death, while compound JNJ-3940447 did not induce toxicity within either the GBM cells or Jurkat T cells except at very high concentrations (40 μM). The lack of direct correlation between the potency of DGKα inhibition and toxicity within cancer cells suggests that there may be additional specific properties of these drugs affecting their action in cells, such as cell permeability, retention, or inhibition of other targets.

In addition to their direct effects on cancer cells, novel inhibitors to DGKα have potential to become valuable as adjuncts to cancer immunotherapies. The ability of ritanserin to upregulate T cell activation is an attractive benefit of DGKα inhibition, since immunotherapies have emerged as very effective treatments for some cancer patients. Treatment of immunogenic malignancies such as melanoma have yielded major improvements in patient survival with the advent of immune checkpoint inhibitors. These treatments reverse the immunosuppressive effects of PD-1/PD-L1 and CTLA4, enabling T cells to combat tumor progression. Combining these drugs with an agent such as ritanserin could prove valuable in the clinic, with possible synergistic effects; notably, DGKα has been shown to potentially mediate some of the resistance to PD-1 inhibitors.[175] We sought to determine if JNJ-3790339 and JNJ-3940447 could also promote T cell activation, using a human T cell line and primary T cells isolated from WT and DGKα$^{-/-}$ mice. The

range of analogs we tested enabled us to get a preliminary sense of correlations between DGKα inhibitory potency and T cell activation. We observed in both mouse primary T cells and the Jurkat human T cell line that JNJ-3790339 enhanced the upregulation of CD69 gene expression, an early marker for T cell activation, and exhibited an improved response over ritanserin (Fig. A6). JNJ-3790892 displayed a significant increase in CD69 expression above DMSO in primary T cells but no improvement in potency or selectivity over ritanserin. Importantly, we confirm that these effects are DGKα-mediated, as primary T cells harvested from the spleens of DGKα$^{-/-}$ mice do not show enhanced T cell activation upon treatment with DGKα inhibitors (Fig. A6).

In summary, through these experiments we have identified compounds that more potently and selectively inhibit the promising immunotherapy and cancer target DGKα. In particular, we have identified JNJ-3790339 as a compound with superior selectivity for DGKα, similar induction of toxicity in malignant cells, and improved ability to upregulate T cell activation. JNJ-3790339 shares a high degree of structural similarity to ritanserin and would likely behave similarly *in vivo*. Further investigation is needed to determine a complete structure-activity relationship for this class of drugs, as well as cell permeability and retention, their activity against serotonin receptors, and their *in vivo* pharmacokinetic profile. The potential clinical benefit of these drugs alone and in combinations with available immunotherapies underscores the importance of further pursuit of these repurposed analogs.

FIGURES AND TABLES

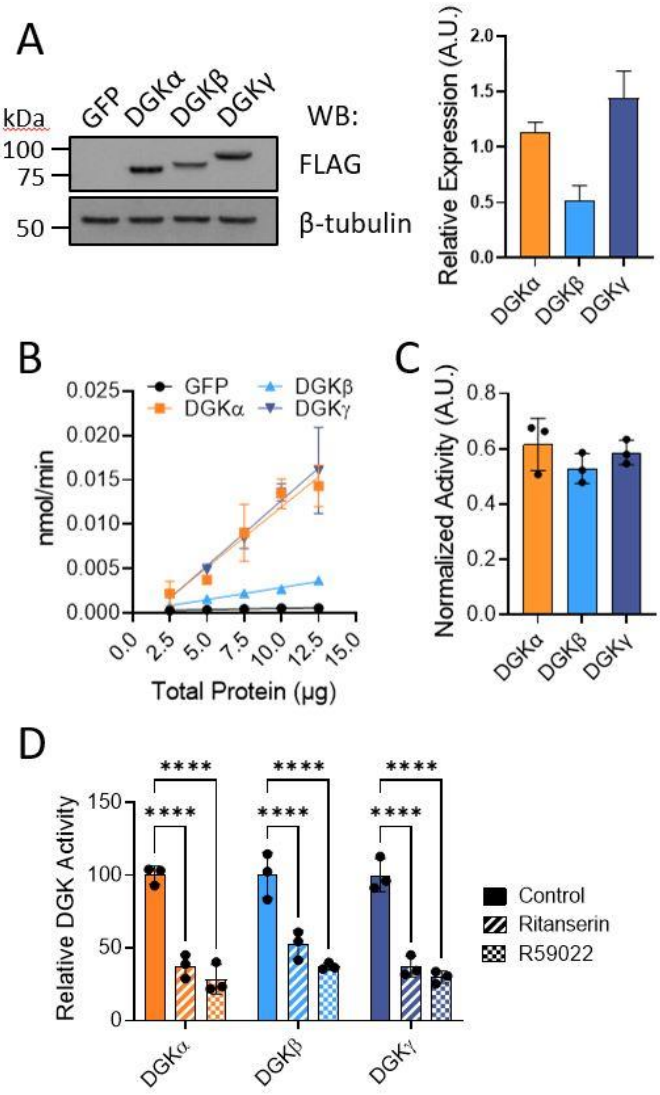

Figure A1: Ritanserin exhibits significant inhibition of all type I DGK isoforms. (A) Representative western blot and quantification for GFP control or indicated FLAG-tagged DGK constructs expressed in HEK-293T cells and harvested 48 hours after transfection. Expression was quantified and normalized relative to β-tubulin. (B) Enzyme activity as a function of the total protein concentration in cell lysates expressing GFP or indicated DGK isoform and measured as nmol of ATP incorporation into PA per minute. (C) Enzyme activity of type I DGKs when assayed with 5 µg total protein of cell lysate, expressed in nmol of ATP incorporation into PA per minute per mg total protein and normalized to the relative expression of each respective DGK. (D) Relative DGK activity with DMSO vehicle or 50 µM of ritanserin or R59022 for type I DGK isoforms. ****p<0.0001, Two-way ANOVA

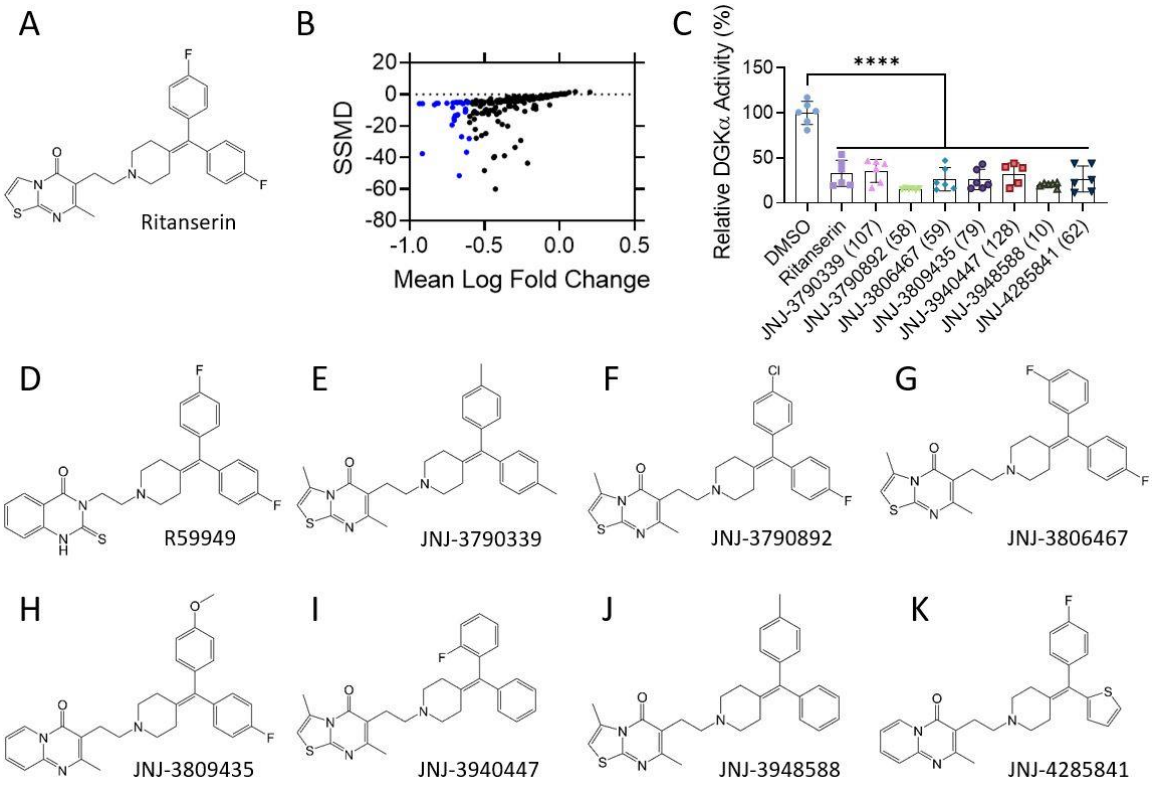

Figure A2: Screening a library of ritanserin analogues reveals additional inhibitors against DGKα. (A) Molecular structure of ritanserin. (B) Dual-flashlight plot for all compounds screened against DGKα. Blue points indicate compounds that met the selection criteria for strictly standardized mean difference (SSMD) and mean log fold change. (C) Relative DGKα activity in confirmation screen. FLAG-tagged DGKα was overexpressed in HEK-293T cells, and DGK activity in 5 µg of protein lysates was measured. DMSO concentration was 0.5% in all assays and all compounds at 50 µM. (D) Molecular structure of the DGK inhibitor R59949. (E-K) Molecular structures for all identified compounds as indicated. ****p<0.0001, One-way ANOVA

Compound (Library #)	SSMD	Log Fold Change
3	-13.47	-0.70
10	-15.15	-0.70
29	-13.24	-0.68
32	-11.19	-0.63
33	-10.17	-0.63
34	-12.81	-0.68
38	-8.30	-0.71
39	-9.41	-0.63
52	-5.12	-0.66
53	-5.59	-0.75
54	-5.04	-0.69
55	-5.38	-0.68
56	-5.99	-0.93
58	-5.75	-0.82
59	-5.73	-0.81
61	-5.03	-0.61
62	-5.96	-0.91
63	-5.38	-0.71
79	-5.01	-0.67
106	-28.00	-0.60
107	-16.45	-0.70
110	-26.87	-0.65
120	-37.52	-0.92
125	-51.47	-0.67
126	-36.56	-0.62
128	-19.41	-0.72
136	-5.20	-0.61
139	-6.61	-0.83
140	-5.18	-0.61
141	-5.97	-0.64

Table A1: Candidate compounds resulting from the primary screening campaign. A list of all 27 compounds identified by the primary screening campaign with a mean log fold-change in DGKα enzymatic activity of ≤-0.6 relative to DMSO, and a strictly standardized mean difference (SSMD) of ≤-5.

Compound	IC_{50} (μM)	IC_{90} (μM)
Ritanserin	27.4	123.3
Ketanserin	-	-
JNJ-3790339 (107)	9.6	429.8
JNJ-3790892 (58)	25.5	260.2
JNJ-3806467 (59)	32.9	223.9
JNJ-3809435 (79)	142.0	>1 mM
JNJ-3940447 (128)	17.5	387.2
JNJ-3948588 (10)	33.0	262.3
JNJ-4285841 (62)	88.4	>1 mM

Table A2: DGKα IC_{50} and IC_{90} values for candidate compounds. All IC_{50} and IC_{90} values for ritanserin and each of the identified candidate compounds calculated from a 5-point dose response curve ranging from 0.1 – 1000 μM. The negative control ketanserin produced no significant inhibition at any concentration, and values above 1 mM are not listed due to lack of sufficient data for accurate calculation.

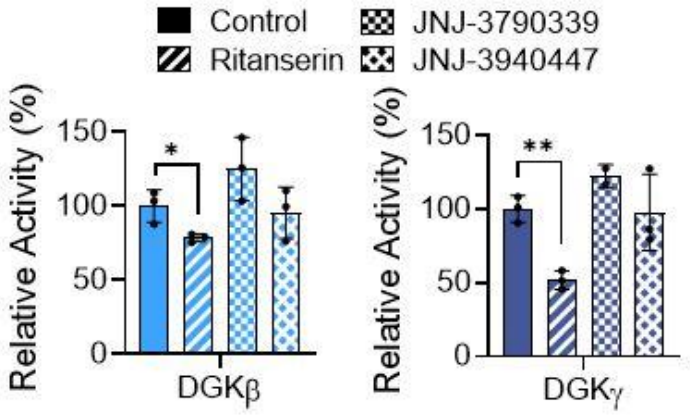

Figure A3: Screening candidates do not exhibit inhibition against other type I DGK isoforms. Inhibitory activity for ritanserin and top candidate compounds against DGKβ and DGKγ. Enzyme assays were performed in the presence of each compound at its calculated IC_{50} value and compared to the relative activity in the presence of an equivalent treatment with DMSO vehicle control. *$p<0.05$, **$p<0.01$, One-way ANOVA

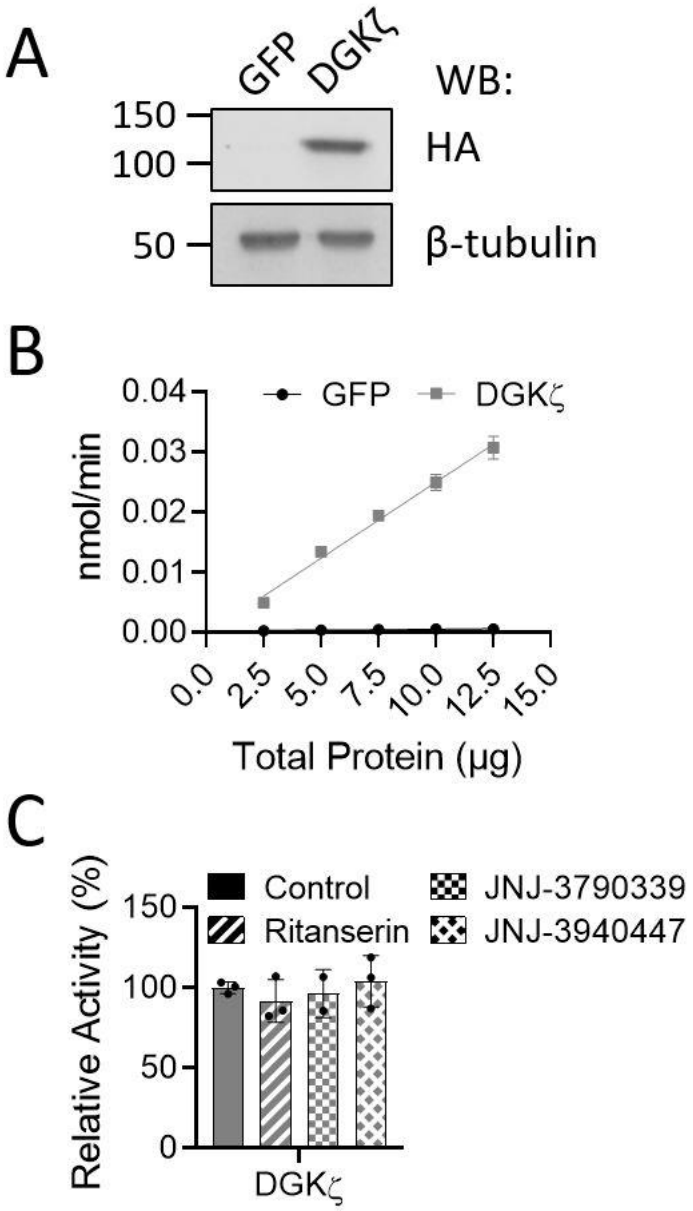

Figure A4: Ritanserin analogues do not significantly inhibit DGKζ. (A) GFP control or HA-tagged DGKζ constructs were expressed in HEK-293T cells, harvested 48 hours after transfection, and expression checked by immunoblot for the HA tag at the appropriate molecular weight. (B) Enzyme activity for cell lysate with overexpressed DGKζ was tested for the range of linearity prior to subsequent experiments. (C) Inhibitory activity against DGKζ for ritanserin and lead candidate compounds at the respective DGKα IC_{50} concentrations, compared to relative activity with DMSO vehicle control.

	DGKβ		DGKγ		DGKζ	
Compound	Relative Activity	p-value	Relative Activity	p-value	Relative Activity	p-value
Ritanserin	0.79	0.6721	0.52	0.0404	0.92	0.9994
Ketanserin	1.08	0.9972	0.91	0.9939	0.93	0.9996
JNJ-3790339	1.25	0.5073	1.42	0.0915	1.38	0.491
JNJ-3790892	0.93	0.9994	0.56	0.0699	1.00	>0.9999
JNJ-3806467	1.09	0.9936	0.71	0.3568	0.81	0.9579
JNJ-3809435	1.14	0.9488	0.52	0.0461	0.75	0.8425
JNJ-3940447	0.95	0.9996	0.98	0.9998	1.04	0.9997
JNJ-3948588	1.05	0.9996	0.75	0.5154	0.91	0.9994
JNJ-4285841	0.62	0.139	0.33	0.0037	0.73	0.7975

Table A3. Specificity at the IC_{50} for all screening candidates. Inhibitory activity for ritanserin, ketanserin, and all identified candidate compounds was determined for DGKβ, DGKγ, and DGKζ at the calculated IC50 values for each compound, or 50 μM for ketanserin. Activity is listed as fold-change relative to DMSO vehicle control.

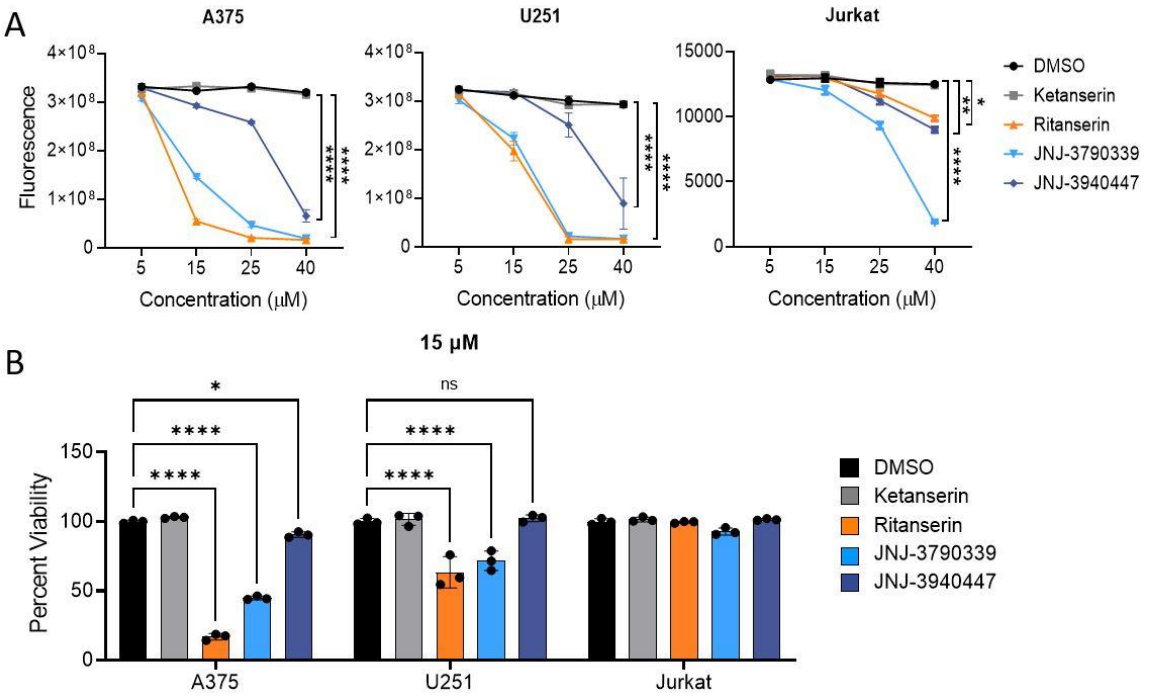

Figure A5: Cytotoxic efficacy of ritanserin, JNJ-3790339, and JNJ-3940447 against cancer cell lines. (A) Dose response curve for cytotoxicity that measures alamarBlue fluorescence from A375, U251, and malignant Jurkat T cells treated with vehicle (DMSO), and the indicated concentrations of ketanserin, ritanserin, and analog compounds JNJ-3790339 and JNJ-3940447. (B) Percent viability of malignant cells treated with 15 μM ritanserin, JNJ-3790339, and JNJ-3940447. *p<0.05, **p<0.01, ****p<0.0001, ns, not significant, Two-way ANOVA

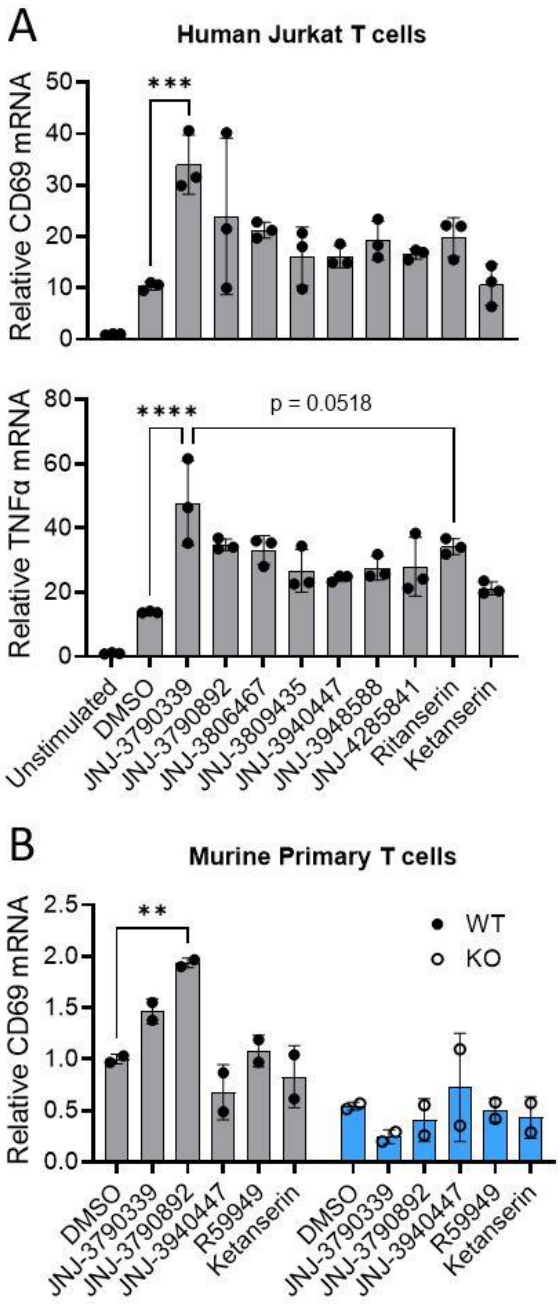

Figure A6: Ritanserin analogs JNJ-3790339 and JNJ-3790892 promote activation of primary murine T cells. (A) The human-derived Jurkat T cell line was unstimulated, or stimulated with 1 μg/mL functional antibodies against CD3/CD28 and treated for 6 hours with DMSO or indicated ritanserin analogs at 5 μM. T cell activation was assessed by qPCR measurement of CD69 and TNFα mRNA levels. (B) Primary isolated murine T cells from WT and DGK$\alpha^{-/-}$ (KO) mice were stimulated and treated for 6 hours with DMSO or indicated inhibitors and T cell activation assessed by CD69 expression as described in (A). **p<0.01, ***p<0.001, ****p<0.0001, one-way ANOVA (A) or two-way ANOVA (B)

METHODS

Materials

[γ^{32}P]-ATP (6000Ci/mmol) was from Perkin Elmer (Boston, MA). The lipid species used in the preparation of liposomes included: 1,2-dioleoyl-sn-glycerol (dioleoyl; 18:1, 18:1), 1,2-dioleoyl-sn-glycero-3-[phospho-L-serine] (PS), and 1,2-dioleoyl-sn-glycero-3-phosphocholine (PC). All lipids and other materials for the preparation of liposomes were from Avanti Polar Lipids (Alabaster, AL). FLAG M2 and HA antibodies, rabbit and mouse alkaline-phosphatase conjugated secondary antibodies, ritanserin, and R59022 were from Sigma-Aldrich (St. Louis, MO). DMSO was from Thermo Fisher Scientific (Waltham, MA). The β-tubulin antibody was from Cell Signaling Technology (Danvers, MA). Ketanserin was from Tocris Bioscience (Avonmouth, Bristol, UK). Anti-Human CD3, clone HIT3a and Anti-Human CD28, clone CD28.2 were obtained from BD Biosciences (San Jose, CA). All other commonly used reagents were from Sigma-Aldrich, unless otherwise indicated. All cell lines were obtained from ATCC (Rockville, MD).

Construction of expression plasmids

The expression plasmids, pcDNA3-FLAG-rat-DGKα[176], pcDNA3-FLAG-rat-DGKβ[177], and pcDNA3-FLAG-rat-DGKγ were gifted to Dr. Kevin Lynch (University of Virginia, School of Medicine) by Dr. Kaoru Goto (Yamagata University, School of Medicine) and were kindly shared with us by Dr. Lynch. The expression plasmid pCMV-rat-DGKζ-HA was a gift from Dr. Matthew Topham (University of Utah, School of Medicine).

Overexpression of DGK isoenzymes

To study the inhibitory activity of compounds against type I DGK isoenzymes (α, β, γ) and DGKζ, human embryonic kidney (HEK 293T) cells (ATCC, Manassas, VA) were cultured in DMEM with 5% fetal bovine serum (FBS) (Gemini Bio-Products, Foundation FBS, West Sacramento, CA) and 1% antibiotic/antimycotic (Fisher Scientific, Waltham, MA). Ten-cm plates of cells were transiently transfected with 5 µg of plasmid DNA for the appropriate plasmid expressing DGK or GFP as a control using polyethyleneimine, 25 kDa linear (Polysciences, Warrington, PA). Cells were fed with fresh media 24 hours after transfection, and 48 hours following the transfection, the cells were harvested and homogenized with a 22 G needle using 300 µL/plate of buffer A (20 mM HEPES, pH 7.2, 150 mM NaCl, 0.5 mM DTT, 0.1% Brij-35, and the protease inhibitors phenylmethylsulfonyl fluoride (PMSF), leupeptin, and pepstatin). The cell lysates were cleared by centrifugation at 16,000 g for 10 min at 4°C. The supernatant was collected and immediately stored at -80°C. For normalizing protein loading in enzyme activity assays, total protein concentration was measured using a BCA protein assay (Thermo Scientific, Waltham, MA).

Western immunoblot analysis

To verify the expression of the DGK isotypes, 50 µg of total protein from cell lysates was separated by 8.75% SDS-PAGE under reducing conditions and transferred onto a polyvinylidene difluoride (PVDF) membrane (Immobilon, Darmstadt, Germany). The membrane was blocked by incubation in Tris-buffered saline with detergent Tween 20

(TBST) containing 10% (w/v) dried milk for 1 hour at room temperature. The TBST contained the following: 50 mM Tris, 150 mM NaCl, and 0.05% (w:v) Tween 20, pH 7.4. The membrane was incubated with monoclonal M2 anti-FLAG antibody (Sigma, F1804) or monoclonal anti-HA (Sigma, H6908) antibody (1:1000) in TBST, at room temperature for 2 hours with gentle agitation. The membranes were then washed with three 5-minute washes with TBST and gentle agitation, and incubated with alkaline phosphatase-conjugated mouse (Sigma, A3562) or rabbit (Sigma, A3687) secondary antibody (1:10,000) diluted in TBST with 2% (w/v) dried milk, for 1 h at room temperature. After three 15-min washes with TBST, the membrane was briefly incubated in chemiluminescent alkaline phosphatase substrate, Applied Biosystems (Poster City, CA). The immunoreactivity was detected using a Fuji LAS 4000. For a loading control, the membranes were stripped using a mild stripping buffer (1.5% (w/v) glycine, pH 2.2, 1% (v/v) Tween 20, and 0.1% (w/v) SDS), blocked again for 1 hour, and incubated with anti-β-tubulin followed by rabbit secondary antibody and chemiluminescent detection as above. Western blot images were quantified using ImageQuant software.

Preparation of liposomes

The preparation of liposomes was modified from our previously reported methods.[163,178] Briefly, PC and DAG were dissolved in $CHCl_3$, and PC was dissolved in 10% isopropyl alcohol in $CHCl_3$; all lipids were combined, and dried under N_2 gas to remove all solvent. The total liposomal concentration of lipids was 10 mol% DAG, 20 mol% PS, and 70 mol% PC. The lipids were hydrated to 10 mM in buffer B (50 mM (3-(N-morpholino)propanesulfonic acid) (MOPS), pH 7.5, 100 mM NaCl, and 5 mM $MgCl_2$).

The lipids were then subjected to five freeze-thaw cycles in liquid nitrogen, followed by extrusion through a 100 nm polycarbonate filter 11 times to generate liposomes with an average diameter of 100 nm.

Kinase assays

The protocol for measurement of DGK activity was modified from our previously reported methods.[163,178] Briefly, the reactions contained buffer B, 0.1 mM $CaCl_2$, 1 mM dithiothreitol (DTT), cell lysate expressing the appropriate DGK or GFP control, and 2 mM lipids. Because enzyme activity can vary between separate preparations due to differences in transfection efficiency, the total protein amount of cell lysate used in each assay was always confirmed to exhibit DGK activity that falls within the linear range. For primary screening of DGKα, 2.8 μg of total protein was used. Five μg of total protein was used for all other corresponding DGK assays. Total protein amount for GFP control was always matched for each DGK. The reactions were initiated by the addition of 10 μL of 10 mM ATP spiked with [γ^{32}P]-ATP to a final volume of 100 μL, and allowed to proceed for 20 min at 30°C. All reactions were terminated with the addition of 0.5 ml of methanol with 0.1 N HCl, followed by 1 ml of ethyl acetate. To facilitate separation of the organic phase, 1 mL of 1 M $MgCl_2$ was added and the solution thoroughly vortexed. To measure the incorporation of [^{32}P] into DAG, 0.5 ml of the organic phase was removed, and the radioactivity was measured using a scintillation counter. The activities of lysates overexpressing DGKs (signal) were normalized to activities of lysates expressing only GFP (background). The specific activities of lysates with GFP represented less than 10% of the signal for all DGKs and were not detectably altered by the presence of inhibitors or DMSO.

The specific activity for each assay was calculated as nmol of product formed per minute per mg of total protein, and then normalized according quantification of Western Blot images to control for differences in DGK isoform expression. Thus, activity is listed as nmol/min/mg/AU of FLAG immunoreactivity, shown as AU. All kinase assays were performed in triplicate or as indicated for inhibitor screening.

Inhibitor Screening

For primary screening of potential inhibitor compounds against DGKα, compounds were dissolved in DMSO, diluted in buffer B, and added directly to kinase assays for a final concentration of 50 μM. The final concentration of DMSO in the reactions was 0.5% (v/v) and did not affect the enzyme activity; DMSO was used as a vehicle control for all screening runs. Screening assays were allowed to equilibrate for 5 min at room temperature following the addition of compound before being initiated with ATP. All compounds were screened in duplicate, and 50 μM ritanserin was used as an internal positive control for all screening runs. All hits were rescreened using the same protocol with a minimum of three biological replicates for confirmation. Inhibitory activity of compounds against other DGKs was similarly tested by diluting the compounds and adding directly to kinase assays for the appropriate IC_{50} concentration, with 5 min for equilibration.

Dose Response for IC_{50} Determination

To determine the IC50 value for ritanserin and all candidate compounds, a 5-point dose response curve was performed with each compound ranging in concentration from 100 nM to 500 μM. Measurements for each dose with all compounds were made with three

independent experiments containing two technical replicates each.

Cell culture and cytotoxicity assay

Human Jurkat malignant T cells, A375 melanoma cell line, and U251 GBM cell line were cultured in DMEM with 10% FBS and 1% penicillin-streptomycin. Cells were plated in 96-well plates and treated in triplicate with 5, 15, 25, and 40 μM of analog compounds or equivalent amounts of DMSO vehicle control. After 48 h, alamarBlue assay was performed to measure cell viability (Bio-Rad, #BUF012B).

Primary T cell harvest and activation assay

Complete RPMI (cRPMI) was prepared with 500 mL RPMI 1640 (Gibco, #11875093), 10% FBS, 1% non-essential amino acids, 1% pen/strep, 1% pyruvate, and 0.1% 2-ME. Spleens from two C57BL/6J and two DGK$\alpha^{-/-}$ mice (10-week) were harvested into 2 mL cRPMI, then dissociated through a 40 μm cell strainer. The cell suspension was centrifuged at 1200 rpm for 5 min, then treated with RBC lysis buffer (0.83% [w/v] NH_4Cl). Cells were pelleted once more and suspended in cRPMI for further T cell isolation with Invitrogen Dynabeads Untouched Mouse T Cells Kit (#11413D) according to the manufacturer's protocols. Isolated T cells were stimulated with 1 μg/mL functional antibodies against CD3/CD28 and simultaneously incubated with 5 μM analogs for 6 hours prior to harvest for subsequent qPCR analysis. Human Jurkat malignant T cells were also similarly stimulated and treated with ritanserin analogs for downstream processing.

Real-Time qPCR

RNA preparation was performed using Qiagen RNeasy Mini Kit, and cDNA synthesis accomplished with Qiagen QuantiTect Reverse Transcription kit according to the manufacturer's instructions. Real-time qPCR was performed using Applied Biosystems Power SYBR Green PCR Master Mix. Expression of target mRNA was normalized to ribosomal 18S RNA and calculated using the $2^{-\Delta\Delta CT}$ method. Primers used were Mouse 18S Forward: GTAACCCGTTGAACCCCATT, Reverse: CCATCCAATCGGTAGTAGCG; Mouse CD69 (PrimerBank ID 221554485c1) Forward: CCCTTGGGCTGTGTTAATAGTG, Reverse: AACTTCTCGTACAAGCCTGGG; Human 18S Forward: CTACCACATCCAAGGAAGCA, Reverse: TTTTTCGTCACTACCTCCCCG; Human CD69 Forward: ATTGTCCAGGCCAATACACATT, Reverse: CCTCTCTACCTGCGTATCGTTTT; Human TNFα Forward: CCTCTCTCTAATCAGCCCTCTG, Reverse: GAGGACCTGGGAGTAGATGAG. Mouse CD69, Human CD69, and Human TNFα primers were sourced from the PrimerBank of the Center for Computational and Integrative Biology of Massachusetts General Hospital and Harvard University.[81–83] Quantification of target amplification was quantified as the relative fold change above DMSO-treated WT controls.

Statistical Analyses

Comparisons between groups were analyzed by either one-way Analysis of Variance (ANOVA) with Dunnett's multiple comparisons test or two-way ANOVA with Dunnett's multiple comparisons test as appropriate and as indicated in the figure legends.

After performing dose-response experiments, a GraphPad Prism function called log [inhibitor] vs. response -- Variable slope (four parameters) was used to calculate IC_{50} values. All values are reported as the mean of triplicate values ± SD. Data shown are representative of at least three independent experiments, except Figure 6 where independent values are shown. Significance was set to $p < 0.05$, and p-values are reported as indicated in the figure legends.

For selection of hits from our primary screen, strictly standardized mean difference (SSMD) was calculated as an estimate of unpaired replicates with unequal variance. Hits were selected based on the criteria of SSMD ≤ -5 and Log_{10} (Fold-change) < -0.6.

APPENDIX B

PHOSPHOREGULATION OF LIPIN 1

PREFACE

This appendix contains a collection of both published and unpublished data regarding the phosphoregulation of the protein lipin 1. In collaboration with the lab of Dr. George Carman, we were able to demonstrate that lipin 1 is a substrate of casein kinase 2 (CK2), that CK2 phosphorylates lipin 1 at two serine residues, Ser-285 and Ser-287, located within a serine-rich domain, and that phosphorylation of these sites regulates lipin 1's interaction with 14-3-3β which has a known role in controlling lipin 1's cytosolic versus nuclear localization [179]. In addition to this published work, we evaluated the involvement of this serine-rich domain in the phosphoregulation of lipin 1's enzymatic activity, as well as the involvement of the specific residues phosphorylated by CK2. This work remains inconclusive in its current state, yet still adds to the current understanding of the phosphoregulation of lipin 1 enzymatic activity and poses new questions which require further investigation. This appendix will cover our evaluation of the serine-rich domain as a regulatory site for lipin 1 enzymatic acitivity, our investigation into the role of Ser-285 and Ser-287 in lipin 1 enzymatic activity, and finally our demonstration of the importance of Ser-285 and Ser-287 for lipin 1's interaction with 14-3-3β. Some figures within this appendix have been previously published, and while the data used to produce these figures

was generated within our lab, credit goes to the lab of Dr. George Carman for the assembly of these figures. Credit is attributed for these figures within the figure legends.

ABSTRACT

The lipin family of enzymes are phosphatidic acid (PA) phosphatases responsible for converting PA to diacylglycerol (DAG), a critical step in the synthesis of triglycerides. Genetic alterations within the lipin family are known to cause severe metabolic and inflammatory abnormalities in both animals and humans, while increased levels of Lipin 1 within adipose tissue of transgenic mice have been shown to improve glucose homeostasis. Lipin 1 is a highly phosphorylated protein, and phosphorylation regulates both its intracellular localization and its enzymatic activity. Phosphorylated lipin 1 interacts with 14-3-3β proteins which facilitates its retention in the cytoplasm. Our lab has previously shown that phosphorylation also negatively regulates the enzymatic activity of lipin 1 in the presence of dianionic PA. Here we present evidence using *in vitro* PA phosphatase assays that loss of phosphorylation within a serine-rich domain (SRD) results in complete ablation of phosphoregulation of lipin 1 enzymatic activity. Dr. George Carman's group, in collaboration with our lab, identified the residues Ser-285 and Ser-287 within the SRD which are phosphorylated by casein kinase 2, a protein kinase which is essential to cell cycle progression. We found no conclusive evidence that these residues are involved in the phosphoregulation of lipin 1 enzymatic activity, however substitution of these residues with non-phosphorylatable alanine resulted in an attenuation of the interaction between lipin 1 and 14-3-3β. Together these results show that the SRD is important for the phosphoregulation of both localization and enzymatic activity of lipin 1. Further, these data provide new insights into the cellular pathways which regulate lipin 1 localization.

INTRODUCTION

Lipin 1 is part of the lipin family of Mg^{2+}-dependent phosphatidic acid phosphatases (PAPs) and is involved in both the synthesis of triacylglycerol and phospholipids as well as transcriptional regulation [180–182]. Lipin 1 catalyzes the conversion of phosphatidic acid (PA) to diacylglycerol (DAG) in the penultimate step of triglyceride synthesis [181,183,184]. Enzymatic activity is dependent on two conserved domains: the NLIP domain located at the amino terminus which contains a conserved glycine residue, and the CLIP domain located at the c-terminus which contains a haloacid dehalogenase-like DXDX(T/V) catalytic motif. The transcriptional activity of lipin 1 is dependent on an LXXIL motif located within the CLIP domain which enables it to regulate fatty acid oxidation genes as a co-activator of PGC-1α [185].

Lipin 1 regulates cellular lipid metabolism at multiple levels through both its enzymatic PAP activity and its transcriptional activity. Lipin 1 deficiency in mice results in lipodystrophy, hepatic steatosis, insulin resistance, peripheral neuropathy, and rhabdomyolysis [182,186,187]. Humans deficient in lipin 1 PAP activity also exhibit rhabdomyolysis, and polymorphisms within the *LPIN1* gene are associated with the development of metabolic syndrome [188,189]. Both the enzymatic activity and transcriptional activity of lipin 1 are regulated by its cellular location which is controlled by post-translational modifications such as phosphorylation, acetylation, and sumoylation [190–194]. The phosphorylation of lipin 1 has been shown to promote the retention of lipin 1 in the cytoplasm and exclusion from the nucleus by facilitating its interaction with 14-3-3 proteins, and negatively regulate both the ability of lipin 1 to bind to PA containing

membranes and its PAP activity [195–197]. Numerous serine and threonine residues modified by phosphorylation have been identified within lipin 1, yet most of these sites have not been associated with either an upstream protein kinase or downstream functional effects [179,190,198]. Given the clear importance of lipin 1 to lipid metabolism, it is critical that we acquire a deeper understanding of the pathways which regulate its enzymatic and transcriptional activities.

Located between the NLIP and CLIP domains, lipin 1 contains a serine-rich domain (SRD) which possesses 7 serine and threonine residues which have been identified as sites of phosphorylation [179]. In this appendix, we present evidence that the phosphosites responsible for regulating lipin 1's ability to associate with PA and catalyze its PAP activity are located within the SRD. In collaboration with Dr. George Carman's lab, we demonstrated that casein kinase 2 (CK2) phosphorylates lipin 1 at two sites within the SRD: Ser-285 and Ser-287 [179]. Herein, we show evidence that these sites are important for the interaction of lipin 1 with 14-3-3β. However, studies on the involvement of Ser-285 and Ser-287 in the regulation of lipin 1 enzymatic activity were inconclusive. Taken together, these data demonstrate that phosphorylation within the SRD of lipin 1 is important for regulating both its interaction with 14-3-3 proteins and its enzymatic activity, but further work is needed to identify the specific phosphosites and protein kinases responsible for the regulation of enzymatic activity.

RESULTS

The SRD is required for the phosphoregulation of PA binding and PAP activity of lipin 1

Our lab has previously shown that phosphorylation regulates lipin 1's association with and enzymatic conversion of dianionic PA [196,197]. Dianionic PA is stable at higher pH levels (≥7.9), but is stabilized at physiological pH levels in the presence of positively charged lipids such as phosphatidylethanolamine (PE) through the hydrogen bond switch mechanism [199]. More details on this mechanism may be found in the introduction of Appendix C. In previously unpublished data from the lab, two truncation mutants of lipin 1β were generated in order to narrow down the location of the phosphosites responsible for this regulation. The first truncation mutant contained the first 316 amino acids (lipin $1^{\Delta 316}$) which critically retains the SRD, while the second truncation mutant contained the first 180 amino acids (lipin $1^{\Delta 180}$) which retains the conserved NLIP domain and nuclear localization sequence/polybasic domain (NLS/PBD) but does not contain the SRD (Fig B1 A). These constructs were purified under conditions in which they were either endogenously phosphorylated or treated with λ-phosphatase to produce a dephosphorylated purified protein. Liposome floatation assays were then used to measure the association of these constructs with PA-containing membranes with 45mol% PE. Both truncation mutants were able to associate with PA at similar levels to WT lipin 1β when dephosphorylated, agreeing with previous studies which have demonstrated that the amino-terminal region of lipin 1 is responsible for binding to PA (Fig B1 B, credit: Sankeerth Takellepati). However, the association with PA was reduced under non-phosphatase treated conditions for lipin $1^{\Delta 316}$,

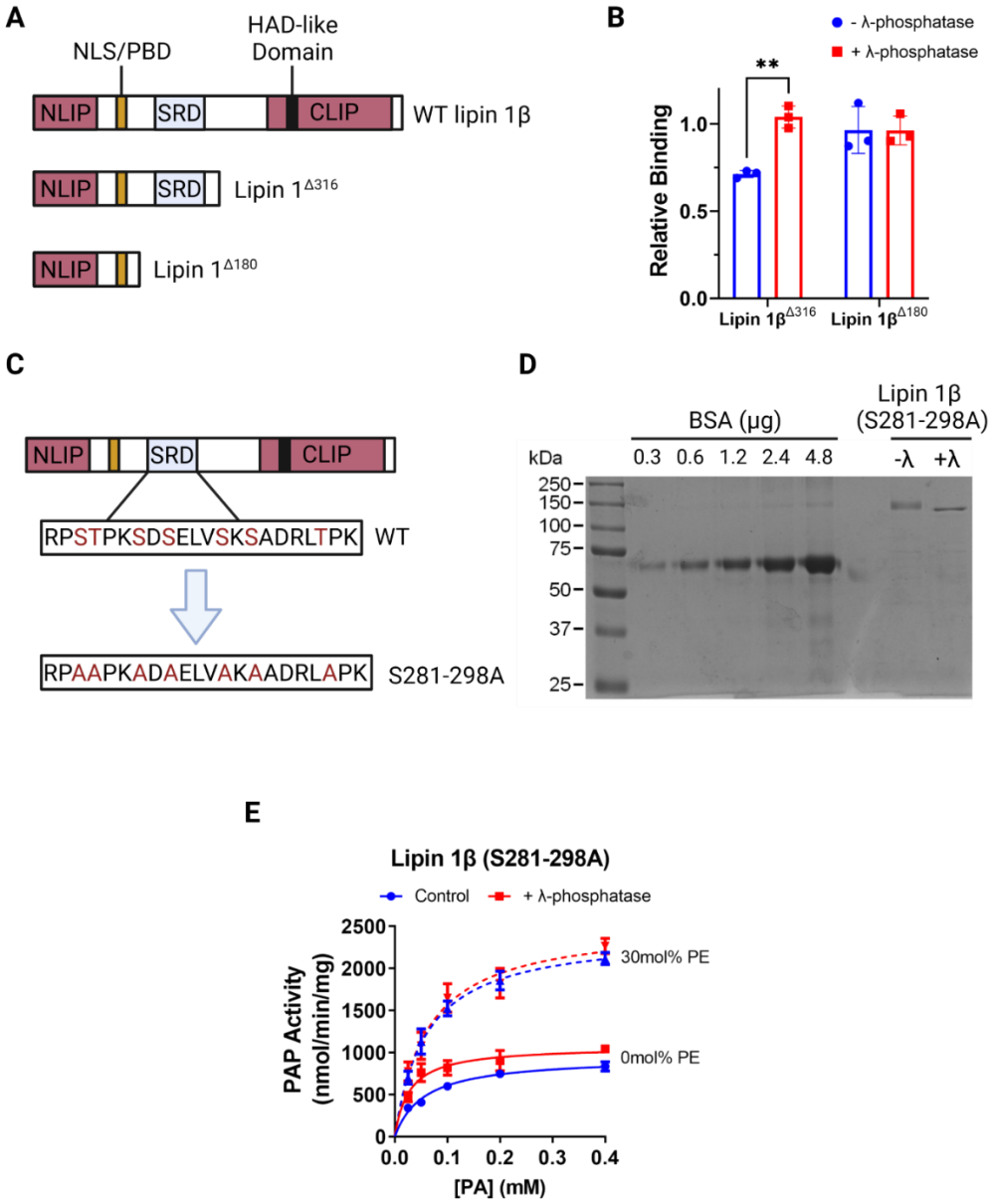

Figure B1: Loss or mutation of the SRD eliminates the phosphoregulation of PA binding and PAP activity by lipin 1β. (A) Diagram of lipin 1β and the truncation mutants containing the first 316 amino acids (Lipin $1^{\Delta316}$) or the first 180 amino acids (Lipin $1^{\Delta180}$) and the functional domains contained within each. (B) Binding of control or λ-phosphatase-treated lipin 1β truncation mutants to PA-containing liposomes with 45mol% PE relative to the total binding observed with λ-phosphatase-treated WT lipin 1β. (C) Diagram of the 7 identified sites of phosphorylation within the SRD and their mutation to alanine within the S281-298A mutant. (D) FLAG-tagged lipin 1β (S281-298A) was overexpressed in HeLa cells and affinity-purified with and without prior incubation with 2000 units of λ-phosphatase. Phosphorylated (-λ) and dephosphorylated (+λ) lipin 1β (S281-298A) proteins were separated by SDS-PAGE along with BSA standards and stained with Coomassie Blue. (E) PAP activity of purified lipin 1β (S281-298A) using PC/PA (0mol% PE, solid lines) and PC/PE/PA (30mol% PE, dashed lines) liposomes. All liposomes contained 10mol% PA. -λ (control, blue) and +λ (red) activities were assayed at pH 7.4.

but not for lipin $1^{\Delta 180}$. This suggested that the phosphosites responsible for regulating lipin 1's enzymatic activity and association with PA may be located within the SRD.

The SRD contains 7 serine and threonine residues located between amino acids 281 and 298 which have all been identified as sites of phosphorylation within lipin 1. We generated a FLAG-tagged mutant in which all 7 of these sites have been mutated to alanine which cannot be phosphorylated (S281-298A, Fig B1 C). We purified this construct by immunoprecipitation under endogenously phosphorylated control or λ-phosphatase-treated conditions (Fig B1 D). We measured the enzymatic activity of this construct on PA-containing liposomes at physiological pH in either the absence or presence of 30mol% PE. As expected, the incorporation of 30mol% PE into the liposomes significantly increased the enzymatic activity of S281-298A (Fig B1 E). However, the activity of the S281-298A mutant was equally enhanced by PE for both the endogenously phosphorylated and dephosphorylated purifications, suggesting that phosphorylation no longer negatively regulates lipin 1 in the absence of the phosphosites located within the SRD.

The target residues of CK2 phosphorylation do not regulate lipin 1 PAP activity

In collaboration with Dr. George Carman's lab, we determined that CK2 phosphorylates lipin 1β at two residues located within the SRD: Ser-285 and Ser-287 [179]. We therefore wondered whether these residues might be responsible for the phosphoregulation of lipin 1 enzymatic activity. We generated and purified a mutant in which each of these residues was mutated to the non-phosphorylatable alanine under

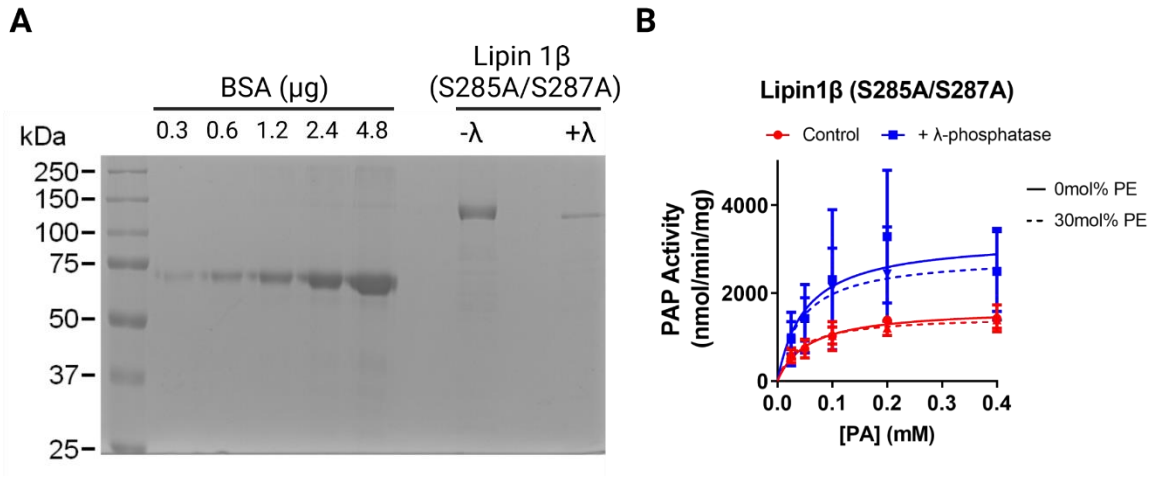

Figure B2: Phosphorylation of Ser-285 and Ser-287 do not regulate lipin 1 PAP activity. (A) FLAG-tagged lipin 1β (S285A/S287A) was overexpressed in HeLa cells and affinity-purified with and without prior incubation with 2000 units of λ-phosphatase. Phosphorylated (-λ) and dephosphorylated (+λ) lipin 1β (S285A/S287A) proteins were separated by SDS-PAGE along with BSA standards and stained with Coomassie Blue. (B) PAP activity of purified lipin 1β (S285A/S287A) using PC/PA (0mol% PE, solid lines) and PC/PE/PA (30mol% PE, dashed lines) liposomes. All liposomes contained 10mol% PA. -λ (control, blue) and +λ (red) activities were assayed at pH 7.4.

control or λ-phosphatase-treated conditions (S285A/S287A, Fig B2 A). When we measured PAP activity, however, we found that λ-phosphatase treatment still enhanced the enzymatic activity of lipin 1β S285A/S287A (Fig B2 B). Unexpectedly, this enhancement in activity occurred even in the absence of PE incorporation within the liposomes. Further, the incorporation of 30mol% PE did not produce any enhancement of PAP activity for either control or λ-phosphatase-treated lipin 1β S285A/S287A. We performed PAP assays for three separate purifications, and while activity was quite variable between separate purifications, this trend in enhanced activity with λ-phosphatase and no change in activity with PE incorporation remained consistent. Since Ser-285 and Ser-287 did not appear to be involved in the phosphoregulation of lipin 1 PAP activity, and we did not have a suitable explanation for the loss of response to dianionic PA in the presence of PE, we did not pursue the involvement of these residues in the regulation of lipin 1 PAP activity further.

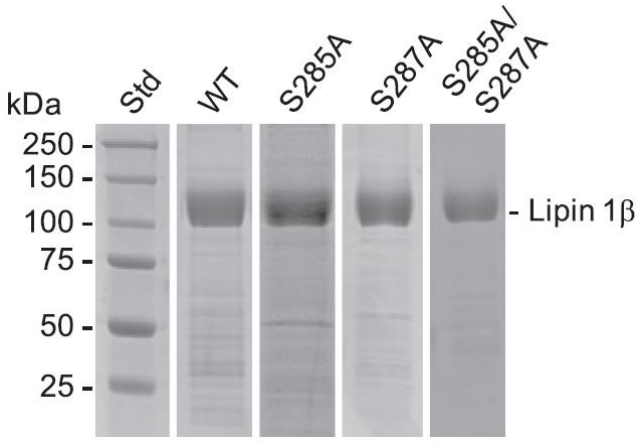

Figure B3: SDS-PAGE analysis of purified mouse lipin 1β proteins. Mouse FLAG-tagged lipin 1β was expressed in HeLa cells and purified by affinity chromatography. Samples of the purified preparations of the WT (3.9 µg), S285A (1.7 µg), S287A (4.8 µg), and S285A/S287A (1.4 µg) lipin 1β were subjected to SDS-PAGE and stained with Coomassie Blue. The positions of lipin 1β and molecular mass standards (Std) are indicated. Credit for the assembly of this figure goes to the lab of Dr. George Carman.

Loss of phosphorylation at CK2 target residues attenuates the interaction of lipin 1 with 14-3-3β

Since phosphorylation is also important in the regulation of lipin 1's cellular localization through its interaction with 14-3-3 proteins, we next chose to investigate the involvement of Ser-285 and Ser-287 in lipin 1 and 14-3-3 binding. In order to investigate this, we first generated and purified mutants in which each of these residues was mutated individually to the non-phosphorylatable alanine, as well as the previously generated double mutant S285A/S287A (Fig B3). We then performed pulldown assays with a GST-tagged 14-3-3β incubated with the WT, S285A, S287A, and S285A/S287A forms of FLAG-tagged lipin 1β. WT lipin 1β was found to interact with 14-3-3β, which is consistent with the previously published finding that lipin 1α interacts with 14-3-3β (Fig B4 A) [195]. Further, while WT lipin 1β was present following pulldown with GST-tagged 14-3-3β, it was not present following pulldown with GST indicating that this interaction was specific (Fig B4 B). We compared the relative inputs of each lipin 1β construct in order to determine the efficiency of pulldown for WT lipin 1β and each of the mutations (Fig B4 C). We found

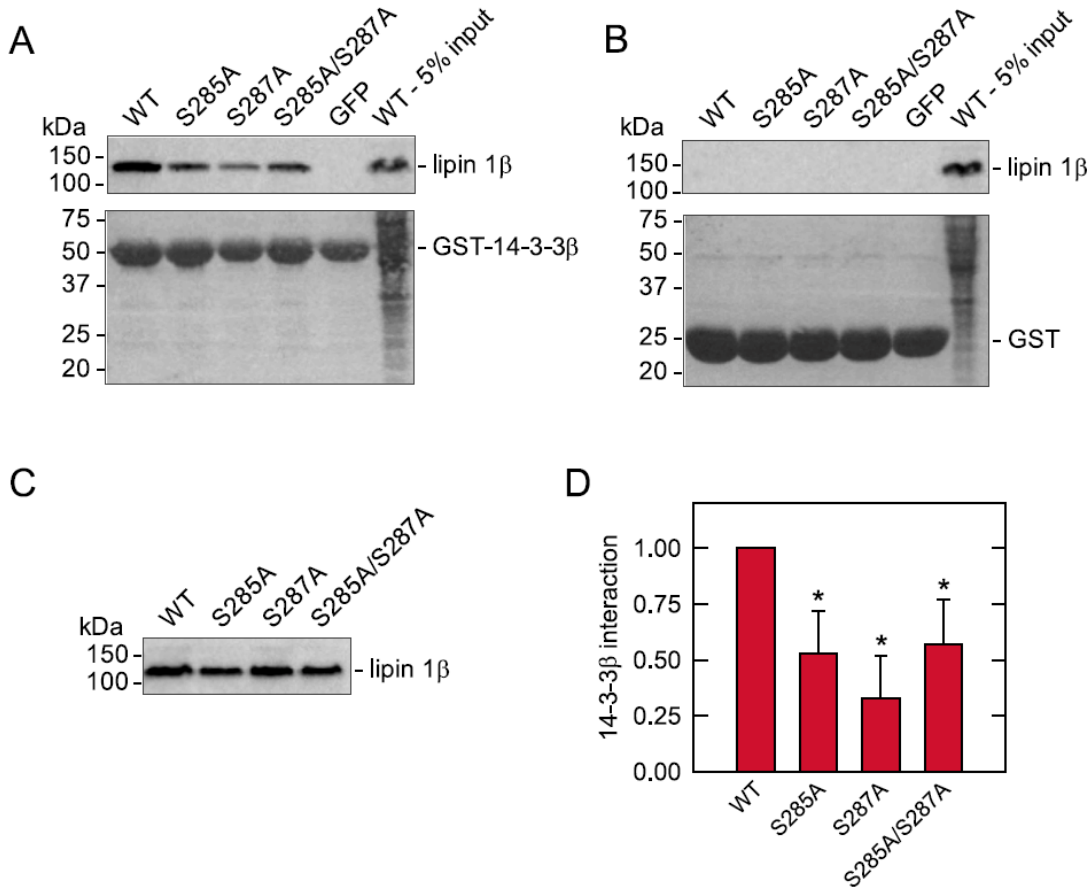

Figure B4: Effects of the phosphorylation-deficient mutations of lipin 1β on its interaction with 14-3-3β protein. (A,B) GSH-Sepharose bound GST-14-3-3β (A) or GST (B) was incubated with the HEK-293T cell lysate (1 mg of protein) containing the WT or the S285A, S287A, or S285A/S287A mutant form of lipin 1β at 4 °C for 2 h. Following the collection of the resin and extensive washing, the proteins were eluted and separated by SDS-PAGE. The resolved proteins were transferred to PVDF membrane and analyzed for lipin 1β by immunoblotting with anti-FLAG antibodies. The lipin 1β signals on the immunoblots were acquired with a Fuji LAS 4000 analyzer and quantified with Multi Gauge software. The GST-14-3-3β and GST proteins on the blots were visualized by staining with Ponceau S. (C) A blot showing the lipin 1β input (5%) of the experiment. (D) Quantification of the amount of lipin 1β after pulldown normalized to input and relative to WT. GFP was included as a negative control. The positions of lipin 1β, GST-14-3-3β, GST, and molecular mass standard are indicated. The data shown in A–C are representative of four independent experiments, whereas the data in D are the average of the four experiments ± S.D. (error bars). *, $p < 0.05$ versus WT by one-way ANOVA. Credit for the assembly of this figure goes to the lab of Dr. George Carman.

that, relative to WT lipin 1β, all of the mutant forms displayed reduced interaction with 14-3-3β (Fig B4 D). There was, however, no significant difference in the amount of interaction with 14-3-3β between the mutant forms.

DISCUSSION

Lipin 1 is a key regulatory protein in lipid metabolism through both its enzymatic PAP activity and its transcriptional effects on fatty acid oxidation genes [180–182]. This is readily apparent by the many pathophysiological defects which manifest upon the loss of lipin 1 function [182,187–189,200]. Lipin 1 is a highly phosphorylated protein with 44 serine and threonine residues having been identified as sites of phosphorylation so far, and phosphorylation regulates both its subcellular localization and its enzymatic activity [179,190,195–198]. In this work, we show that the serine rich domain is necessary for the effects of phosphorylation on PA binding by lipin 1. Mutation of only 7 residues within the SRD to alanine eliminated the phosphoregulation of lipin 1 PAP activity. Two of these residues, Ser-285 and Ser-287, were identified as targets of CK2 activity. Mutation of these two residues alone to alanine did not eliminate the regulation of lipin 1 PAP activity by phosphorylation. However, mutation of either or both of these residues to alanine significantly attenuated the interaction of lipin 1β with 14-3-3β. Taken together, these data indicate that the SRD in lipin 1β is a critical site of phosphoregulation which is involved in the regulation of lipin 1 subcellular localization, PA binding, and PAP activity.

Phosphorylation is well established as an important regulator of lipin 1 PA binding [196,197]. In previously unpublished data from our lab, truncation mutants of lipin 1β were used to investigate the region responsible for this phosphoregulation. In this experiment, a truncation of lipin 1β containing only the first 180 amino acids was able to exhibit the same amount of PA binding as dephosphorylated WT lipin 1β (Fig B1 B). This is consistent with previously published literature showing that the polybasic domain is the major site

involved in PA binding [197]. The SRD has previously been implicated in regulating the subcellular localization of lipin 1, and the high density of identified phosphosites in this region indicate that it is a key regulatory site [195]. It was therefore unsurprising that residues within the SRD were necessary to the regulation of both PA binding and PAP activity (Fig B1). At the same time, this work significantly narrows down the residues critical for this phosphoregulation and provides a foundation for further investigations into the pathways which regulate lipin 1 activity.

The identification of lipin 1 as a target of CK2 provides new insights into the cellular pathways which regulate lipin 1 [179]. CK2 is essential to cell viability and cell cycle progression, and interestingly lipin 1 has recently been linked to the regulation of ER membrane biogenesis during mitosis [201–204]. CK2 is also activated by insulin, and lipin 1 is known to be phosphorylated at multiple sites outside of the SRD in response to insulin suggesting that the regulation of lipin 1 by insulin is complex and multifaceted [198,205–207]. The maintained phosphoregulation of lipin 1 when Ser-285 and Ser-287 are mutated alanine may indicate that CK2 is not involved in directly controlling lipin 1 PAP activity, or it may simply indicate that multiple phosphosites controlled by multiple kinases are involved in the full phosphoregulation of PAP activity (Fig B2). More extensive work is needed to further investigate the involvement of all 7 phosphosites located within the SRD. The identification of Ser-285 and Ser-287 as both targets of CK2 and important phosphosites for the interaction of lipin 1 and 14-3-3 proteins, however, suggests that CK2 is primarily involved in regulating lipin 1 subcellular localization (Fig B3,4). Since lipin 1 localized in the cytoplasm is associated with lower PAP activity, CK2 would be expected

to attenuate lipin 1 enzymatic activity, consistent with its negative regulation of other lipid synthesis enzymes such as acetyl-CoA carboxylase [207]. Overall, this work advances our understanding of the regulatory pathways involved in lipin 1 function as well as the regulation of lipid metabolism by CK2.

METHODS

Cell culture

Human cervical cancer cells (HeLa) and HEK-293T cells were cultured in DMEM supplemented with 5% FBS (VMR Life Science Seradigm, Radnor, PA) and 1% antibiotic/antimycotic (Life Technologies, Inc.).

Preparation of lipin 1β proteins

Venus-tagged WT lipin 1β was generated by subcloning the Venus cDNA in frame with the N terminus of lipin 1β downstream from the FLAG epitope tag in the pcDNA3 vector. Truncation mutants were generated by PCR subcloning. The S281-298A, S285A, S287A, and S285A/S287A mutations in mouse lipin 1β were made using PCR site-directed mutagenesis in the pcDNA3 vector with FLAG-tagged lipin 1β inserts. The mutagenesis was confirmed by DNA sequencing. The FLAG-tagged lipin 1β cDNAs were placed into pAdTRACK-CMV; the shuttle vector was recombined with pAdEasy, and adenovirus was made by transformation of the linearized recombined plasmid in HEK-293 cells. The lipin 1β proteins were prepared by infection of HeLa cells and harvesting 3 days post-infection and purified after incubation with or without λ-phosphatase treatment as described in Appendix C.

For the GST-14-3-3β interaction studies, the FLAG-tagged WT or mutant forms of lipin 1β were expressed in HEK-293T by transient transfection. HEK-293T cells in a 10-cm plate were transfected with 5 μg of pcDNA3-FLAG-Lpin1β (WT, S285A, S287A, or

S285A/S287A). Three days post-transfection, the cells were scraped in 10 mM Na2HPO4 buffer (pH 7.4) containing 50mM β-glycerophosphate, 50mM NaF, 1mM EDTA, 1mM EGTA, 0.1% Nonidet P-40, 10 µg/ml leupeptin, 10 µg/ml pepstatin A, and 1 mM PMSF and centrifuged at 16,000 × g for 10 min at 4 °C to obtain the clarified cell lysate.

PA binding assays

Binding of lipin to liposome vesicles was measured as previously described with minor modifications [208]. In brief, PC/PE/PA (35mol% PC, 45mol% PE, 20mol% PA) were hydrated to 10mM in buffer A (50 mM Tris-HCl, 1 mM EDTA, pH 7.2). Liposomes were prepared as in Appendix C. The reaction volume was 100 µl and contained Venus-FLAG-tagged WT lipin 1β or truncation mutants as indicated, 2 mM PA, and buffer C and binding was allowed to proceed for 30 min at 30 °C with gentle agitation. An equal volume of 80% sucrose (w/v) was added, and this mixture was carefully layered over 270 µl of 80% sucrose (w/v) in 5 × 41-mm Beckman centrifuge tubes, then overlaid by 150 µl of 20% sucrose (w/v) and finally 100 µl of buffer C. The sucrose gradients were centrifuged in an SW55Ti swinging bucket rotor containing nylon inserts at 240,000 × g for 1 h. After centrifugation, the top 100 µl of the gradients containing the liposomes and bound lipin proteins were collected, and PC-pyrene and Venus absorption were measured. The Venus absorption from samples was normalized to input Venus readout from protein and buffer only. Similarly, PC-pyrene from samples was normalized to input PC-pyrene measurement from liposomes and buffer only. To determine the fraction of lipins bound to liposomes, Venus absorption values were normalized to that of PC-pyrene.

PAP assays

The method for performing PAP assays is extensively described in Appendix C.

Preparation of GST-14-3-3β protein

Escherichia coli BL21 (DE3) pLysS cells were transformed with pGEX4T3 or pGEX4T3-14-3-3β. The E. coli transformant was inoculated into 800 ml of lysogeny broth medium containing 100 μg/ml ampicillin and grown to A600 nm = 0.5. Transgene expression was induced with the addition of 0.5 mM isopropyl-β-D-1-thiogalactopyranoside, and cultures were incubated for an additional 2 h. The E. coli culture was harvested by centrifugation and lysed by sonication in PBS (pH 7.4) containing 0.5% Nonidet P-40, 10 μg/ml leupeptin, 10 μg/ml pepstatin A, and 1 mM PMSF. The sonicate was centrifuged at 16,000 × g for 10 min at 4 °C, and the supernatant was used as cell lysate. The lysate containing the overexpressed GST or GST-14-3-3β (850 μg of protein) was incubated with GSH-Sepharose at 4 °C for 1 h, followed by washing of the resin three times with sonication buffer.

Analysis of lipin 1β interaction with GST-14-3-3β protein

GSH-Sepharose–bound GST-14-3-3β or GST was incubated with the HEK-293T lysate (1 mg of protein) containing the WT or the S285A, S287A, and S285A/S287A

mutant forms of lipin 1β at 4 °C for 2 h with rotation and washed three times with 10mM Na2HPO4 buffer (pH 7.4) containing 50mM β-glycerophosphate, 50 mM NaF, 1 mM EDTA, 1 mM EGTA, 0.1% Nonidet P-40, 10 μg/ml leupeptin, 10 μg/ml pepstatin A, and 1 mM PMSF, followed by two additional washes with the same buffer containing 450 mM NaCl. Proteins were eluted from GSH-Sepharose by incubation in Laemmli's sample buffer at 70 °C, followed by SDS-PAGE, transfer to PVDF membrane, and immunoblot analysis. Mouse anti-FLAG and alkaline-conjugated goat anti-mouse antibodies were used at dilutions of 1:1,000 and 1:30,000, respectively. GST-14-3-3β or GST on the PVDF membrane was visualized by staining with Ponceau S. The images of immunoblot signals and Ponceau S staining were acquired with a Fuji LAS 4000 analyzer, and lipin 1β proteins were quantified with Multi Gauge software.

APPENDIX C

PURIFICATION OF LIPIN AND MEASUREMENT OF PHOSPHATIDIC ACID PHOSPHATASE ACTIVITY FROM LIPOSOMES

PREFACE

The following appendix was published as a methods chapter within Methods in Molecular Biology [178]. This chapter describes a method for the purification of mammalian lipins, and the assaying of their enzymatic PAP activity with the use of radiolabeled, PA-containing liposomes. I would like to acknowledge the work of Dr. James Eaton and Dr. Salome Boroda who initially established this method within the lab.

ABSTRACT

The lipin family of enzymes are phosphatidic acid (PA) phosphatases responsible for converting PA to diacylglycerol (DAG). Lipins therefore occupy a central node in the synthesis of triacylglycerol (TAG) and phospholipids, and may play a role in regulating the levels of PA and DAG as signaling molecules. Some enzymatic assays used to measure PA phosphatase activities use detergents above their critical micelle concentration to present substrate; however, these methods do not represent the physiological membrane bilayers found in cells and these conditions can drastically alter phosphatase activities. Other assays use poorly defined mixtures of phosphatidylcholine (PC), PA, and high concentrations of BSA to present substrate. In this chapter, we describe methods for affinity purification of FLAG-tagged lipin proteins, and an alternative enzymatic assay using small unilamellar vesicles, also known as liposomes, to investigate specific activities of PA phosphatases. These activities are measured using an acidified Bligh–Dyer extraction to separate the water-soluble, radiolabeled, inorganic phosphate released during the assay from the chloroform-soluble PA.

INTRODUCTION

Lipins are a class of mammalian Mg^{2+}-dependent phosphatidic acid phosphatases (PAPs) that are centrally involved in the synthesis of triacylglycerol and phospholipids [180–182]. The lipin family consists of three members (lipins 1-3) which convert phosphatidic acid (PA) to diacylglycerol (DAG) [181,183,184]. Additionally, lipin 1 plays a role as a transcriptional co-activator in the activation of fatty acid oxidation genes [185]. The lipin family members are amphiphilic, and their translocation from the cytosol to various membranes is required for their enzymatic activity [191,209]. The subcellular localization of the lipins is regulated by both nutrient and hormonal signaling and is thought to occur via post-translation regulation [190,195,198,210]. Phosphorylation has been shown to both regulate lipin subcellular localization [190,195,198] and to negatively regulate the enzymatic activity of lipin 1, however the mechanisms behind this regulation remain unclear [196,197].

Amphiphilic lipid modifying enzymes exhibit surface dilution kinetics due to the 2D surface nature of cellular membranes. Amphiphilic lipid modifying enzymes depend not only on the bulk concentration of substrate, but also the surface concentration of substrate within the two-dimensional membrane surface [211]. Properly assaying such enzymes requires the determination of kinetics for both the bulk step, in which the enzyme binds to the lipid surface, as well as the surface step, in which the enzyme binds to its lipid-substrate molecule. The use of nonionic detergent micelles, particularly Triton X-100, has been suggested as an ideal method for such assays (Carman, Raymond, & Dennis 1995). Triton X-100 can form homogenous mixed micelles with a variety of lipids, and surface

dilution experiments may be performed with minimal effects to the surface characteristics such as size, charge, or area per molecule. However, while micelles present uniform characteristics ideal for such kinetic analyses, they do not represent the native membrane bilayers that are the targets of lipid modifying enzymes. It is therefore possible that with this method of substrate presentation, various aspects of enzymatic activity may be constrained or overemphasized.

Because the lipin family members are amphiphilic, the method used to present the PA substrate can have drastic effects on specific activity. Indeed, the lipin family displays significantly higher specific activity when assayed in Triton micelles as compared to liposomes, and the molecular basis for this observation remains elusive [196,197]. In addition, both the specific activity and the post-translational regulation of lipin is clearly dependent on the context of substrate presentation [196,197,212]. At physiological pH, PA exists as a mono-anionic lipid species, yet lipin 1 has been shown to have preferential binding to di-anionic PA [196,199,213]. The hydrogen bond switch mechanism has been proposed as the method by which positively charged lipids such as phosphatidylethanolamine (PE) stabilize di-anionic PA at physiological pH to enhance lipin binding [199]. Using liposomes with 30 mol% PE, representative of the endoplasmic membrane, the presence of PE has been shown to enhance lipin activity, and phosphorylation has been shown to negatively regulate lipin 1 enzymatic activity only in the presence of PE [196,214]. In this chapter, we describe a method for preparing unilamellar liposomes with a uniform size of 100-nm containing 10 mol% of radiolabeled [^{32}P]PA, and their use for assaying PAP specific activity. Similar to previously described

micelle methods, these activities are measured by extracting the water-soluble radiolabeled inorganic phosphates released during the reaction.

PURIFICATION OF LIPINS

Equipment

1. 150-mm treated tissue culture dish
2. Cell scraper
3. 22-gauge needle
4. 5 mL syringe
5. Disposable filter column (Fisher Scientific, 11-387-50)
6. 50 mL polypropylene conical tubes
7. 15 mL polypropylene conical tubes
8. 1.5 mL microcentrifuge tubes

Buffers and Reagents

1. Anti-FLAG M2 Affinity Gel beads (Sigma, A2220)
2. FLAG peptide (Sigma, F3290)
3. λ-phosphatase (NEB, P0753L)
4. Phosphate buffered saline
5. Lysis Buffer A (150 mM NaCl, 20 mM HEPES, 0.1% Brij 35, 10 μg/mL Leupeptin, 10 μg/mL Pepstatin A, 1 mM PMSF, 0.5 mM dithiothreitol, pH 7.2)
6. Phosphatase Buffer B (100 mM NaCl, 50 mM HEPES, 2 mM dithiothreitol, 1 mM $MnCl_2$, pH 7.0)
7. Wash Buffer C (150 mM NaCl, 20 mM HEPES, 10 μg/mL Leupeptin, 10 μg/mL Pepstatin A, 1 mM PMSF, 0.5 mM dithiothreitol, pH 7.2)

8. Elution Buffer D (150 mM NaCl, 20 mM HEPES, FLAG peptide 1.0 mg/mL, pH 7.2)

The cloning of the mammalian PAP enzymes allows assays to be run with purified, recombinant enzyme to enable accurate calculations of specific activity. This method may also be used with cleared cell lysates for qualitative comparisons of specific activity. The addition of the FLAG tag (Sigma, DYKDDDDK) allows for single-step affinity purification to a high degree of purity, as has been previously described [215,216].

The lipin family are highly phosphorylated, and the phosphorylation status of lipin 1 correlates with its subcellular localization[190]. As phosphorylation of the lipin family may impact enzymatic activity, it may be of interest to isolate lipin proteins in a non-phosphorylated form. This can be achieved post-isolation by phosphatase treatment of the protein during purification.

1. For a typical purification of 100-500 μg of lipin divided into phosphatase treated and untreated, infect 40 × 150-mm plates of HeLa cells with an adenovirus containing an N-terminal FLAG tagged (DYKDDDDK) lipin construct. For best expression we seek >90% infection efficiency. Transfection of HEK-293T cells may also be used. (See note 1)
2. Allow the cells to grow for 48-72 hours to achieve maximal expression. Add fresh media 24 hours prior to harvesting.

3. Prior to harvesting cells, cool 500 mL of PBS on ice and place 2 sterile 50 mL conical tubes on ice. Additionally, place culture dishes of the infected HeLa cells on ice immediately prior to harvesting. (See note 2)
4. Aspirate off all media, and rinse the cells with 5 mL of cold PBS.
5. Aspirate off all PBS, then add another 2 mL of cold PBS. Use a scraper to dislodge all cells from the surface of the culture dish and pipette them into the sterile 50 mL conical tubes on ice.
6. Centrifuge the harvested cells at 200 g for 5 minutes to pellet, then aspirate off all supernatant. (See note 3)
7. Lysis Buffer A (150 mM NaCl, 20 mM HEPES, 0.1% Brij 35, pH 7.2) may be prepared in advance and stored at 4 °C. Add protease inhibitors (10 μg/mL Leupeptin, 10 μg/mL Pepstatin A, 1 mM PMSF) and 0.5 mM dithiothreitol to Buffer A immediately prior to use.
8. To each pellet, add 500 μL of lysis Buffer A per 150-mm plate harvested in the pellet.
9. Pass the cells through a 22-gauge needle 6-7 times using a 5 mL syringe to homogenize the cells and ensure complete shearing of cellular membranes.
10. Pipette the homogenate into 1.5 mL microcentrifuge tubes, and spin in a 4°C centrifuge at 16,000 g for 10 minutes.
11. During the 10 minute spin, prepare Anti-FLAG M2 Affinity Gel beads (Sigma, A2220). Add the beads to a 1.5 mL microcentrifuge tube using 15 μL compacted gel volume of beads per 150-mm plate harvested, and spin at 1000 g for 1 minute to pellet.

12. Aspirate off the storage buffer from the beads and suspend the beads in 500 µL lysis Buffer A.
13. Combine homogenate supernatants into a 50 mL conical tube, and add the Anti-FLAG M2 Affinity Gel beads to the homogenate. Use the homogenate to rinse the beads out of the microcentrifuge tube to collect all of the beads.
14. Place the combined homogenate with affinity gel beads on a rotating wheel/with agitation at 4 °C for 2-4 hours.
15. During the incubation step, prepare phosphatase Buffer B (100 mM NaCl, 50 mM HEPES, pH 7.0). Add 2 mM dithiothreitol and 1 mM $MnCl_2$ immediately prior to use. Thaw FLAG peptide (Sigma, F3290) on ice during this period as well. (See note 4)
16. Remove the homogenate from the rotator and centrifuge for 1 minute at 200 g to pellet the beads.
17. Aspirate off the supernatant, taking care not to remove any beads. Suspend the beads in 2 mL of lysis Buffer A, and split the beads evenly between two 1.5 mL microcentrifuge tubes. Designate one tube for λ-phosphatase treatment and one for control. Label the tubes accordingly, and do not mix the two groups for the remainder of the protocol.
18. Centrifuge the tubes for 1 minute at 200 g and check the beads to ensure they are evenly split. Aspirate off the lysis Buffer A, and add 500 µL of phosphatase Buffer B to each tube to suspend the beads.
19. Centrifuge for 1 minute at 200 g, aspirate off the supernatant, and add 200 µL of phosphatase Buffer B to each tube.

20. Add 5 μL (2,000 units) of λ-phosphatase (NEB, P0753L) to the tube designated for λ-phosphatase treatment and none to the control. Incubate both tubes with agitation at 30 °C for 25 minutes. (See note 5)
21. During the incubation step, prepare the following:
    a. Wash Buffer C (150 mM NaCl, 20 mM HEPES pH 7.2). Immediately before use add 10 μg/mL Leupeptin, 10 μg/mL Pepstatin A, 1 mM PMSF, and 0.5 mM dithiothreitol
    b. Elution Buffer D (150 mM NaCl, 20 mM HEPES, pH 7.2), immediately before use add FLAG peptide to a final concentration of 1.0 mg/mL
22. Transfer the beads to two separate 15 mL conical tubes and add 7 mL of lysis Buffer A to each. Gently mix the beads by inverting the tubes several times. Centrifuge for 1 minute at 200 g to pellet the beads and aspirate off the supernatants. Repeat the wash with another 7 mL of lysis Buffer A to each and centrifuge to pellet.
23. For the final wash step, aspirate off the supernatants and add 7 mL of wash Buffer C to each tube. Gently mix the beads by inverting the tubes several times. Centrifuge for 1 minute at 200 g to pellet the beads.
24. Aspirate the supernatants down to a volume of around 1 mL, then transfer the beads to two separate 1.5 mL microcentrifuge tubes. Centrifuge for 1 minute at 200 g to pellet the beads, and aspirate off all remaining wash Buffer C from each.
25. Add 500 μL of elution Buffer D to each tube. Incubate tubes with agitation at 4 °C for 15 minutes to elute.
26. Equilibrate two screening columns with lysis Buffer A and label appropriately.

27. Remove the microcentrifuge tubes from agitation and centrifuge for 1 minute at 200 g.
28. Place each previously equilibrated screening column over an appropriately labeled 1.5 mL microcentrifuge tube. Carefully transfer the supernatant of each tube to the appropriate screening column, allow to flow through, and catch the eluate in the microcentrifuge tubes.
29. Place the eluates on ice. Repeat the elution in step 25 with a second fraction of 500 µL of elution Buffer D to each of the bead pellets.
30. Place the appropriate screening column over the microcentrifuge tubes containing the first elution fraction. Transfer the beads and eluate to the appropriate screening columns, and catch the eluate in the tube containing the first fraction to combine.
31. Briefly vortex the combined fractions to mix, and divide the purified protein into aliquots (20-50 µL).
32. Store the aliquots at -80 °C. Freeze-thaw cycles will reduce specific activity, and the aliquots should be used or discarded after thawing. (See note 6)
33. Proteins may be quantified by running the purified proteins on a polyacrylamide gel with a standard curve of serially diluted BSA standards, and staining with Coomassie Brilliant Blue G-250, or other appropriate protein stain (Fig. C1).

Notes

1. For large scale purification we have found that overexpression of lipin family members in a fast-growing cell line like HeLa or HEK-293T cells is optimal. Lipin

family proteins can be efficiently and economically expressed by adenovirus expression or via transient transfection using previously described protocols [217–220]. Transfections are allowed 72 hours of expression before harvesting.

2. Lipins are heat sensitive and are quickly inhibited by incubation at higher temperatures (Han & Carman, 2010). Lysates and proteins should be kept at 4 °C throughout the purification process.
3. Harvested cell pellets may be stored at -80 °C prior to immunoprecipitation.
4. Flag peptide (Sigma, F3290) is suspended at a stock concentration of 5 mg/mL in elution Buffer D and stored at -20 °C.
5. We have found that lipin degradation occurs when treated with λ-phosphatase at 30 °C for a prolonged time.
6. We have observed that prolonged storage of purified lipin protein, even when stored at -80°C, also reduces specific activity. For best results, use purified enzyme within three months.

PHOSPHATIDIC ACID PHOSPHATASE ASSAY

Equipment

1. Glass tubes (12 × 75 mm)
2. Polypropylene tubes (12 × 75 mm)
3. 15 mL polypropylene conical tubes
4. 1.5 mL microcentrifuge tubes
5. Thin layer chromatography (TLC) plates, silica gel 60, 20 cm x 20 cm
6. Autoradiography film
7. TLC chamber
8. Mini-Extruder set (Avanti, 610000)
9. Polycarbonate membrane, 0.1 μm pore size (Sigma, WHA800309)
10. Filter supports (Sigma, WHA230300)
11. Scintillation vials

Buffers and Reagents

1. *Escherichia coli* DAG kinase (Sigma, D3065)
2. Cardiolipin
3. Dioleoyl-diacylglycerol
4. Dioleoyl-phosphatidic acid (DOPA)
5. Dioleoyl-phosphatidylcholine (DOPC)
6. Dioleoyl-phosphatidylethanolamine (DOPE)
7. β-mercaptoethanol

8. 1 M $MgCl_2$
9. 100 mM ATP
10. 10 mM [γ-^{32}P]ATP (6000 Ci/mmol)
11. 500 mM Tris-HCl, pH 7.5
12. PA Phosphatase Buffer E (50 mM Tris-HCl, 0.5 mM $MgCl_2$, 10 mM β-mercaptoethanol, pH 7.5)
13. Chloroform/methanol/1 N HCl (1:2:0.8, v/v)
14. Chloroform/methanol/water (65:25:4, v/v)
15. 0.1N HCl
16. 0.1N HCl in methanol

Preparation of PA Substrate

To prepare the ^{32}P radiolabeled PA substrate, *E. coli* DAG kinase is used to enzymatically phosphorylate DAG using [γ-^{32}P]ATP as previously described [222,223]. PA is then isolated by thin-layer chromatography (TLC).

Caution: The generation of [^{32}P]PA substrate and its subsequent incorporation into liposomes involves multiple steps using ^{32}P with a relatively high specific activity. Be sure to minimize exposure by keeping manipulations behind a ½" or greater acrylic shield. Use of a radioactive material handling glove box is recommended.

1. Mix 1 μmol of DAG and 9 μg of cardiolipin in a 1.5 mL microcentrifuge tube and dry down under N_2 gas. (See note 1)

2. To the dried lipids, add 20 μL of 5X DGK buffer (250 mM imidazole-HCl, 250 mM octyl-β-D-glucopyranoside, 250 mM NaCl, 62.5 mM $MgCl_2$, 5 mM EGTA, pH 6.6), 10 μL of 100 mM β-mercaptoethanol, 5 μL of 100 mM ATP, 5 μL of 10 mM [γ-^{32}P]ATP (6000 Ci/mmol), and 40 μL of water. (See note 2)
3. Add 20 μL of *E. coli* DAG Kinase to start the reaction. Mix and incubate with agitation for 45 minutes at 30 °C.
4. Stop the reaction with the addition of 0.5 mL of 0.1 N HCl in methanol and transfer to a 15 mL polypropylene tube.
5. Add 1.0 mL of chloroform, followed by 1.5 mL of 1 M $MgCl_2$. Vortex and centrifuge for 1 minute at 100 g.
6. Transfer the organic (bottom) phase to a new polypropylene tube, add 0.5 mL of 0.1 N HCl in methanol followed by 1.5 mL of 1 M $MgCl_2$. Vortex and centrifuge for 1 minute at 100 g.
7. Transfer the organic (bottom) phase to a glass tube and dry down under N_2 gas to around 100 μL total volume.
8. Spot the sample onto a TLC plate. Rinse the tube with 50 μL of chloroform and spot the sample again.
9. Develop the TLC plate in a TLC chamber with the chloroform/methanol/water (65:25:4, v/v) running buffer. Allow the buffer to run until 2-3 cm from the top of the plate, approximately 1-2 hours.
10. Remove the TLC plate from the chamber and allow to dry in a fume hood (5 – 10 minutes).

11. Wrap the TLC plate in plastic wrap, and expose to an autoradiography film for approximately 1 minute.
12. Develop the film.
13. Remove the plastic wrap from the TLC plate, and align the developed film. Mark the region of [^{32}P]PA through the film using a razor blade. (See note 3)
14. Moisten the radioactive region with water, place a sheet of weighing paper underneath the TLC plate, and use the razor blade to scrape the silica within the region off the plate and onto the weighing paper.
15. Transfer the silica into a 15 mL polypropylene tube and add 1.0 mL of chloroform/methanol/1 N HCl (1:2:0.8, v/v). (See note 4)
16. Vortex vigorously and centrifuge for 1 minute at 100 g. Transfer the supernatant into a new 15 mL polypropylene tube.
17. Repeat the extraction in steps 15 and 16 with the silica scrapings and combine the extractions.
18. Add 0.5 mL of chloroform followed by 0.6 mL of 0.1 N HCl (in water) to the combined extractions. Vortex and centrifuge for 1 minute at 100 g.
19. Transfer the organic (bottom) phase to a new 15 mL polypropylene tube. Add 1 mL of methanol and 1 mL of 0.1 N HCl (in water) to combined extractions, vortex and centrifuge for 1 minute at 200 g.
20. Transfer the organic (bottom) phase to a 2 mL glass tube with cap. Store at -20 °C.
21. Add 5-10 μL of the [^{32}P]PA to scintillation vials in duplicate, and count with a scintillation counter to determine the radioactive concentration (cpm/μL). Radioactive concentration will need to be determined each day that liposomes are

prepared (see next section) to calculate the volume of [^{32}P]PA to incorporate into liposomes.

Notes

1. Cardiolipin is added along with other components of the DG Kinase Buffer to provide optimal conditions for *E. coli* DG kinase [224].
2. 5X DGK buffer may be prepared in advance and stored at -20 °C.
3. During a typical separation by TLC, PA migrates to around 4-5 cm from the solvent front. A good quality separation of PA should be free of smearing.
4. The chloroform/methanol/1 N HCl (1:2:0.8, v/v) mixture should not phase separate.

Preparation of Liposomes

PA phosphatase activities are measured using 100 nm liposomes containing 10 mol% PA at a bulk concentration of 1 mM. Lipin activity is induced by di-anionic PA, and the phosphoregulation of lipin 1 activity only becomes apparent in the presence of di-anionic PA. The use of liposomes containing PE stabilizes di-anionic PA at a physiological pH [199]. In this protocol, 100 nm liposomes are generated using the mini-extruder from Avanti Lipids Polar, Inc. (Avanti, 610000) with 100 nm pore size polycarbonate membranes according to manufacturer recommendations. The preparation of liposomes using extrusion techniques has been extensively covered in previous protocols [225,226]. Liposomes should be used for phosphatase assays immediately after they are generated.

1. At room temperature, prepare PA phosphatase Buffer E (50 mM Tris-HCl, 0.5 mM $MgCl_2$, 10 mM β-mercaptoethanol, pH 7.5). (See note 1)
2. In a glass tube, mix 9 μmol of DOPC with 1 μmol of DOPA dissolved in chloroform. This tube will be used to generate PC:PA (9:1) liposomes. In a second glass tube, mix 6 μmol of DOPC, 3 μmol of DOPE, and 1 μmol of DOPA dissolved in chloroform. This tube will be used to generate PC:PE:PA (6:3:1) liposomes.
3. To each tube, add [^{32}P]PA to 5,000 cpm/nmol DOPA. Mix and use N_2 gas to dry down each tube to a thin film. (See note 2)
4. Suspend the lipid film in 1 mL of PA phosphatase Buffer E. Pipette up and down, then vortex vigorously to ensure complete suspension. Transfer the lipid suspensions into a 1.5 mL microcentrifuge tube. (See note 3)
5. To disrupt large multi-lamellar vesicles, snap freeze the lipids in liquid N_2, then place in a room temperature water bath and allow to thaw. Vortex vigorously when completely thawed. Repeat to perform 5 freeze/thaw cycles.
6. Use a 1 mL mini-extruder to pass the lipid suspension through a polycarbonate filter membrane with a 0.1 μm pore size. Pass through the membrane 11 times.
7. Carefully transfer the prepared liposomes into a 1.5 mL microcentrifuge tube and place on ice while preparing phosphatase assays.

Notes

1. $MgCl_2$ and β-mercaptoethanol should be added immediately prior to use.

2. Generating a thin, even film of lipids will reduce aggregation during subsequent lipid suspensions and liposome preparations. While drying under N_2 gas, angle the glass tubes to the side and rotate slowly to dry the lipids in a thin film around the bottom of the tube.
3. Suspending lipids using vortexing alone may cause the lipids to aggregate, particularly in mixtures containing PE. Mixing up and down with a pipette will help to disperse any lipid aggregates.

PA Phosphatase Assay

In this assay, specific activity is determined by measuring the radiolabeled, inorganic phosphates released by the enzyme during the reaction. An acidified Bligh-Dyer extraction is used to separate the water-soluble inorganic phosphates from the chloroform-soluble PA. For example, Michaelis-Menten steady-state kinetic constants may be determined by increasing bulk concentration of PA, while maintaining a constant PA surface concentration. All assay conditions are performed in triplicate.

1. In 1.5 mL microcentrifuge tubes, combine PA phosphatase Buffer E and appropriate liposomes to a total volume of 90 μL. For example, create a range of bulk concentrations of PA by varying the amount of liposomes added to generate a binding curve of velocity versus substrate concentration (Fig. C2). (See note 1)
2. Start each phosphatase reaction with the addition of 10 μL of purified enzyme. (See note 2)

3. Incubate each reaction with agitation for 20 minutes at 30 °C.
4. Stop each reaction with the addition of 0.5 mL of 0.1N HCl in methanol. Transfer to a polypropylene centrifuge tube. (See note 3)
5. Add 1 mL of chloroform followed by 1 mL of 1 M $MgCl_2$. Mix by gentle vortexing and centrifuge for 1 minute at 100 g.
6. Transfer 0.5 mL of the aqueous (top) phase to a scintillation vial. Samples may then be measured directly or with the addition of 4 mL of scintillation fluid for aqueous samples.
7. Prepare scintillation vials with direct aliquots of liposomes and measure radioactivity (specific label) for data analysis.

Notes

1. A typical range of bulk concentrations of PA may start at 0.025 mM PA and increase as high as 0.8 mM PA.
2. As always, it is crucial to ensure that the reaction is linear with respect to time and concentration. Thus, the amount of purified enzyme added may need to be adjusted. For the lipin family, we have found that 30 ng to 50 ng usually falls within the linear range.
3. To ensure consistent reaction times, stop each reaction in the same order in which they were begun.

Analysis of Data

Specific activity for an enzyme is expressed as U/mg of protein, or nmol of product/minute/mg. Calculate the specific activity using the following:

$$\text{Specific activity(nmol/min/mg)} = \frac{3.2\ (\text{correction factor}) * \text{cpm (corrected for background)}}{\text{specific label } \left(\frac{\text{cpm}}{\text{nmol}}\right) * \text{time (minutes)} * \text{purified enzyme (mg)}}$$

Notes

1. A correction factor of 3.2 is applied for measuring 0.5 mL of aqueous phase from a total 1.6 mL volume of aqueous phase in step 6 under the PA Phosphatase assay.
2. Specific label, measured as described by step 7 under the PA Phosphatase assay, refers to the counts per minute per nmol of PA within the liposomes.

SUMMARY AND CONCLUSION

Amphiphilic lipid enzymes must translocate to membrane surfaces in order to access substrate and catalyze their activity. Translocation between cytosolic and membrane fractions is regulated for many such amphiphilic enzymes, and seems to target them to specific cellular membranes [190,227,228]. The method of substrate presentation can play a critical role in the regulation and specificity of translocation, as is the case for lipin 1 in which the presence of PE is necessary for appropriate phosporegulation of PAP activity at a physiological pH (Fig C2) [196]. Current methods using detergent micelles or BSA to present lipid substrates display drastically altered *in vitro* enzyme kinetics when compared with lipid bilayers, and do not represent the native presentation of lipid substrates *in vivo* [196,197]. Liposomes provide an ideal method for a physiological presentation of substrate by enabling the generation of well-defined lipid bilayers. We have described a method for using liposomes to assay lipin PAP activity, however this method was also used to measure the specific activity of diacylglycerol kinases by making minor alterations to the reaction buffer and lipid composition, and measuring the incorporation of ^{32}P into the organic phase [163]. This method may therefore be more broadly applied to other amphiphilic lipid enzymes with minor modifications.

FIGURES

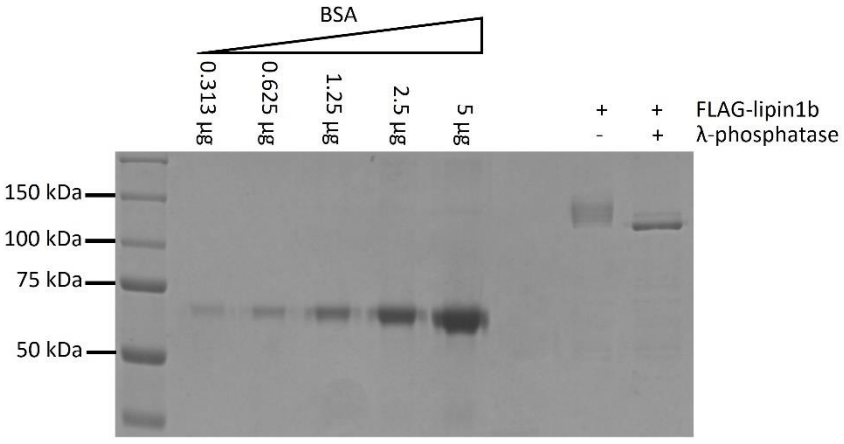

	Concentration(µg/mL)	Purity
-λ	79.7	92.8 %
+λ	47.2	92.3 %

Fig C1. SDS-PAGE gel stained with Coomassie Brilliant Blue G-250 showing a BSA standard curve and a typical yield of purified lipin from an adenoviral infection of 20 x 150-mm plates of HeLa cells. Concentration and purity values are listed for a 1 mL yield of purified protein.

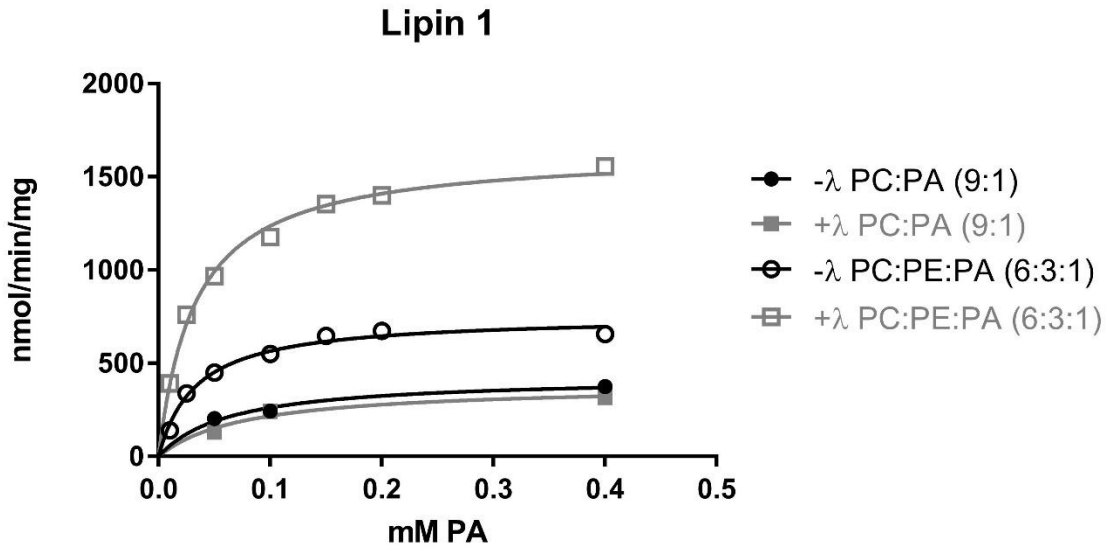

Fig C2. Velocity versus substrate concentration for lipin 1 PAP activity in PC:PA (9:1) and PC:PE:PA (6:3:1) liposomes. Binding curves are shown for control treated (-λ) and λ-phosphatase treated (+λ) lipin 1 [196].

RESULTING PUBLICATIONS

Granade ME, Hargett SR, Lank DS, Lemke MC, Luse MA, Isakson BE, Bochkis IM, Linden J, Harris TE. *Accepted*. Feeding desensitizes A1 adenosine receptors in adipose through FOXO1-mediated transcriptional regulation. Molecular Metabolism.

Granade ME*, Manigat LC*, Lemke MC, Purow BW, Harris TE. 2022. Identification of ritanserin analogs that display DGK isoform specificity. Biochemical Pharmacology. 197: 114908.

Merta H, Carasquillo Rodríguez JW, Anjur-Dietrich MI, Vitale T, **Granade ME**, Harris TE, Needleman DJ, Bahmanyar S. 2021. Cell cycle regulation of ER membrane biogenesis protects against chromosome missegregation. Developmental Cell. 56:1-16.

Manigat LC, **Granade ME**, Suchet T, Miller CA, Vass LR, Zhong X, Harris TE, Purow BW. 2021. Loss of diacylglycerol kinase α enhances macrophage responsiveness. Frontiers in Immunology. 12:722469.

Huang T, Hosseinibarkooie S, Borne AL, **Granade ME**, Brulet JW, Harris TE, Ferris HA, Hsu KL. 2021. Chemoproteomic profiling of kinases in live cells using electrophilic sulfonyl triazole probes. Chemical Science. 12(9):3295-3307.

Bottermann K, **Granade ME**, Oenarto V, Fischer JW, Harris TE. 2021. Atglistatin pretreatment preserves remote myocardium function following myocardial infarction. Journal of Cardiovascular Pharmacology and Therapeutics. 26(3):289-297.

Raje V, Howell NL, Martinez BA, Ahern KW, Oenarto V, **Granade ME**, Kim JW, Tundup S, Bottermann K, Gödecke A, Keller SR, Kadl A, Bland ML, Harris TE. 2020. Adipocyte lipolysis drives acute stress-induced insulin resistance and hyperglycemia. Scientific Reports. 10(1):18166.

Martinez BA, Hoyle RG, Yeudall S, **Granade ME**, Harris TE, Castle JD, Leitinger N, Bland ML. 2020. Innate immune signaling in Drosophila shifts anabolic lipid metabolism from triglyceride storage to phospholipid synthesis to support immune function. PLOS Genetics. 16(11):e1009192.

Ware TB, Franks CE, **Granade ME**, Zhang M, Kim KB, Park KS, Gahlmann A, Harris TE, Hsu KL. 2020. Reprogramming fatty acyl specificity of lipid kinases via C1 domain engineering. Nature Chemical Biology. 16(2):170-178.

Hennessy M, **Granade ME**, Hassaninasab A, Wang D, Kwiatek JM, Han GS, Harris TE, Carman GM. 2019. Casein kinase II-mediated phosphorylation of lipin 1β phosphatidate phosphatase at Ser-285 and Ser-287 regulates its interaction with 14-3-3β protein. Journal of Biological Chemistry. 294(7):2365-2374.

Granade ME and Harris TE. 2018. Purification of Lipin and Measurement of Phosphatidic Acid Phosphatase Activity from Liposomes in Karen Allen (Ed.), *Methods in Enzymology* Vol. 607 (*pp. 373-388*) Cambridge, MA: Academic Press.

Boroda S, Takkellapati S, Lawrence RT, Entwisle SW, Pearson JM, **Granade ME**, Mullins GR, Eaton JM, Villén J, and Harris TE. 2017. The Phosphatidic Acid-Binding, Polybasic Domain is Responsible for the Differences in the Phosphoregulation of Lipins 1 and 3. Journal of Biological Chemistry. 292(50):20481-20493.

REFERENCES

[1] Frühbeck, G., Méndez-Giménez, L., Fernández-Formoso, J.A., Fernández, S., Rodríguez, A., 2014. Regulation of adipocyte lipolysis. vol. 27.

[2] Oberer, M., Boeszoermenyi, A., Nagy, H.M., Zechner, R., 2011. Recent insights into the structure and function of CGI-58. Current Opinions in Lipidology 22(3): 149–58, Doi: 10.1097/MOL.0b013e328346230e.Recent.

[3] Haemmerle, G., Lass, A., Zimmermann, R., Gorkiewicz, G., Meyer, C., Rozman, J., et al., 2006. Defective Lipolysis and Altered Energy Metabolism in Mice Lacking Adipose Triglyceride Lipase. Science 312: 734–7.

[4] Schoiswohl, G., Stefanovic-Racic, M., Menke, M.N., Wills, R.C., Surlow, B.A., Basantani, M.K., et al., 2015. Impact of reduced ATGL-mediated adipocyte lipolysis on obesity-associated insulin resistance and inflammation in male mice. Endocrinology 156(10): 3610–24, Doi: 10.1210/en.2015-1322.

[5] Jaworski, K., Sarkadi-Nagy, E., Duncan, R.E., Ahmadian, M., Sul, H.S., 2007. Regulation of triglyceride metabolism. IV. Hormonal regulation of lipolysis in adipose tissue. American Journal of Physiology. Gastrointestinal and Liver Physiology 293(7): G1–4, Doi: 10.1152/ajpgi.00554.2006.Regulation.

[6] Petersen, M.C., Shulman, G.I., 2018. Mechanisms of insulin action and insulin resistance. Physiological Reviews 98(4): 2133–223, Doi: 10.1152/physrev.00063.2017.

[7] Czech, M.P., Tencerova, M., Pedersen, D.J., Aouadi, M., 2013. Insulin signalling mechanisms for triacylglycerol storage. Diabetologia 56(5): 949–64, Doi: 10.1007/s00125-013-2869-1.

[8] Carpentier, A.C., 2021. 100th anniversary of the discovery of insulin perspective: Insulin and adipose tissue fatty acid metabolism. American Journal of Physiology - Endocrinology and Metabolism 320(4): E653–70, Doi: 10.1152/AJPENDO.00620.2020.

[9] Carpene, C., Chalaux, E., Lizarbe, M., Estrada, A., Mora, C., Palacin, M., et al., 1993. Beta 3-adrenergic receptors are responsible for the adrenergic inhibition of insulin-stimulated glucose transport in rat adipocytes. Biochem J 296 (Pt 1: 99–105.

[10] Green, A., 1983. Catecholamines inhibit insulin-stimulated glucose transport in adipocytes, in the presence of adenosine deaminase. FEBS Letters 152(2): 261–4.

[11] Mullins, G.R., Wang, L., Raje, V., Sherwood, S.G., Grande, R.C., Boroda, S., et al., 2014. Catecholamine-induced lipolysis causes mTOR complex dissociation and inhibits glucose uptake in adipocytes. Proceedings of the National Academy of Sciences 111(49): 17450–5, Doi: 10.1073/pnas.1410530111.

[12] Chait, A., den Hartigh, L.J., 2020. Adipose Tissue Distribution, Inflammation and Its Metabolic Consequences, Including Diabetes and Cardiovascular Disease. Frontiers in Cardiovascular Medicine 7(February): 1–41, Doi: 10.3389/fcvm.2020.00022.

[13] Lee, M., Wu, Y., Fried, S., 2013. Adipose tissue heterogeneity: implication of depot differences in adipose tissue for obesity complications. Molecular Aspects of Medicine 34(1): 1–11, Doi: 10.1016/j.mam.2012.10.001.Adipose.

[14] Guglielmi, V., Sbraccia, P., 2018. Obesity phenotypes: Depot-differences in adipose tissue and their clinical implications. Eating and Weight Disorders 23(1): 3–14, Doi: 10.1007/s40519-017-0467-9.

[15] Gómez-Hernández, A., Beneit, N., Díaz-Castroverde, S., Escribano, Ó., 2016. Differential Role of Adipose Tissues in Obesity and Related Metabolic and Vascular Complications. International Journal of Endocrinology 2016, Doi: 10.1155/2016/1216783.

[16] Björntorp, P., 1991. Metabolic implications of body fat distribution. Diabetes Care 14(12): 1132–43, Doi: 10.2337/diacare.14.12.1132.

[17] Hellmér, J., Marcus, C., Sonnenfeld, T., Arner, P., 1992. Mechanisms for differences in lipolysis between human subcutaneous and omental fat cells. Journal of Clinical Endocrinology and Metabolism 75(1): 15–20.

[18] Kahn, S., Hull, R., Utzschneider, K., 2006. Mechanisms linking obesity to insulin resistance and type 2 diabetes. Nature 444(12): 840–6.

[19] Lowell, B., S-Susulic, V., Hamann, A., Lawitts, J., Himms-Hagen, J., Boyer, B., et al., 1993. Development of obesity in transgenic mice after genetic ablation of brown adipose tissue. Nature 366(6457): 740–2.

[20] Yang, X., Enerbäck, S., Smith, U., 2003. Reduced expression of FOXC2 and brown adipogenic genes in human subjects with insulin resistance. Obesity Research 11(10): 1182–91.

[21] Almind, K., Manieri, M., Sivitz, W., Cinti, S., Kahn, C., 2007. Ectopic brown adipose tissue in muscle provides a mechanism for differences in risk of metabolic syndrome in mice. Proceedings of the National Academy of Sciences of the United States of America 104(7): 2366–71.

[22] Cypess, A.M., Lehman, S., Williams, G., Tal, I., Rodman, D., Goldfine, A.B., et al., 2009. Identification and importance of brown adipose tissue in adult humans. Obstetrical and Gynecological Survey 64(8): 519–20, Doi: 10.1097/OGX.0b013e3181ac8aa2.

[23] Hales, C., Carroll, M., Fryar, C., Ogden, C., 2017. Prevalence of obesity among adults and youth: United States, 2015-2016. NCHS Data Brief: 1–8.

[24] Zhou, B., Lu, Y., Hajifathalian, K., Bentham, J., Di Cesare, M., Danaei, G., et al.,

2016. Worldwide trends in diabetes since 1980: A pooled analysis of 751 population-based studies with 4.4 million participants. The Lancet 387(10027): 1513–30, Doi: 10.1016/S0140-6736(16)00618-8.

[25] Bray, G.A., Edelstein, S.L., Crandall, J.P., Aroda, V.R., Franks, P.W., Fujimoto, W., et al., 2012. Long-term safety, tolerability, and weight loss associated with metformin in the diabetes prevention program outcomes study. Diabetes Care 35(4): 731–7, Doi: 10.2337/dc11-1299.

[26] Padwal, R.S., Rucker, D., Li, S.K., Curioni, C., Lau, D.C.W., 2003. Long-term pharmacotherapy for obesity and overweight. Cochrane Database of Systematic Reviews 2010(1), Doi: 10.1002/14651858.CD004094.pub2.

[27] Shah, M., Vella, A., 2014. Effects of GLP-1 on appetite and weight. Reviews in Endocrine and Metabolic Disorders 15(3): 181–7, Doi: 10.1007/s11154-014-9289-5.

[28] Samuel, V.T., Liu, Z.X., Wang, A., Beddow, S.A., Geisler, J.G., Kahn, M., et al., 2007. Inhibition of protein kinase Cε prevents hepatic insulin resistance in nonalcoholic fatty liver disease. Journal of Clinical Investigation 117(3): 739–45, Doi: 10.1172/JCI30400.

[29] Kumar, A., Lawrence, J.C., Jung, D.Y., Ko, H.J., Keller, S.R., Kim, J.K., et al., 2010. Fat Cell – Specific Ablation of Rictor in Mice Impairs insulin-regulated fat cell and whole-body glucose and lipid metabolism. Diabetes 59(6): 1397–406, Doi: 10.2337/db09-1061.

[30] Rosen, E., Spiegelman, B., 2006. Adipocytes as regulators of energy balance and glucose homeostasis. Nature 444(12): 847–53.

[31] Rebrin, K., Steil, G.M., Mittelman, S.D., Bergman, R.N., 1996. Causal linkage between insulin suppression of lipolysis and suppression of liver glucose output in dogs. Journal of Clinical Investigation 98(3): 741–9, Doi: 10.1172/JCI118846.

[32] Bergman, R.N., Iyer, M.S., 2017. Indirect regulation of endogenous glucose production by Insulin: The single gateway hypothesis revisited. Diabetes 66(7): 1742–7, Doi: 10.2337/db16-1320.

[33] Jacobson, K.A., Tosh, D.K., Jain, S., Gao, Z.-G., 2019. Historical and Current Adenosine Receptor Agonists in Preclinical and Clinical Development. Frontiers in Cellular Neuroscience 13: 1–17, Doi: 10.3389/fncel.2019.00124.

[34] Albrecht-Küpper, B.E., Leineweber, K., Nell, P.G., 2012. Partial adenosine A1 receptor agonists for cardiovascular therapies. Purinergic Signalling 8(SUPPL. 1): 91–9, Doi: 10.1007/s11302-011-9274-3.

[35] Fredholm, B.B., IJzerman, A.P., Jacobson, K.A., Linden, J., Müller, C.E., 2011. International union of basic and clinical pharmacology. LXXXI. Nomenclature and classification of adenosine receptors - An update. Pharmacological Reviews

63(1): 1–34, Doi: 10.1124/pr.110.003285.

[36] Newby, A.C., 1984. Adenosine and the concept of "retaliatory metabolites." Trends in Biochemical Sciences 9(2): 42–4, Doi: 10.1016/0968-0004(84)90176-2.

[37] Stone, T., 1981. Commentary: Physiological roles for adenosine and adenosine 5'-triphosphate in the nervous system. Neuroscience 6(4): 523–55.

[38] Burnstock, G., 2006. Historical review: ATP as a neurotransmitter. Trends in Pharmacological Sciences 27(3 SPEC. ISS.): 166–76, Doi: 10.1016/j.tips.2006.01.005.

[39] Lerman, B., Belardinelli, L., 1991. Cardiac Electrophysiology of Adenosine. Basic and clinical concepts. Circulation 83(5): 1499–509.

[40] Linden, J., Thai, T., Figler, H., Jin, X., Robeva, A.S., 1999. Characterization of human A(2B) adenosine receptors: Radioligand binding, Western blotting, and coupling to G(q) in human embryonic kidney 293 cells and HMC-1 mast cells. Molecular Pharmacology 56(4): 705–13.

[41] Sheth, S., Brito, R., Mukherjea, D., Rybak, L.P., Ramkumar, V., 2014. Adenosine receptors: Expression, function and regulation. International Journal of Molecular Sciences 15(2): 2024–52, Doi: 10.3390/ijms15022024.

[42] Yan, L., Burbiel, J., Maaß, A., Müller, C.E., 2003. Adenosine receptor agonists: from basic medicinal chemistry to clinical development. Expert Opinions on Emerging Drugs 8(2): 537–76.

[43] Xiao, C., Liu, N., Jacobson, K.A., Gavrilova, O., Reitman, M.L., 2019. Physiology and effects of nucleosides in mice lacking all four adenosine receptors. PLoS Biology 17(3): 1–26, Doi: 10.1371/journal.pbio.3000161.

[44] Gharibi, B., Abraham, A.A., Ham, J., Evans, B.A.J., 2012. Contrasting effects of A1 and A2b adenosine receptors on adipogenesis. International Journal of Obesity 36(3): 397–406, Doi: 10.1038/ijo.2011.129.

[45] Koupenova, M., Ravid, K., 2013. Adenosine, Adenosine Receptors and Their Role in Glucose Homeostasis and Lipid Metabolism. Journal of Cellular Physiology 228(8): 1703–12, Doi: 10.1002/jcp.24352.

[46] Szkudelski, T., Szkudelska, K., Nogowski, L., 2009. Effects of adenosine A1 receptor antagonism on lipogenesis and lipolysis in isolated rat adipocytes. Physiological Research 58(6): 863–71, Doi: 10.33549/physiolres.931467.

[47] Gnad, T., Scheibler, S., Kugelgen, I. Von., Scheele, C., Kilic, A., Glode, A., et al., 2014. Adenosine activates brown adipose tissue and recruits beige adipocytes via A2A receptors. Nature 516(7531): 395–9, Doi: 10.1038/nature13816.

[48] Gnad, T., Navarro, G., Lahesmaa, M., Reverte-Salisa, L., Copperi, F., Cordomi, A., et al., 2020. Adenosine/A2B Receptor Signaling Ameliorates the Effects of

Aging and Counteracts Obesity. Cell Metabolism 32(1): 56-70.e7, Doi: 10.1016/j.cmet.2020.06.006.

[49] Johansson, S.M., Lindgren, E., Yang, J.N., Herling, A.W., Fredholm, B.B., 2008. Adenosine A1 receptors regulate lipolysis and lipogenesis in mouse adipose tissue - Interactions with insulin. European Journal of Pharmacology 597: 92–101, Doi: 10.1016/j.ejphar.2008.08.022.

[50] Duncan, R.E., Ahmadian, M., Jaworski, K., Sarkadi-Nagy, E., Sul, H.S., 2007. Regulation of Lipolysis in Adipocytes. Annual Review of Nutrition 27(1): 79–101, Doi: 10.1146/annurev.nutr.27.061406.093734.

[51] Zisman, A., Michael, M.D., Mauvais-Jarvis, F., Wojtaszewski, J.F.P., Hirshman, M.F., Virkamaki, A., et al., 2000. Targeted disruption of the glucose transporter 4 selectively in muscle causes insulin resistance and glucose intolerance. Nature Medicine 6(8): 924–8, Doi: 10.1038/78693.

[52] Raje, V., Ahern, K.W., Martinez, B.A., Howell, N.L., Oenarto, V., Granade, M.E., et al., 2020. Adipocyte lipolysis drives acute stress-induced insulin resistance. Scientific Reports 10(1): 18166, Doi: 10.1038/s41598-020-75321-0.

[53] DeFronzo, R.A., 2010. Insulin resistance, lipotoxicity, type 2 diabetes and atherosclerosis: The missing links. The Claude Bernard Lecture 2009. Diabetologia 53(7): 1270–87, Doi: 10.1007/s00125-010-1684-1.

[54] Green, A., 1987. Adenosine receptor down-regulation and insulin resistance following prolonged incubation of adipocytes with an A1 adenosine receptor agonist. Journal of Biological Chemistry 262(32): 15702–7, Doi: 10.1016/s0021-9258(18)47784-8.

[55] Fredholm, B.B., Sollevi, A., 1981. The release of adenosine and inosine from canine subcutaneous adipose tissue by nerve stimulation and noradrenaline. The Journal of Physiology 313(1): 351–67, Doi: 10.1113/jphysiol.1981.sp013670.

[56] Lonnroth, P., Jansson, P.A., Fredholm, B.B., Smith, U., 1989. Microdialysis of intercellular adenosine concentration in subcutaneous tissue in humans. American Journal of Physiology - Endocrinology and Metabolism 256(2), Doi: 10.1152/ajpendo.1989.256.2.e250.

[57] Liang, H.X., Belardinelli, L., Ozeck, M.J., Shryock, J.C., 2002. Tonic activity of the rat adipocyte A1-adenosine receptor. British Journal of Pharmacology 135(6): 1457–66, Doi: 10.1038/sj.bjp.0704586.

[58] Schwabe, U., Ebert, R., Erbler, H., 1973. Adenosine release from isolated fat cells and its significance for the effects of hormones on cyclic 3',5'-AMP levels and lipolysis. Naunyn-Schmiedeberg's Archives of Pharmacology 276: 133–48.

[59] Fain, J.N., Wieser, P.B., 1975. Effects of adenosine deaminase on cyclic adenosine monophosphate accumulation, lipolysis, and glucose metabolism of fat cells.

Journal of Biological Chemistry 250(3): 1027–34, Doi: 10.1016/s0021-9258(19)41887-5.

[60] Hoffman, B.B., Chang, H., Farahbakhsh, Z., Reaven, G., 1984. Inhibition of lipolysis by adenosine is potentiated with age. Journal of Clinical Investigation 74(5): 1750–5, Doi: 10.1172/JCI111593.

[61] Joost, H.-G., Steinfelder, H.-J., 1982. Modulation of insulin sensitivity by adenosine. Effects on glucose transport, lipid synthesis, and insulin receptors of the adipocyte. Molecular Pharmacology 22: 614–8.

[62] Heseltine, L., Webster, J.M., Taylor, R., 1995. Adenosine effects upon insulin action on lipolysis and glucose transport in human adipocytes. Molecular and Cellular Biochemistry 144(2): 147–51, Doi: 10.1007/BF00944394.

[63] Vannucci, S.J., Nishimura, H., Satoh, S., Cushman, S.W., Holman, G.D., Simpson, I.A., 1992. Cell surface accessibility of GLUT4 glucose transporters in insulin-stimulated rat adipose cells. Modulation by isoprenaline and adenosine. Biochemical Journal 288(1): 325–30, Doi: 10.1042/bj2880325.

[64] Dixon, A.K., Gubitz, A.K., Sirinathsinghji, D.J.S., Richardson, P.J., Freeman, T.C., 1996. Tissue distribution of adenosine receptor mRNAs in the rat. British Journal of Pharmacology 118(6): 1461–8, Doi: 10.1111/j.1476-5381.1996.tb15561.x.

[65] Schoelch, C., Kuhlmann, J., Gossel, M., Mueller, G., Neumann-Haefelin, C., Belz, U., et al., 2004. Characterization of adenosine-A1 receptor-mediated antilipolysis in rats by tissue microdialysis, 1H-spectroscopy, and glucose clamp studies. Diabetes 53(7): 1920–6, Doi: 10.2337/diabetes.53.7.1920.

[66] Dhalla, A.K., Santikul, M., Chisholm, J.M., Belardinelli, L., Reaven, G.M., 2009. Comparison of the antilipolytic effects of an A1 adenosine receptor partial agonist in normal and diabetic rats. Diabetes, Obesity and Metabolism 11(2): 95–101, Doi: 10.1111/j.1463-1326.2008.00902.x.

[67] Staehr, P., Dhalla, A., Zack, J., Wang, X., Ho, Y., Bingham, J., et al., 2013. Reduction of free fatty acids, safety, and pharmacokinetics of oral GS-9667, an A(1) adenosine receptor partial agonist. Journal of Clinical Investigation 53(4): 385–92.

[68] Kaartinen, J.M., Hreniuk, S.P., Martin, L.F., Ranta, S., LaNoue, K.F., Ohisalo, J.J., 1991. Attenuated adenosine-sensitivity and decreased adenosine-receptor number in adipocyte plasma membranes in human obesity. Biochemical Journal 279(1): 17–22, Doi: 10.1042/bj2790017.

[69] Green, A., Johnson, J.L., DiPette, D.J., 1990. Decrease in A1 adenosine receptors in adipocytes from spontaneously hypertensive rats. Metabolism 39(12): 1334–8, Doi: 10.1016/0026-0495(90)90193-G.

[70] Faulhaber-Walter, R., Jou, W., Mizel, D., Li, L., Zhang, J., Kim, S.M., et al., 2011. Impaired glucose tolerance in the absence of adenosine A1 receptor signaling. Diabetes 60(10): 2578–87, Doi: 10.2337/db11-0058.

[71] Yang, G.K., Fredholm, B.B., Kieffer, T.J., Kwok, Y.N., 2012. Improved blood glucose disposal and altered insulin secretion patterns in adenosine A 1 receptor knockout mice. American Journal of Physiology - Endocrinology and Metabolism 303(2): 180–90, Doi: 10.1152/ajpendo.00050.2012.

[72] Johansson, S.M., Salehi, A., Sandström, M.E., Westerblad, H., Lundquist, I., Carlsson, P.O., et al., 2007. A1 receptor deficiency causes increased insulin and glucagon secretion in mice. Biochemical Pharmacology 74(11): 1628–35, Doi: 10.1016/j.bcp.2007.08.006.

[73] Dong, Q., Ginsberg, H.N., Erlanger, B.F., 2001. Overexpression of the A1 adenosine receptor in adipose tissue protects mice from obesity-related insulin resistance. Diabetes, Obesity and Metabolism 3(5): 360–6, Doi: 10.1046/j.1463-1326.2001.00158.x.

[74] Johansson, B., Halldner, L., Dunwiddie, T. V., Masino, S.A., Poelchen, W., Giménez-Llort, L., et al., 2001. Hyperalgesia, anxiety, and decreased hypoxic neuroprotection in mice lacking the adenosine A1 receptor. Proceedings of the National Academy of Sciences of the United States of America 98(16): 9407–12, Doi: 10.1073/pnas.161292398.

[75] Blundon, J.A., Roy, N.C., Teubner, B.J.W., Yu, J., Eom, T.Y., Sample, K.J., et al., 2017. Restoring auditory cortex plasticity in adult mice by restricting thalamic adenosine signaling. Science 356(6345): 1352–6, Doi: 10.1126/science.aaf4612.

[76] Vannucci, S.J., Klim, C.M., Martin, L.F., LaNoue, F., 1989. A1-adenosine receptor-mediated inhibition of adipocyte adenylate cyclase and lipolysis in Zucker rats. American Journal of Physiology - Endocrinology and Metabolism 257(20): E871–8.

[77] Soto, M., Orliaguet, L., Reyzer, M.L., Manier, M.L., Caprioli, R.M., Kahn, C.R., 2018. Pyruvate induces torpor in obese mice. Proceedings of the National Academy of Sciences of the United States of America 115(4): 810–5, Doi: 10.1073/pnas.1717507115.

[78] Antonioli, L., Pacher, P., Haskó, G., 2022. Adenosine and inflammation: it's time to (re)solve the problem. Trends in Pharmacological Sciences 43(1): 43–55, Doi: 10.1016/j.tips.2021.10.010.

[79] Elks, M.L., Jackson, M., Manganiello, V.C., Vaughan, M., 1987. Effect of N6-(L-2-phenylisopropyl)adenosine and insulin on cAMP metabolism in 3T3-L1 adipocytes. American Journal of Physiology - Cell Physiology 252(21): C342–8, Doi: 10.1152/ajpcell.1987.252.3.c342.

[80] Raje, V., Ahern, K.W., Martinez, B.A., Howell, N.L., Oenarto, V., Granade, M.E.,

et al., 2020. Adipocyte lipolysis drives acute stress-induced insulin resistance. Scientific Reports 10(1): 18166, Doi: 10.1038/s41598-020-75321-0.

[81] Wang, X., Seed, B., 2003. A PCR primer bank for quantitative gene expression analysis. Nucleic Acids Research 31(24): e154–e154, Doi: 10.1093/nar/gng154.

[82] Spandidos, A., Wang, X., Wang, H., Dragnev, S., Thurber, T., Seed, B., 2008. A comprehensive collection of experimentally validated primers for Polymerase Chain Reaction quantitation of murine transcript abundance. BMC Genomics 9(1): 1–17, Doi: 10.1186/1471-2164-9-633.

[83] Spandidos, A., Wang, X., Wang, H., Seed, B., 2009. PrimerBank: A resource of human and mouse PCR primer pairs for gene expression detection and quantification. Nucleic Acids Research 38(SUPPL.1): D792–9, Doi: 10.1093/nar/gkp1005.

[84] Untergasser, A., Cutcutache, I., Koressaar, T., Ye, J., Faircloth, B., Remm, M., et al., 2012. Primer3--new capabilities and interfaces. Nucleic Acids Research 40(15): e115.

[85] Koressaar, T., Remm, M., 2007. Enhancements and modifications of primer design program Primer3. Bioinformatics 23(10): 1289–91.

[86] Aherne, C.M., Kewley, E.M., Eltzschig, H.K., 2011. The resurgence of A2B adenosine receptor signaling. Biochimica et Biophysica Acta - Biomembranes 1808(5): 1329–39, Doi: 10.1016/j.bbamem.2010.05.016.

[87] Harada, H., Asano, O., Hoshino, Y., Yoshikawa, S., Matsukura, M., Kabasawa, Y., et al., 2001. 2-alkynyl-8-aryl-9-methyladenines as novel adenosine receptor antagonists: Their synthesis and structure-activity relationships toward hepatic glucose production induced via agonism of the A2B receptor. Journal of Medicinal Chemistry 44(2): 170–9, Doi: 10.1021/jm990499b.

[88] Johnston-Cox, H., Eisenstein, A.S., Koupenova, M., Carroll, S., Ravid, K., 2014. The macrophage A2b adenosine receptor regulates tissue insulin sensitivity. PLoS ONE 9(6): 1–13, Doi: 10.1371/journal.pone.0098775.

[89] Csóka, B., Koscsó, B., Töro, G., Kókai, E., Virág, L., Németh, Z.H., et al., 2014. A2B Adenosine receptors prevent insulin resistance by inhibiting adipose tissue inflammation via maintaining alternative macrophage activation. Diabetes 63(3): 850–66, Doi: 10.2337/db13-0573.

[90] Figler, R.A., Wang, G., Srinivasan, S., Jung, D.Y., Zhang, Z., Pankow, J.S., et al., 2011. Links between Insulin resistance, adenosine A2B receptors, and inflammatory markers in mice and humans. Diabetes 60(2): 669–79, Doi: 10.2337/db10-1070.

[91] Treadway, J., Sacca, R., Jones, B., 2006. Adenosine A2B receptor knock-out mice display an improved metabolic phenotype. Diabetologia 49(Suppl1): 44–5.

[92] Johnston-Cox, H., Koupenova, M., Yang, D., Corkey, B., Gokce, N., Farb, M.G., et al., 2012. The A2b adenosine receptor modulates glucose homeostasis and obesity. PLoS ONE 7(7): e40584, Doi: 10.1371/journal.pone.0040584.

[93] Koupenova, M., Johnston-Cox, H., Vezeridis, A., Gavras, H., Yang, D., Zannis, V., et al., 2012. A 2b adenosine receptor regulates hyperlipidemia and atherosclerosis. Circulation 125(2): 354–63, Doi: 10.1161/CIRCULATIONAHA.111.057596.

[94] Hilaire, C.S.T., Carroll, S.H., Chen, H., Ravid, K., 2009. Mechanisms of induction of adenosine receptor genes and its functional significance. Journal of Cellular Physiology 218(1): 35–44, Doi: 10.1002/jcp.21579.

[95] Vassaux, G., Gaillard, D., Mari, B., Ailhaud, G., Negrel, R., 1993. Differential expression of adenosine A1 and A2 receptors in preadipocytes and adipocytes. Biochemical and Biophysical Research Communications 193(3): 1123–30.

[96] Zhang, X., Gan, L., Pan, H., Guo, S., He, X., Olson, S.T., et al., 2002. Phosphorylation of serine 256 suppresses transactivation by FKHR (FOXO1) by multiple mechanisms: Direct and indirect effects on nuclear/cytoplasmic shuttling and DNA binding. Journal of Biological Chemistry 277(47): 45276–84, Doi: 10.1074/jbc.M208063200.

[97] Cheng, Z., White, M.F., 2011. Targeting forkhead Box O1 from the concept to metabolic diseases: Lessons from mouse models. Antioxidants and Redox Signaling 14(4): 649–61, Doi: 10.1089/ars.2010.3370.

[98] Nakae, J., Kitamura, T., Kitamura, Y., Biggs, W.H., Arden, K.C., Accili, D., 2003. The forkhead transcription factor Foxo1 regulates adipocyte differentiation. Developmental Cell 4(1): 119–29, Doi: 10.1016/S1534-5807(02)00401-X.

[99] Nagashima, T., Shigematsu, N., Maruki, R., Urano, Y., Tanaka, H., Shimaya, A., et al., 2010. Discovery of novel forkhead box O1 inhibitors for treating type 2 diabetes: Improvement of fasting glycemia in diabetic db/db mice. Molecular Pharmacology 78(5): 961–70, Doi: 10.1124/mol.110.065714.

[100] Lee, C., Huang, C.H., 2013. LASAGNA-search: An integrated web tool for transcription factor binding site search and visualization. BioTechniques 54(3): 141–53, Doi: 10.2144/000113999.

[101] Lin, Y., Bai, L., Chen, W., Xu, S., 2010. The NF-κB activation pathways, emerging molecular targets for cancer prevention and therapy. Expert Opinion on Therapeutic Targets 14(1): 45–55, Doi: 10.1517/14728220903431069.

[102] Fitzgerald, K.A., McWhirter, S.M., Faia, K.L., Rowe, D.C., Latz, E., Golenbock, D.T., et al., 2003. IKKE and TBKI are essential components of the IRF3 signalling pathway. Nature Immunology 4(5): 491–6, Doi: 10.1038/ni921.

[103] Ohisalo, J.J., Ranta, S., Huhtaniemi, I.T., 1986. Attenuated adenosine R-site effect

in adipocytes in obesity. Metabolism 35(2): 143–6, Doi: 10.1016/0026-0495(86)90115-0.

[104] Ramsay, D.S., Woods, S.C., 2014. Clarifying the roles of homeostasis and allostasis in physiological regulation. Psychological Review 121(2): 225–47, Doi: 10.1037/a0035942.Clarifying.

[105] Sterling, P., Eyer, J., 1988. Allostasis: A new paradigm to explain arousal pathology. In: Fisher, S., Reason, J., editors. Handbook of Life Stress, Cognition and Health, New York, NY: John Wiley & Sons p. 629–49.

[106] Cunha, R.A., 2019. Signaling by adenosine receptors-Homeostatic or allostatic control? PLoS Biology 17(4): 5–8, Doi: 10.1371/journal.pbio.3000213.

[107] Van der Graaf, P.H., Van Schaick, E.A., Visser, S.A., De Greef, H.J., Ijzerman, A.P., Danhof, M., 1999. Mechanism-based pharmacokinetic-pharmacodynamic modeling of antilipolytic effects of adenosine A(1) receptor agonists in rats: prediction of tissue-dependent efficacy in vivo. The Journal of Pharmacology and Experimental Therapeutics 290(2): 702–9.

[108] Ciruela, F., Saura, C., Canela, E.I., Mallol, J., Lluís, C., Franco, R., 1997. Ligand-induced phosphorylation, clustering, and desensitization of A1 adenosine receptors. Molecular Pharmacology 52(5): 788–97, Doi: 10.1124/mol.52.5.788.

[109] Berkich, D.A., Luthin, D.R., Woodard, R.L., Vannucci, S.J., Linden, J., LaNoue, K.F., 1995. Evidence for regulated coupling of A1 adenosine receptors by phosphorylation in Zucker rats. American Journal of Physiology - Endocrinology and Metabolism 268(4 31-4), Doi: 10.1152/ajpendo.1995.268.4.e693.

[110] Klaasse, E.C., IJzerman, A.P., de Grip, W.J., Beukers, M.W., 2008. Internalization and desensitization of adenosine receptors. Purinergic Signalling 4(1): 21–37, Doi: 10.1007/s11302-007-9086-7.

[111] Kohno, T., Kubo, Y., Yasui, K., Haraguchi, M., Shigematsu, S., Chua, K.J., et al., 2012. Serum starvation activates NF-κB through G protein β2 subunit-mediated signal. DNA and Cell Biology 31(11): 1636–44, Doi: 10.1089/dna.2012.1666.

[112] Sun, Y., Huang, P., 2016. Adenosine A2B receptor: From cell biology to human diseases. Frontiers in Chemistry 4(AUG): 1–11, Doi: 10.3389/fchem.2016.00037.

[113] Hinz, S., Lacher, S.K., Seibt, B.F., Müller, C.E., 2014. BAY60-6583 acts as a partial agonist at adenosine A2B receptors. Journal of Pharmacology and Experimental Therapeutics 349(3): 427–36, Doi: 10.1124/jpet.113.210849.

[114] Whitton, H., Singh, L.N., Patrick, M.A., Price, A.J., Osorio, F.G., López-Otín, C., et al., 2018. Changes at the nuclear lamina alter binding of pioneer factor Foxa2 in aged liver. Aging Cell 17(3): e12742, Doi: 10.1111/acel.12742.

[115] Strange, P.G., 2000. Agonist binding to G-protein coupled receptors. British Journal of Pharmacology 129(4): 820–1, Doi: 10.1038/sj.bjp.0702991.

[116] Tupone, D., Madden, C.J., Morrison, S.F., 2013. Central activation of the A1 adenosine receptor (A1AR) induces a hypothermic, torpor-like state in the rat. Journal of Neuroscience 33(36): 14512–25, Doi: 10.1523/JNEUROSCI.1980-13.2013.

[117] Bailey, I.R., Laughlin, B., Moore, L.A., Bogren, L.K., Barati, Z., Drew, K.L., 2017. Optimization of thermolytic response to a1 adenosine receptor agonists in rats. Journal of Pharmacology and Experimental Therapeutics 362(3): 424–30, Doi: 10.1124/jpet.117.241315.

[118] Henry, B.A., Dunshea, F.R., Gould, M., Clarke, I.J., 2008. Profiling postprandial thermogenesis in muscle and fat of sheep and the central effect of leptin administration. Endocrinology 149(4): 2019–26, Doi: 10.1210/en.2007-1311.

[119] Serin, Y., Acar Tek, N., 2019. Effect of Circadian Rhythm on Metabolic Processes and the Regulation of Energy Balance. Annals of Nutrition and Metabolism 74(4): 322–30, Doi: 10.1159/000500071.

[120] Jagannath, A., Varga, N., Dallmann, R., Rando, G., Gosselin, P., Ebrahimjee, F., et al., 2021. Adenosine integrates light and sleep signalling for the regulation of circadian timing in mice. Nature Communications 12(1): 1–11, Doi: 10.1038/s41467-021-22179-z.

[121] Heyde, I., Begemann, K., Oster, H., 2021. Contributions of White and Brown Adipose Tissues to the Circadian Regulation of Energy Metabolism. Endocrinology (United States) 162(3): 1–14, Doi: 10.1210/endocr/bqab009.

[122] Lund, J., Arendt, J., Hampton, S.M., English, J., Morgan, L.M., 2001. Postprandial hormone and metabolic responses amongst shift workers in Antarctica. Journal of Endocrinology 171(3): 557–64, Doi: 10.1677/joe.0.1710557.

[123] Louvel, J., Guo, D., Soethoudt, M., Mocking, T.A.M., Lenselink, E.B., Mulder-Krieger, T., et al., 2015. Structure-kinetics relationships of Capadenoson derivatives as adenosine A<inf>1</inf> receptor agonists. European Journal of Medicinal Chemistry 101: 681–91, Doi: 10.1016/j.ejmech.2015.07.023.

[124] Sabbah, H.N., Gupta, R.C., Kohli, S., Wang, M., Rastogi, S., Zhang, K., et al., 2013. Chronic therapy with a partial adenosine a1-receptor agonist improves left ventricular function and remodeling in dogs with advanced heart failure. Circulation: Heart Failure 6(3): 563–71, Doi: 10.1161/CIRCHEARTFAILURE.112.000208.

[125] Bottermann, K., Granade, M.E., Oenarto, V., Fischer, J.W., Harris, T.E., 2021. Atglistatin Pretreatment Preserves Remote Myocardium Function Following Myocardial Infarction. Journal of Cardiovascular Pharmacology and Therapeutics 26(3): 289–97, Doi: 10.1177/1074248420971113.

[126] Viswanadha, S., Londos, C., 2006. Optimized conditions for measuring lipolysis in murine primary adipocytes. Journal of Lipid Research 47(8): 1859–64, Doi:

10.1194/jlr.D600005-JLR200.

[127] Baltos, J.A., Vecchio, E.A., Harris, M.A., Qin, C.X., Ritchie, R.H., Christopoulos, A., et al., 2017. Capadenoson, a clinically trialed partial adenosine A1 receptor agonist, can stimulate adenosine A2B receptor biased agonism. Biochemical Pharmacology 135: 79–89, Doi: 10.1016/j.bcp.2017.03.014.

[128] Das, S.K., Eder, S., Schauer, S., Diwoky, C., Temmel, H., Guertl, B., et al., 2011. Adipose triglyceride lipase contributes to cancer-associated cachexia. Science 333(6039): 233–8, Doi: 10.1126/science.1198973.

[129] Challis, R.A.J., Budohoski, L., McManus, B., Newsholme, E.A., 1984. Effects of an adenosine-receptor antagonist on insulin-resistance in soleus muscle from obese Zucker rats. Biochemical Journal 221(3): 915–7, Doi: 10.1042/bj2210915.

[130] Budohoski, L., Challiss, R.A.J., Cooney, G.J., McManus, B., Newsholme, E.A., 1984. Reversal of dietary-induced insulin resistance in muscle of the rat by adenosine deaminase and an adenosine-receptor antagonist. Biochemical Journal 224(1): 327–30, Doi: 10.1042/bj2240327.

[131] Baiyang, X.U., Berkich, D.A., Grist, G.H., Lanoue, K.F., 1998. AI adenosine receptor antagonism improves glucose tolerance in Zucker rats. American Journal of Physiology 274(2 PART 1): 271–9.

[132] Crist, G., Baiyang, X., LaNoue, K., Lang, C., 1998. Tissue-specific effects of in vivo adenosine receptor blockade on glucose uptake in Zucker rats. FASEB Journal 12: 1301–8.

[133] Han, D., Hansen, P. a., Nolte, L. a., Holloszy, J.O., 1998. Removal of adenosine decreases the responsiveness of muscle glucose transport to insulin and contractions. Diabetes 47: 1671–5.

[134] Thong, F.S.L., Lally, J.S.V., Dyck, D.J., Greer, F., Bonen, A., Graham, T.E., 2007. Activation of the A1 adenosine receptor increases insulin-stimulated glucose transport in isolated rat soleus muscle. Applied Physiology, Nutrition and Metabolism 32(4): 701–10, Doi: 10.1139/H07-039.

[135] Derave, W., Hespel, P., 1999. Role of adenosine in regulating glucose uptake during contractions and hypoxia in rat skeletal muscle. Journal of Physiology 515(1): 255–63, Doi: 10.1111/j.1469-7793.1999.255ad.x.

[136] Vergauwen, L., Hespel, P., Richter, E.A., 1994. Adenosine receptors mediate synergistic stimulation of glucose uptake and transport by insulin and by contractions in rat skeletal muscle. Journal of Clinical Investigation 93(3): 974–81, Doi: 10.1172/JCI117104.

[137] Granade, M.E., Manigat, L.C., Lemke, M.C., Purow, B.W., Harris, T.E., 2022. Identification of ritanserin analogs that display DGK isoform specificity. Biochemical Pharmacology 197(December 2021), Doi:

10.1016/j.bcp.2022.114908.

[138] Luo, B., Regier, D.S., Prescott, S.M., Topham, M.K., 2004. Diacylglycerol kinases. Cellular Signalling 16(9): 983–9, Doi: 10.1016/j.cellsig.2004.03.016.

[139] Krishna, S., Zhong, X.P., 2013. Regulation of lipid signaling by diacylglycerol kinases during T cell development and function. Frontiers in Immunology 4: 1–14, Doi: 10.3389/fimmu.2013.00178.

[140] Lim, H.K., Choi, Y.A., Park, W., Lee, T., Ryu, S.H., Kim, S.Y., et al., 2003. Phosphatidic Acid Regulates Systemic Inflammatory Responses by Modulating the Akt-Mammalian Target of Rapamycin-p70 S6 Kinase 1 Pathway. Journal of Biological Chemistry 278(46): 45117–27, Doi: 10.1074/jbc.M303789200.

[141] Shulga, Y. V., Topham, M.K., Epand, R.M., 2011. Regulation and functions of diacylglycerol kinases. Chemical Reviews 111(10): 6186–208, Doi: 10.1021/cr1004106.

[142] Topham, M.K., 2006. Signaling roles of diacylglycerol kinases. Journal of Cellular Biochemistry 97(3): 474–84, Doi: 10.1002/jcb.20704.

[143] Purow, B.W., 2015. Molecular pathways: targeting diacylglycerol kinase alpha in cancer. Clinical Cancer Research 21(22): 5008–12, Doi: 10.1158/1078-0432.CCR-15-0413.

[144] Yanagisawa, K., Yasuda, S., Kai, M., Imai, S. ichi., Yamada, K., Yamashita, T., et al., 2007. Diacylglycerol kinase α suppresses tumor necrosis factor-α-induced apoptosis of human melanoma cells through NF-κB activation. Biochimica et Biophysica Acta - Molecular and Cell Biology of Lipids 1771(4): 462–74, Doi: 10.1016/j.bbalip.2006.12.008.

[145] Dominguez, C.L., Floyd, D.H., Xiao, A., Mullins, G.R., Benjamin, K.A., Xin, W., et al., 2013. Diacylglycerol kinase alpha is a critical signaling node and novel therapeutic target in glioblastoma and other cancers. Cancer Discovery 3(7): 782–97, Doi: 10.1158/2159-8290.CD-12-0215.Diacylglycerol.

[146] Sanjuán, M.A., Jones, D.R., Izquierdo, M., Mérida, I., 2001. Role of diacylglycerol kinase α in the attenuation of receptor signaling. Journal of Cell Biology 153(1): 207–19, Doi: 10.1083/jcb.153.1.207.

[147] Riese, M.J., Moon, E.K., Johnson, B.D., Albelda, S.M., 2016. Diacylglycerol kinases (DGKs): Novel targets for improving T cell activity in cancer. Frontiers in Cell and Developmental Biology 4(OCT): 1–7, Doi: 10.3389/fcell.2016.00108.

[148] Sanjuán, M.A., Pradet-Balade, B., Jones, D.R., Martínez-A, C., Stone, J.C., Garcia-Sanz, J.A., et al., 2003. T Cell Activation In Vivo Targets Diacylglycerol Kinase α to the Membrane: A Novel Mechanism for Ras Attenuation. The Journal of Immunology 170(6): 2877–83, Doi: 10.4049/jimmunol.170.6.2877.

[149] Zha, Y., Marks, R., Ho, A.W., Peterson, A.C., Janardhan, S., Brown, I., et al.,

2006. T cell anergy is reversed by active Ras and is regulated by diacylglycerol kinase-α. Nature Immunology 7(11): 1166–73, Doi: 10.1038/ni1394.

[150] Prinz, P.U., Mendler, A.N., Masouris, I., Durner, L., Oberneder, R., Noessner, E., 2012. High DGK-α and Disabled MAPK Pathways Cause Dysfunction of Human Tumor-Infiltrating CD8 + T Cells That Is Reversible by Pharmacologic Intervention. The Journal of Immunology 188(12): 5990–6000, Doi: 10.4049/jimmunol.1103028.

[151] Olenchock, B.A., Guo, R., Carpenter, J.H., Jordan, M., Topham, M.K., Koretzky, G.A., et al., 2006. Disruption of diacylglycerol metabolism impairs the induction of T cell anergy. Nature Immunology 7(11): 1174–81, Doi: 10.1038/ni1400.

[152] Moon, E.K., Wang, L.-C., Dolfi, D. V., Wilson, C.B., Ranganathan, R., Sun, J., et al., 2014. Multifactorial T cell hypofunction that is reversible can limit the efficacy of chimeric antibody receptor-transduced human T cells in solid tumors. Clinical Cancer Research 20(16): 4262–73, Doi: 10.1038/jid.2014.371.

[153] Jung, I.Y., Kim, Y.Y., Yu, H.S., Lee, M., Kim, S., Lee, J., 2018. CRISPR/Cas9-Mediated Knockout of DGK Improves Antitumor Activities of Human T Cells. Cancer Research 78(16): 4692–703, Doi: 10.1158/0008-5472.CAN-18-0030.

[154] Noessner, E., 2017. DGK-α: A checkpoint in cancer-mediated immuno-inhibition and target for immunotherapy. Frontiers in Cell and Developmental Biology 5(MAR): 1–7, Doi: 10.3389/fcell.2017.00016.

[155] Joshi, R.P., Schmidt, A.M., Das, J., Pytel, D., Riese, M.J., Lester, M., et al., 2014. The zeta isoform of diacylglycerol kinase plays a predominant role in regulatory T cell development and TCR-mediated Ras signaling. Science Signaling 6(303): 1–34.

[156] Tsuchiya, R., Tanaka, T., Hozumi, Y., Nakano, T., Okada, M., Topham, M.K., et al., 2015. Downregulation of diacylglycerol kinase ζ enhances activation of cytokine-induced NF-κB signaling pathway. Biochimica et Biophysica Acta 1853(2): 361–9, Doi: 10.1016/j.bbamcr.2014.11.011.

[157] Faris, M., Kokot, N., Lee, L., Nel, A.E., 1996. Regulation of interleukin-2 transcription by inducible stable expression of dominant negative and dominant active mitogen-activated protein kinase kinase kinase in jurkat T cells: Evidence for the importance of Ras in a pathway that is controlled by dual . Journal of Biological Chemistry 271(44): 27366–73, Doi: 10.1074/jbc.271.44.27366.

[158] Takeishi, K., Taketomi, A., Shirabe, K., Toshima, T., Motomura, T., Ikegami, T., et al., 2012. Diacylglycerol kinase alpha enhances hepatocellular carcinoma progression by activation of Ras-Raf-MEK-ERK pathway. Journal of Hepatology 57(1): 77–83, Doi: 10.1016/j.jhep.2012.02.026.

[159] Bozelli, J.C., Yune, J., Takahashi, D., Sakane, F., Epand, R.M., 2021. Membrane morphology determines diacylglycerol kinase α substrate acyl chain specificity.

FASEB Journal 35(6): 1–11, Doi: 10.1096/fj.202100264R.

[160] Sakane, F., Mizuno, S., Takahashi, D., Sakai, H., 2018. Where do substrates of diacylglycerol kinases come from? Diacylglycerol kinases utilize diacylglycerol species supplied from phosphatidylinositol turnover-independent pathways. Advances in Biological Regulation 67: 101–8, Doi: 10.1016/j.jbior.2017.09.003.

[161] Sakai, H., Kado, S., Taketomi, A., Sakane, F., 2014. Diacylglycerol kinase δ phosphorylates phosphatidylcholinespecific phospholipase C-dependent, palmitic acid containing diacylglycerol species in response to high glucose levels. Journal of Biological Chemistry 289(38): 26607–17, Doi: 10.1074/jbc.M114.590950.

[162] Mizuno, S., Kado, S., Goto, K., Takahashi, D., Sakane, F., 2016. Diacylglycerol kinase ζ generates dipalmitoyl-phosphatidic acid species during neuroblastoma cell differentiation. Biochemistry and Biophysics Reports 8(September): 352–9, Doi: 10.1016/j.bbrep.2016.10.004.

[163] Boroda, S., Niccum, M., Raje, V., Purow, B.W., Harris, T.E., 2017. Dual activities of ritanserin and R59022 as DGKα inhibitors and serotonin receptor antagonists. Biochemical Pharmacology 123: 29–39, Doi: 10.1016/j.bcp.2016.10.011.

[164] Wiesel, F.A., Nordström, A.L., Farde, L., Eriksson, B., 1994. An open clinical and biochemical study of ritanserin in acute patients with schizophrenia. Psychopharmacology (Berl) 114(1): 31–8.

[165] Velnati, S., Massarotti, A., Antona, A., Talmon, M., Fresu, L.G., Galetto, A.S., et al., 2020. Structure activity relationship studies on Amb639752: toward the identification of a common pharmacophoric structure for DGKα inhibitors. Journal of Enzyme Inhibition and Medicinal Chemistry 35(1): 96–108, Doi: 10.1080/14756366.2019.1684911.

[166] Liu, K., Kunii, N., Sakuma, M., Yamaki, A., Mizuno, S., Sato, M., et al., 2016. A novel diacylglycerol kinase α-selective inhibitor, CU-3, induces cancer cell apoptosis and enhances immune response. Journal of Lipid Research 57(3): 368–79, Doi: 10.1194/jlr.M062794.

[167] Franks, C.E., Campbell, S.T., Purow, B.W., Harris, T.E., Hsu, K.-L., 2017. The Ligand Binding Landscape of Diacylglycerol Kinases. Cell Chemical Biology 24(7): 870–80, Doi: 10.1016/j.chembiol.2017.06.007.The.

[168] McCloud, R.L., Franks, C.E., Campbell, S.T., Purow, B.W., Harris, T.E., Hsu, K.-L., 2018. Deconstructing lipid kinase inhibitors by chemical proteomics. Biochemistry 57(2): 231–6, Doi: 10.1021/acs.biochem.7b00962.

[169] Olmez, I., Love, S., Xiao, A., Manigat, L., Randolph, P., McKenna, B.D., et al., 2018. Targeting the mesenchymal subtype in glioblastoma and other cancers via inhibition of diacylglycerol kinase alpha. Neuro-Oncology 20(2): 192–202, Doi: 10.1093/neuonc/nox119.

[170] Campbell, S.T., Franks, C.E., Borne, A.L., Shin, M., Zhang, L., Hsu, K.L., 2018. Chemoproteomic discovery of a ritanserin-targeted kinase network mediating apoptotic cell death of lung tumor cells. Molecular Pharmacology 94(5): 1246–55, Doi: 10.1124/mol.118.113001.

[171] Joshi, R.P., Koretzky, G.A., 2013. Diacylglycerol kinases: Regulated controllers of T cell activation, function, and development. International Journal of Molecular Sciences 14(4): 6649–73, Doi: 10.3390/ijms14046649.

[172] Arranz-Nicolás, J., Ogando, J., Soutar, D., Arcos-Pérez, R., Meraviglia-Crivelli, D., Mañes, S., et al., 2018. Diacylglycerol kinase α inactivation is an integral component of the costimulatory pathway that amplifies TCR signals. Cancer Immunology, Immunotherapy 67(6): 965–80, Doi: 10.1007/s00262-018-2154-8.

[173] Cerami, E., Demir, E., Schultz, N., Taylor, B.S., Sander, C., 2010. Automated network analysis identifies core pathways in glioblastoma. PLoS ONE 5(2), Doi: 10.1371/journal.pone.0008918.

[174] Koshy, M., Villano, J.L., Dolecek, T.A., Howard, A., Mahmood, U., Chmura, S.J., et al., 2012. Improved survival time trends for glioblastoma using the SEER 17 population-based registries. Journal of Neuro-Oncology 107(1): 207–12, Doi: 10.1007/s11060-011-0738-7.

[175] Fu, L., Li, S., Xiao, W.W., Yu, K., Li, S., Yuan, S., et al., 2021. DGKA mediates resistance to PD-1 blockade. Cancer Immunology Research 9(4): OF1–15, Doi: 10.1158/2326-6066.CIR-20-0216.

[176] Goto, K., Watanabe, M., Kondo, H., Yuasa, H., Sakane, F., Kanoh, H., 1992. Gene cloning, sequence, expression and in situ localization of 80 kDa diacylglycerol kinase specific to oligodendrocyte of rat brain. Molecular Brain Research 16(1–2): 75–87, Doi: 10.1016/0169-328X(92)90196-I.

[177] Goto, K., Kondo, H., 1993. Molecular cloning and expression of a 90-kDa diacylglycerol kinase that predominantly localizes in neurons. Proceedings of the National Academy of Sciences of the United States of America 90(16): 7598–602, Doi: 10.1073/pnas.90.16.7598.

[178] Granade, M.E., Harris, T.E., 2018. Purification of Lipin and Measurement of Phosphatidic Acid Phosphatase Activity from Liposomes. vol. 607, 1st ed., Elsevier Inc.

[179] Hennessy, M., Granade, M.E., Hassaninasab, A., Wang, D., Kwiatek, J.M., Han, G.S., et al., 2019. Casein kinase II–mediated phosphorylation of lipin 1 phosphatidate phosphatase at Ser-285 and Ser-287 regulates its interaction with 14-3-3 protein. Journal of Biological Chemistry 294(7): 2365–74, Doi: 10.1074/jbc.RA118.007246.

[180] Han, G.S., Wu, W.I., Carman, G.M., 2006. The Saccharomyces cerevisiae lipin homolog is a Mg2+-dependent phosphatidate phosphatase enzyme. Journal of

Biological Chemistry 281(14): 9210–8, Doi: 10.1074/jbc.M600425200.

[181] Carman, G.M., Han, G.S., 2009. Phosphatidic acid phosphatase, a key enzyme in the regulation of lipid synthesis. Journal of Biological Chemistry 284(5): 2593–7, Doi: 10.1074/jbc.R800059200.

[182] Péterfy, M., Phan, J., Xu, P., Reue, K., 2001. Lipodystrophy in the fld mouse results from mutation of a new gene encoding a nuclear protein, lipin. Nature Genetics 27(1): 121–4, Doi: 10.1038/83685.

[183] Carman, G.M., Han, G.S., 2006. Roles of phosphatidate phosphatase enzymes in lipid metabolism. Trends in Biochemical Sciences 31(12): 694–9, Doi: 10.1016/j.tibs.2006.10.003.

[184] Reue, K., Zhang, P., 2008. The lipin protein family: dual roles in lipid biosynthesis and gene expression. FEBS Letters 582(1): 90–6, Doi: 10.3174/ajnr.A1256.Functional.

[185] Finck, B.N., Gropler, M.C., Chen, Z., Leone, T.C., Croce, M.A., Harris, T.E., et al., 2006. Lipin 1 is an inducible amplifier of the hepatic PGC-1α/PPARα regulatory pathway. Cell Metabolism 4(3): 199–210, Doi: 10.1016/j.cmet.2006.08.005.

[186] Zhang, P., Verity, M.A., Reue, K., 2014. Lipin-1 regulates autophagy clearance and intersects with statin drug effects in skeletal muscle. Cell Metabolism 20(2): 267–79, Doi: 10.1016/j.cmet.2014.05.003.

[187] Nadra, K., Charles, A.S.D.P., Médard, J.J., Hendriks, W.T., Han, G.S., Grès, S., et al., 2008. Phosphatidic acid mediates demyelination in Lpin1 mutant mice. Genes and Development 22(12): 1647–61, Doi: 10.1101/gad.1638008.

[188] Zeharia, A., Shaag, A., Houtkooper, R.H., Hindi, T., de Lonlay, P., Erez, G., et al., 2008. Mutations in LPIN1 Cause Recurrent Acute Myoglobinuria in Childhood. American Journal of Human Genetics 83(4): 489–94, Doi: 10.1016/j.ajhg.2008.09.002.

[189] Wiedmann, S., Fischer, M., Koehler, M., Neureuther, K., Riegger, G., Doering, A., et al., 2008. Genetic variants within the LPIN1 gene, encoding lipin, are influencing phenotypes of the metabolic syndrome in humans. Diabetes 57(1): 209–17, Doi: 10.2337/db07-0083.

[190] Harris, T.E., Huffman, T.A., Chi, A., Shabanowitz, J., Hunt, D.F., Kumar, A., et al., 2007. Insulin controls subcellular localization and multisite phosphorylation of the phosphatidic acid phosphatase, lipin 1. Journal of Biological Chemistry 282(1): 277–86, Doi: 10.1074/jbc.M609537200.

[191] Grimsey, N., Han, G.S., O'Hara, L., Rochford, J.J., Carman, G.M., Siniossoglou, S., 2008. Temporal and spatial regulation of the phosphatidate phosphatases lipin 1 and 2. Journal of Biological Chemistry 283(43): 29166–74, Doi:

10.1074/jbc.M804278200.

[192] Huffman, T.A., Mothe-Satney, I., Lawrence, J.C., 2002. Insulin-stimulated phosphorylation of lipin mediated by the mammalian target of rapamycin. Proceedings of the National Academy of Sciences of the United States of America 99(2): 1047–52, Doi: 10.1073/pnas.022634399.

[193] Liu, G.H., Gerace, L., 2009. Sumoylation regulates nuclear localization of lipin-1α in neuronal cells. PLoS ONE 4(9): 1–10, Doi: 10.1371/journal.pone.0007031.

[194] Li, T.Y., Song, L., Sun, Y., Li, J., Yi, C., Lam, S.M., et al., 2018. Tip60-mediated lipin 1 acetylation and ER translocation determine triacylglycerol synthesis rate /631/80/458/1275 /631/443/319/2723 /96/1 /96/95 /82/83 /64/60 /13/109 /38/70 /38/88 article. Nature Communications 9(1), Doi: 10.1038/s41467-018-04363-w.

[195] Péterfy, M., Harris, T.E., Fujita, N., Reue, K., 2010. Insulin-stimulated interaction with 14-3-3 promotes cytoplasmic localization of lipin-1 in adipocytes. Journal of Biological Chemistry 285(6): 3857–64, Doi: 10.1074/jbc.M109.072488.

[196] Eaton, J.M., Mullins, G.R., Brindley, D.N., Harris, T.E., 2013. Phosphorylation of lipin 1 and charge on the phosphatidic acid head group control its phosphatidic acid phosphatase activity and membrane association. Journal of Biological Chemistry 288(14): 9933–45, Doi: 10.1074/jbc.M112.441493.

[197] Boroda, S., Takkellapati, S., Lawrence, R.T., Entwisle, S.W., Pearson, J.M., Granade, M.E., et al., 2017. The phosphatidic acid-binding, polybasic domain is responsible for the differences in the phosphoregulation of lipins 1 and 3. Journal of Biological Chemistry 292(50): 20481–93, Doi: 10.1074/jbc.M117.786574.

[198] Peterson, T.R., Sengupta, S.S., Harris, T.E., Carmack, A.E., Kang, S.A., Balderas, E., et al., 2011. MTOR complex 1 regulates lipin 1 localization to control the SREBP pathway. Cell 146(3): 408–20, Doi: 10.1016/j.cell.2011.06.034.

[199] Kooijman, E.E., Tieleman, D.P., Testerink, C., Munnik, T., Rijkers, D.T.S., Burger, K.N.J., et al., 2007. An electrostatic/hydrogen bond switch as the basis for the specific interaction of phosphatidic acid with proteins. Journal of Biological Chemistry 282(15): 11356–64, Doi: 10.1074/jbc.M609737200.

[200] Zhang, P., Verity, M.A., Reue, K., 2014. Lipin-1 regulates autophagy clearance and intersects with statin drug effects in skeletal muscle. Cell Metabolism 20(2): 267–79, Doi: 10.1016/j.cmet.2014.05.003.

[201] Pinna, L., Meggio, F., 1997. Protein kinase CK2 ("casein kinase-2") and its implication in cell division and proliferation. In: Meijer, L., Guidet, S., Philippe, M., editors. Progress in Cell Cycle Research, Boston, MA: Progress in Cell Cycle Research p. 77–97.

[202] Faust, M., Montenarh, M., 2000. Subcellular localization of protein kinase CK2: A key to its function? Cell and Tissue Research 301(3): 329–40, Doi:

10.1007/s004410000256.

[203] Litchfield, D.W., 2003. Protein kinase CK2: Structure, regulation and role in cellular decisions of life and death. Biochemical Journal 369(1): 1–15, Doi: 10.1042/BJ20021469.

[204] Merta, H., Carrasquillo Rodríguez, J.W., Anjur-Dietrich, M.I., Vitale, T., Granade, M.E., Harris, T.E., et al., 2021. Cell cycle regulation of ER membrane biogenesis protects against chromosome missegregation. Developmental Cell 56(24): 3364-3379.e10, Doi: 10.1016/j.devcel.2021.11.009.

[205] Heesom, K., Avison, M., Diggle, T., Denton, R., 1998. Insulin-stimulated kinase from rat fat cells that phosphorylates initiation factor 4E-binding protein 1 on the rapamycin-insensitive site (serine-111). Biochemical Journal 336(1): 39–48.

[206] Diggle, T., Schmitz-Peiffer, C., Borthwick, A., Welsh, G., Denton, R., 1991. Evidence that insulin activates casein kinase 2 in rat epididymal fat-cells and that this may result in the increased phosphorylation of an acid-soluble 22 kDa protein. Biochemical Journal 279(2): 545–51.

[207] Witters, L.A., Tipper, J.P., Bacon, G.W., 1983. Stimulation of site-specific phosphorylation of acetyl coenzyme A carboxylase by insulin and epinephrine. Journal of Biological Chemistry 258(9): 5643–8, Doi: 10.1016/s0021-9258(20)81941-3.

[208] Höfer, C., Herrmann, A., Müller, P., 2010. Use of liposomes for studying interactions of soluble proteins with cellular membranes. Methods in Molecular Biology 606: 69–82.

[209] Brindley, D.N., 1985. Intracellular Translocation of Phosphatidate Phosphohydrolase and its Possible Role in the Control of Glycerolipid Synthesis. Prog. Lipid Res. 23: 115–33.

[210] Elabbadi, N., Day, C.P., Virden, R., Yeaman, S.J., 2002. Regulation of phosphatidic acid phosphohydrolase 1 by fatty acids. Lipids 37(1): 69–73, Doi: 10.1007/s11745-002-0865-7.

[211] Carman, G.M., Deems, R.A., Dennis, E.A., 1995. Lipid signaling enzymes and surface dlution kinetics. Journal of Biological Chemistry 270(32): 18711–4.

[212] Eaton, J.M., Takkellapati, S., Lawrence, R.T., McQueeney, K.E., Boroda, S., Mullins, G.R., et al., 2014. Lipin 2 binds phosphatidic acid by the electrostatic hydrogen bond switch mechanism independent of phosphorylation. Journal of Biological Chemistry 289(26): 18055–66, Doi: 10.1074/jbc.M114.547604.

[213] Kooijman, E.E., Carter, K.M., Laar, E.G. Van., Chupin, V., Burger, K.N.J., Kruijff, B. De., 2005. What Makes the Bioactive Lipids Phosphatidic Acid and Lysophosphatidic Acid So Special ? What Makes the Bioactive Lipids Phosphatidic Acid and Lysophosphatidic Acid So Special ? †. Biochemistry

44(51): 17007–15, Doi: 10.1021/bi0518794.

[214] Gomez-Muñoz, A., Hatch, G.M., Martin, A., Jamal, Z., Vance, D.E., Brindley, D.N., 1992. Effects of okadaic acid on the activities of two distinct phosphatidate phosphohydrolases in rat hepatocytes. FEBS Letters 301(1): 103–6, Doi: 10.1016/0014-5793(92)80219-7.

[215] Gerace, E., Moazed, D., 2015. Affinity Pull-Down of Proteins Using Anti-FLAG M2 Agarose Beads. Methods in Enzymology 559: 99–110, Doi: 10.1016/bs.mie.2014.11.010.

[216] Tomomori-Sato, C., Sato, S., Conaway, R.C., Conaway, J.W., 2013. Immunoaffinity Purification of Protein Complexes from Mammalian Cells. Methods in Molecular Biology 977: 273–87, Doi: 10.1007/978-1-62703-284-1.

[217] Luo, J., Deng, Z.L., Luo, X., Tang, N., Song, W.X., Chen, J., et al., 2007. A protocol for rapid generation of recombinant adenoviruses using the AdEasy system. Nature Protocols 2(5): 1236–47, Doi: 10.1038/nprot.2007.135.

[218] He, T.-C., Zhou, S., da Costa, L.T., Yu, J., Kinzler, K.W., Vogelstein, B., 1998. A simplified system for generating recombinant adenoviruses. Proceedings of the National Academy of Sciences 95(5): 2509–14, Doi: 10.1073/pnas.95.5.2509.

[219] Ehrhardt, C., Schmolke, M., Matzke, A., Knoblauch, A., Will, C., Wixler, V., et al., 2006. Polyethylenimine, a cost-effective transfection reagent. Signal Transduction 6(3): 179–84, Doi: 10.1002/sita.200500073.

[220] Boussif, O., Lezoualc'h, F., Zanta, M.A., Mergny, M.D., Scherman, D., Demeneix, B., et al., 1995. A versatile vector for gene and oligonucleotide transfer into cells in culture and in vivo: polyethylenimine. Proceedings of the National Academy of Sciences 92(16): 7297–301, Doi: 10.1073/pnas.92.16.7297.

[221] Han, G.S., Carman, G.M., 2010. Characterization of the human LPIN1-encoded phosphatidate phosphatase isoforms. Journal of Biological Chemistry 285(19): 14628–38, Doi: 10.1074/jbc.M110.117747.

[222] Carman, G.M., Lin, Y.-P., 1991. Phosphatidate Phosphatase from Yeast. Methods in Enzymology 197(1991): 548–53, Doi: 10.1128/EC.2.6.1304.

[223] Han, G.-S., Carman, G.M., 2004. Assaying lipid phosphate phosphatase activities. vol. 284, Humana Press.

[224] Walsh, J.P., Bell, R.M., 1986. 1,2-Diacylglycerol Kinase of Escherichia coli. Journal of Biological Chemistry 261(14): 6239–47.

[225] Zhang, H., 2017. Thin-Film Hydration Followed by Extrusion Method for Liposome Preparation. In: D'Souza, G., editor. Methods in Molecular Biology, vol. 1522. 2nd ed. New York, NY: Humana Press p. 17–22.

[226] Mui, B., Chow, L., Hope, M.J., 2003. Extrusion Technique to Generate Liposomes

of Defined Size. Methods in Enzymology 367(1980): 3–14, Doi: 10.1016/S0076-6879(03)67001-1.

[227] Cornell, R.B., Northwood, I.C., 2000. Regulation of CTP : phosphocholine cytidylyltransferase by amphitropism and relocalization. TIBS 25(September): 441–7, Doi: 10.1016/s0968-0004(00)01625-x.

[228] Merino, E., Sanjuán, M.A., Moraga, I., Ciprés, A., Mérida, I., 2007. Role of the diacylglycerol kinase α-conserved domains in membrane targeting in intact T cells. Journal of Biological Chemistry 282(48): 35396–404, Doi: 10.1074/jbc.M702085200.

[229] Santoleri, D., Titchenell, P.M., 2019. Resolving the Paradox of Hepatic Insulin Resistance. Cellular and Molecular Gastroenterology and Hepatology 7(2): 447–56, Doi: 10.1016/j.jcmgh.2018.10.016.